

**DEVELOPMENT AND CHARACTERIZATION OF
A SIDE SCAN SONAR TOWFISH
STABILIZATION DEVICE**

BY

REBECCA ANN CONRAD
University of New Hampshire, 2003

THESIS

Submitted to the University of New Hampshire
In partial fulfillment of
The Requirement for the Degree of

Master of Science

In

Mechanical Engineering

December 2006

This thesis has been examined and approved.

Thesis Director, Lloyd C. Huff
Research Professor of Ocean
Engineering

L. Gordon Kraft
Professor of Electrical and Computer
Engineering

May-Win Thein
Associate Professor of Mechanical
Engineering

Igor Tsukrov
Associate Professor of Mechanical
Engineering

Date

DEDICATION

This work is dedicated to Kali.

ACKNOWLEDGEMENTS

This work was made possible by the NOAA Test Long Range Side Scan Grant (NA04NOS4000259) and The Defence Science and Technology Organization of the Department of Defence Australia (ABN 68706814312). I would like to thank my committee: Dr. Lloyd Huff, Dr. Gordon Kraft, Dr. May-Win Thein, Dr. Igor Tsukrov. The people of UNH Mechanical Engineering and CCOM, which includes: Tracey Harvey, Abby Pagan-Allis, Linda Prescott, Dr. Larry Mayer, Capt. Andy Armstrong, Dr. Ken Baldwin, Dr. Barbaros Celikkol, and Dr. Jindra Novak. Contributors to the project: Paul Lavoie, Ian Berry, Dr. Yuri Rzhakov, Dr. Barbara Kraft, Glenn McGillicuddy, Dr. Barry Fussell, Andy McLeod, Mike Leo, Tianghang Hou, Gretchen Imahori, Shachak Pe'eri, Mashkor Malik, Lorraine Robidoux, Jim Glynn, Bert Franzheim, Val Schmidt, Michelle Weirathmueller, Capt. Ben Smith, Ed Sweeney, Chris Dundorf of Klien, Peter Graham and Roger Neill of Boeing Australia DSTO. Finally, I would like to thank my friends and family.

TABLE OF CONTENTS

DEDICATION.....	iii
ACKNOWLEDGEMENTS.....	iv
LIST OF TABLES.....	viii
LIST OF FIGURES.....	ix
ABSTRACT	xiv
CHAPTER	PAGE
1. INTRODUCTION.....	1
1.1 Background.....	1
1.2 Goals and Objectives	5
1.3 Constraints	5
1.4 Tasks.....	7
2. EXPERIMENTAL SETUP & DESIGN	8
2.1 Major Mechanical Components	8
2.2 Major System Components of the Smart Tail.....	9
2.3 Testing Components	10
3. SENSOR CHARACTERIZATION.....	14
3.1 Sensor Error.....	14
3.2 Sensor Comparison	18
3.3 Sensor Filter Characteristics.....	20

4.	MOTOR CONTROL CHARACTERIZATION.....	24
4.1	Motor Drive.....	24
4.2	Operational Mode Performance	26
4.3	Command Timing.....	28
5.	TOW TANK TESTING.....	31
5.1	Experimental Setup	31
5.2	Pitch Testing.....	32
5.2.1	Transient Response	33
5.2.2	Steady State Response.....	34
5.3	Roll Testing.....	39
5.4	Steady State Coupling.....	40
5.5	Elevator Loading.....	41
6.	FIELD TESTING.....	44
6.1	Testing Objectives	44
6.2	Magnitude of Towfish Response.....	45
6.3	Frequency Content in Towfish Response.....	47
6.4	Test Variable Observations.....	49
7.	MATHEMATICAL MODELING AND SIMULATION.....	51
7.1	Modeling the Plant.....	51
7.1.1	Simulating the Plant	52
7.1.2	Coupling Pitch and Roll	55
7.2	Modeling the Motors.....	55

7.2.1	Simulating the Motors	56
7.2.2	Adding the Motors into the System Model	57
8.	CONTROLLER DESIGN	59
8.1	Feedback and Decoupling.....	59
8.2	Controller Type	65
8.3	Pitch as a Single-input, Single-output System.....	66
8.4	Roll as a Single-input, Single-output System.....	73
8.5	Controller Parameters in the Overall Loop	79
8.6	Test Inputs	84
9.	CONTROLLER PERFORMANCE EVALUATION	91
9.1	Field Observations.....	91
9.2	Magnitude of Towfish Response	94
9.3	Low Frequency Performance	99
9.4	High Frequency Performance	107
10.	CONCLUSIONS	110
	REFERENCES.....	115
	APPENDICES.....	116
	APPENDIX A: CALCULATIONS.....	117
	APPENDIX B: PARTS INFORMATION	119
	APPENDIX C: PRINTS	126
	APPENDIX D: CALIBRATIONS	138
	APPENDIX E: SMART TAIL SOFTWARE.....	141

LIST OF TABLES

Table 5.2.1: Steady state pitch/elevator position gain and vehicle pitch range for tow speeds from 4 to 6 knots.....	38
Table 5.3.1: Steady state gain and time constant results for pitch and roll.	40
Table 5.4.1: Effect of coupling at steady state with swivel degree of freedom in pitch.	41
Table 8.5.1: Controller parameters selected for Version 1 (V1) implementation.....	79
Table 8.5.2: Controller parameters selected for Version 0 (V0) implementation.....	82
Table 9.2.1: Mean and standard deviation values for variables observed in Sections A, B and C of the October 19 th survey.....	99

LIST OF FIGURES

Figure 1.1.1: A typical Side Scan sonar towing arrangement (NOAA).....	1
Figure 1.1.2: Example of Klein System 5000 Side Scan towfishs and reduced-length towfish with Boeing Australia Smart Tail.....	2
Figure 1.1.3: Definition of the six degrees of freedom of a vessel (IMCA).....	3
Figure 2.1.1: Major mechanical features of the Smart Tail.....	8
Figure 2.2.1: Instrument pod electronics stacking disc mount and stepper motor.....	9
Figure 2.2.2: Overall electronics system diagram.	10
Figure 2.3.1: Exploded view of the towfish testing setup.....	11
Figure 2.3.2: Towfish testing setup mounted to the PEL Swivel and Tow Shaft.....	12
Figure 2.3.3: Tow Carriage Apparatus (TCA) mounted to the UNH tow carriage and towfish testing setup.....	12
Figure 3.1.1: Testing setup for the sensor error experiment a) Oscillatory sway actuator b) Cart and potentiometer.....	15
Figure 3.1.2: FFTs of the potentiometer and TCM™ 2.5 data from one trial of the oscillating cart experiment.	16
Figure 3.1.3: TCM™ 2.5 angular error as a function of horizontal acceleration.	17
Figure 3.2.1: TSS™ 335, TCM™ 2.5 and OCTANS™ III tilt sensors mounted to the Tow Carriage Assembly (TCA).....	19
Figure 3.2.2: Results of the sensor comparison performance analysis at 6 kts.....	20
Figure 3.3.1: Experimental setup for TCM™ 2.5 filter characterization.....	21

Figure 3.3.2: Effect of digital damping settings of the TCM™ 2.5 on output to input amplitude ratio as a function of frequency.....	22
Figure 3.3.3: Effect of digital damping settings of the TCM™ 2.5 on phase shift as a function of frequency.....	23
Figure 4.1.1: Weeder Technologies™ Stepper Motor Drive Module command set (Weeder Tech™).....	25
Figure 4.1.2: Position (in steps) reference for elevators (not to scale).....	26
Figure 4.2.1: Potentiometer setup for elevator positioning.	27
Figure 4.2.2: Single-step and ramp mode (R13, V50) position profiles for a 100 step command.	28
Figure 4.3.1: Motor command timing for single-step and ramp modes.	29
Figure 5.1.1 a) Tow tank testing facilities at University of New Hampshire's Chase Engineering Lab b) Towfish mounted to the Tow Carriage Assembly (TCA).....	32
Figure 5.2.1: Pitch step response experimental setup at a) pre-release condition b) post-release, steady state tow condition.	33
Figure 5.2.2: Transient pitch response to a step input.....	34
Figure 5.2.3: Raw pitch data as read into Matlab™ software.	35
Figure 5.2.4: Steady state pitch vs. tow speed at various elevator positions.....	36
Figure 5.2.5: Steady state pitch vs. tow speed for elevator in neutral position case and static balance of 6 degrees bow up.....	37
Figure 5.2.6: Steady state pitch vs. elevator position for 3 to 6 knot tow speeds.....	38
Figure 5.3.1: Transient roll response to a step input.....	39
Figure 5.5.1: Elevator loading experimental setup with elevators positioned parallel to flow...	42
Figure 5.5.2: Results for elevator loading up to 6 knots tow speed.	43

Figure 6.1.1 Research Vessel Gulf Challenger off Portsmouth Harbor.	45
Figure 6.2.1: Pitch and roll magnitude results from R/V Gulf Challenger tow.	46
Figure 6.3.1: Roll spectrogram and roll data from field testing.	47
Figure 6.3.2: Pitch spectrogram compared with major changes in compass heading from field testing.	48
Figure 6.4.1 Observations after free tow from R/V Gulf Challenger.....	49
Figure 7.1.1: Plant model of pitch in Simulink™ workspace.	53
Figure 7.1.2: Pitch step response simulation results as compared to 3 and 4 knot tow tank test data.	53
Figure 7.1.3: Plant model of roll in Simulink™ workspace.	54
Figure 7.1.4: Roll step response simulation results as compared to 3 and 4 knot tow tank test data.	54
Figure 7.1.5: Coupled model of the plant in Simulink™ workspace.	55
Figure 7.2.1: Stepper motor model in Simulink™ workspace.....	56
Figure 7.2.2: Comparison of simulation and stepper motor performance after 100 single-step commands.	57
Figure 7.2.3: System model including motor control.	58
Figure 8.1.1: System coupling in terms of path gains.	60
Figure 8.1.2: Decoupled system model with negative feedback.....	63
Figure 8.1.3: Decoupled system response with -10 degree pitch initial condition.	64
Figure 8.1.4: Decoupled system response with 10 degree roll initial condition.....	65
Figure 8.3.1: SISO pitch system model.	66
Figure 8.3.2: Root Locus vs. K_{p_pitch} in the z-plane for the SISO pitch model.....	69
Figure 8.3.3: Bode plot for the proportional feedback gain (K_{p_pitch}) in the SISO pitch model.	70

Figure 8.3.4: Root Locus vs. K_d _pitch in z-plane of SISO pitch model.....	71
Figure 8.3.5: Bode Diagram for K_d _pitch of the SISO pitch model with K_p _pitch set to half of the critical proportional feedback gain.....	72
Figure 8.4.1: SISO roll system model.....	73
Figure 8.4.2: Root Locus vs. K_p _roll in z-plane of SISO roll model.....	75
Figure 8.4.3: Bode plot for the proportional feedback gain (K_{p_roll}) in the SISO roll model.. ...	76
Figure 8.4.4: Root locus vs. K_d _roll (in the z-plane) for the SISO roll system.....	77
Figure 8.4.5: Bode Diagram for K_d _roll of the SISO roll model with K_p _roll set to half of the critical proportional feedback gain.....	78
Figure 8.5.1: Bode Diagram for overall loop gain of the SISO pitch Version 1 model.....	80
Figure 8.5.2: Bode Diagram for the overall loop gain of the roll Version 1 SISO model.....	81
Figure 8.5.3: Bode Diagram for overall loop gain of the SISO pitch Version 0 model.....	82
Figure 8.5.4: Bode Diagram for overall loop gain of the SISO pitch Version 0 model.....	83
Figure 8.6.1: Multiple-input, multiple-output (MIMO) system model with feedback control. .	84
Figure 8.6.2: System response to a 10 degree pitch step disturbance with PD control.	85
Figure 8.6.3: System response to a pitch ramp disturbance with PD control.....	86
Figure 8.6.4: System response to a 0.5 Hz pitch sinusoid disturbance with PD control.	87
Figure 8.6.5: System response to a 10 degree roll step disturbance with PD control.	88
Figure 8.6.6: System response to a roll ramp disturbance with PD control.....	89
Figure 8.6.7: System response to a 0.5 Hz roll sinusoid disturbance with PD control.	90
Figure 9.1.1: Depth and tension as a function of speed through water for the October 19 th , 2006 survey.....	92
Figure 9.1.2: Comparison of depth and tension vs. speed through water trend lines from Oct. 19 th , 2006 and Oct. 24 th , 2006 surveys.....	93

Figure 9.2.1: Sections A, B, and C from the October 19 th , 2006 survey. Section C is with control Version 0 active.....	95
Figure 9.2.2: Section A of the October 19 th , 2006 survey.....	96
Figure 9.2.3: Section B of the October 19 th , 2006 survey.....	97
Figure 9.2.4: Section C of the October 19 th , 2006 survey.....	98
Figure 9.3.1: A reference data set from the October 24 th data set, post 10:43 am with no control active.....	100
Figure 9.3.2 Section from 10:57 am of data from October 24 th , 2006 survey with control Version 1 active.	101
Figure 9.3.3: 100 seconds after control active on 10:57 am data set from Oct. 24 th , 2006 with Version 1 control.....	103
Figure 9.3.4: Startup condition and reaction of the towfish from the 1101V0 control sequence..	105
Figure 9.3.5: Section from 11:01 am of data from October 24 th , 2006 survey with control Version 0 active.	106
Figure 9.4.1: A 10 second segment of the 1057V1 dataset.....	108
Figure 9.4.2: A 10 second segment of the 1101V0 dataset.....	109

ABSTRACT

DEVELOPMENT AND CHARACTERIZATION OF A SIDE SCAN SONAR TOWFISH STABILIZATION DEVICE

by

Rebecca Ann Conrad

University of New Hampshire, December 2006

The attitude of a side scan sonar towfish may introduce artifacts into the imagery when the towfish attitude exhibits a significant mean offset from horizontal and/or exhibits significant variations over time. The Smart Tail was designed by Boeing Australia for stabilizing the attitude of a Klein System 5000 towfish. This report describes the development and testing of a closed-loop controller for towfish attitude based on the Smart Tail's movable elevators. Transient and steady state response of the towfish pitch and roll motion were evaluated in a tow tank at speeds up to 6 knots. Mathematical modeling and simulation were used to design and build a PD controller for the Smart Tail. Performance of the towfish/Smart Tail assemblage was evaluated via an instrumented field test conducted in a typical seaway. This study concludes that closed-loop active control of a side scan towfish is feasible using controllable elevators.

CHAPTER 1

INTRODUCTION

1.1 Background

Side scan sonar is commonly used to observe sea floor characteristics such as roughness and seabed texture by sending and receiving sonar signals perpendicular to a ship's track. The sonar transducer is integrated into a towfish that trails at depth behind a boat. An example of a side scan sonar towing arrangement is illustrated in Figure 1.1.1.

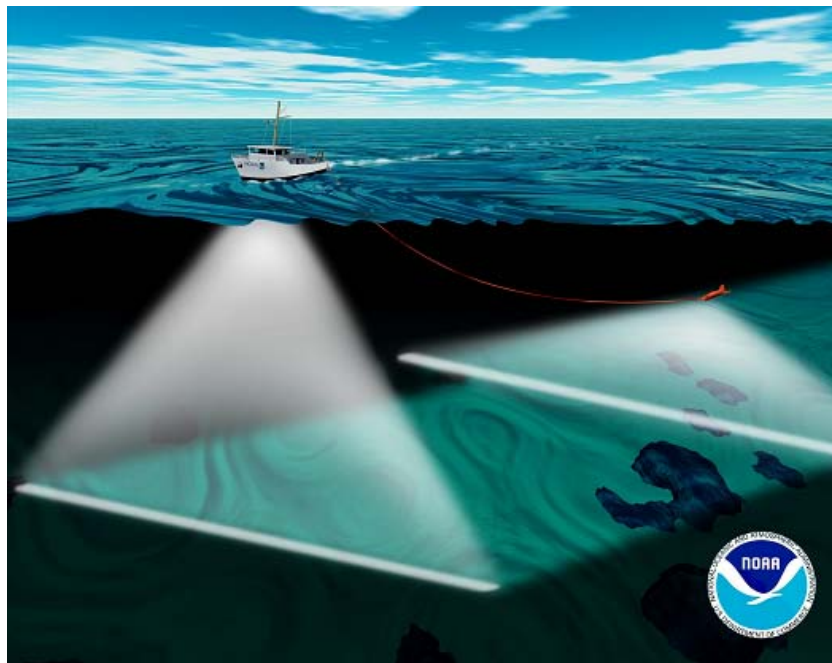


Figure 1.1.1: A typical Side Scan sonar towing arrangement (NOAA).

There are three main mechanical parts to a side scan towfish: the nose, the body and the tail. The nose is a cone shaped mass that is secured to the leading edge of the towfish. The body is cylindrical casing that houses the sonar transceiver. The tail is a cone shaped mass that affixes to the trailing edge of the towfish that typically includes stationary fins for yaw, pitch and roll stabilization.

Two Klein System 5000 Towfish are pictured in Figure 1.1.2.



Figure 1.1.2: Example of Klein System 5000 Side Scan towfish and reduced-length towfish with Boeing Australia Smart Tail.

The Klein System 5000 Towfish has a 76.4 in. body length, weighs 155 lbs in air and can acquire high resolution images of the sea floor at tow speeds up to 10 knots with an overall swath width of 300 meters (Appendix B).

The towfish is subject to six degrees of freedom as it moves through the water – sway, surge, and heave (translational) and pitch, roll, and yaw (rotational).

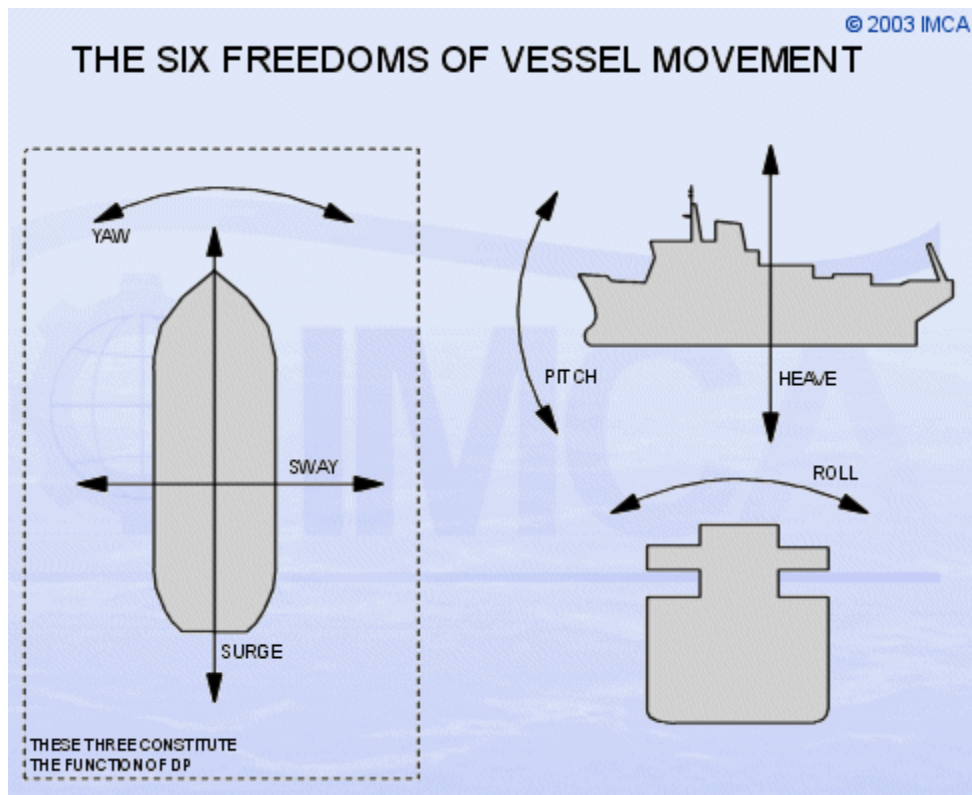


Figure 1.1.3: Definition of the six degrees of freedom of a vessel (IMCA).

The interaction of the towfish with the towing vessel (via the tow cable) along with the effects of wave and currents on the towfish can cause distortions in the side scan sonar image (Unlu 1999). Changes in the speed of the towing vessel causes the towfish to change its altitude and attitude, which may have negative effects on the quality of the imagery.

In the field, a constant towfish roll of 5 degrees is considered enough of a problem to delay survey operations. During tow, if the orientation of one of the tail fins is not parallel to the flow, a local lift force (perpendicular to the flow) results, which causes a torque in the roll direction. Once this applied torque exceeds the opposing torque on the vehicle by the tow cable, the vehicle rotates until the tow cable torque balances the applied torque at a new equilibrium position. Common practice is to haul the towfish out of the water, beat the tail fins with a hammer, and then re-deploy. The operator then reviews the tilt sensor data output stream to see if the towfish roll offset has been corrected and the process is repeated as many times as necessary.

In 1996, a Boeing Australia team of engineers under contract of the Australian Defense Science and Technology (DSTO) office built a “Smart Tail” that had the mechanical capability to remotely operate tail fins (called elevators) by stepper motor drive. An adaptor plate was made to fit the Smart Tail onto the Klein System 5000 Towfish. The project lost momentum and the Smart Tail was placed on the shelf, devoid of several critical system components that were needed for operation. The Smart Tail had not even been wet.

In 2004, an agreement was reached between DSTO and the University of New Hampshire’s (UNH) Center for Coastal and Ocean Mapping (CCOM) which temporarily transferred custody of the Smart Tail assembly to CCOM where the development was to be continued under the direction of Dr. Lloyd Huff.

1.2 Goals and Objectives

This thesis entails a project that continued the development of the Smart Tail to achieve the following objectives:

- Remote operation of towfish tail elevators
- Autonomous low frequency pitch and roll stabilization of a towfish using closed loop feedback control.

Stabilization was initially defined as performance which maintained the towfish within ± 2 degrees of horizontal over an average time of 3 seconds. This project is one step in a chain of research motivated by the reduction of motion artifacts in side scan sonar standard images.

1.3 Constraints

Since this project involves a specific towfish, the Klein System 5000, and a specific tail, the Boeing Smart Tail, there were a number of real and implied constraints that include:

- A power limit of 75 mA at 200V DC
- A horizontal reference provided by a TCMTM2 tilt sensor which had an 8 Hz maximum sampling frequency and up to 15 degree tilt error due to rectilinear acceleration
- Two Stepper motors, each with 11 foot-pound torque stepper motor drive limit after a 30:1 gear reduction

- No continuous feedback sensor for motor position
- No speed through water sensor.

The KGCOMP™ SPN15 12 Volt, 1.5 Amp power supply was provided by CCOM to interface with the Klein System 5000 200V DC power supply. The Klein System 5000 is also equipped with the TCM™2 Tilt Compensated 3-axis Compass Module. The limitations of the TCM™2 include the 8 Hz. maximum sampling frequency and no compensation for tilt error due to translational acceleration of the unit. The RST™ Hybrid Stepper Motors were selected by Boeing Australia and provided with the Smart Tail. The major limitation of the motors is their torque/speed characterization along with no position feedback sensor. The motor drive unit provides motor position feedback by virtue of tracking the step commands. Weeder Technologies™ Stepper Motor Driver Modules were provided by CCOM as the communications interface between the controller PC and the stepper motors. The Weeder™ boards limit the motor stepping speed due to the constrained current draw.

A leak was found in the Smart Tail between the carbon fiber shroud and the cast aluminum main body. A last resort solution was found to prevent water from leaking into the Smart Tail by feeding Tygon™ tubing from a pressure regulated SCUBA tank to a through-hull fitting on the instrument housing. The practicality of towing a fish with Tygon™ tubing fastened alongside the tow cable limited the tow cable to 120 ft. Therefore, the maximum cable that could be in the water during field testing the Smart Tail was approximately 90 ft. Additional caution was taken to install a relative humidity sensor to detect leaks that may have occurred while the Smart Tail was underwater.

Originally, all of the electronics, power, and controller software were all intended to be self-contained within the Smart Tail's pressure tight housing. However, the leak condition changed this plan. A decision was made to have the controller remain topside during Smart Tail testing with power and communication lines running down to the Smart Tail through the tow cable. A 6-pin through hull connector was installed in the instrument housing for compatibility with the Falmat Xtreme-Green™ video cable system available for use at CCOM. The conductors available in the cable and the 6-pin underwater connector limited the number of parameters from the Smart Tail that could be brought topside via the tow cable. The six pins were allotted to: +200V DC, ground, RS232 stepper motor control transmit, RS232 stepper motor control receive, RS232 TCM™2.5 receive, and output from the relative humidity sensor.

1.4 Tasks

The project scope is to install, characterize, and analyze major electro-mechanical and communications components of the Smart Tail in an electronics laboratory setting, observe and analyze overall towfish motion through tow tank and field testing, develop a mathematical model of the tow system and incorporate it into a simulation, design a controller capable of meeting the performance criterion, and provide a final system performance evaluation through field testing.

CHAPTER 2

EXPERIMENTAL SETUP & DESIGN

2.1 Major Mechanical Components

The major mechanical components of the Smart Tail are shown in Figure 2.1.1.

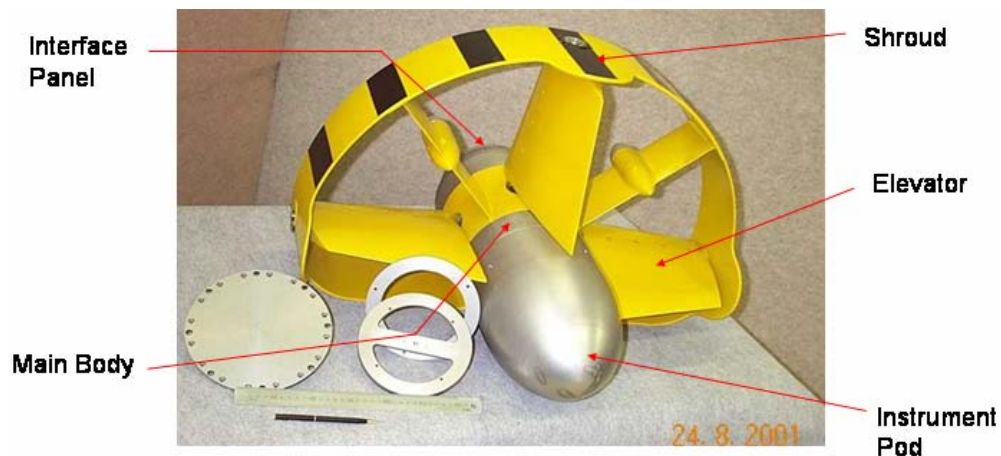


Figure 2.1.1: Major mechanical features of the Smart Tail.

The Smart Tail consists of a carbon fiber Shroud that is integrated with a cast aluminum Main Body. The Instrument Pod is an aluminum pressure bulb that threads into the Main Body and is made water tight with a face-sealing o-ring. The Elevators are mounted to stainless steel shafts that penetrate the Main Body and are sealed with Elastomer Bellows Seals (Appendix

B). The Interface Panel is a mounting plate that connects the Smart Tail to the body of the Klein System 5000 towfish.

2.2 Major System Components of the Smart Tail

Major system components of the Smart Tail include the Weeder Technologies™ Stepper Motor Driver Modules (WTSMD), SPN15 Power Supply, RS™ Hybrid Stepper Motors, TCM™ 2.5 Tilt Compensated Compass Module and a Honeywell™ Relative Humidity (RH) sensor. All system components, except for the stepper motors were mounted into a circular disc bracket, as shown in Figure 2.2.1. The disc on the far left of the figure bolts into the aft end of the Smart Tail's Main Body and is enclosed by the instrument pod housing. The two stepper motors mount into the forward end of the Main Body.

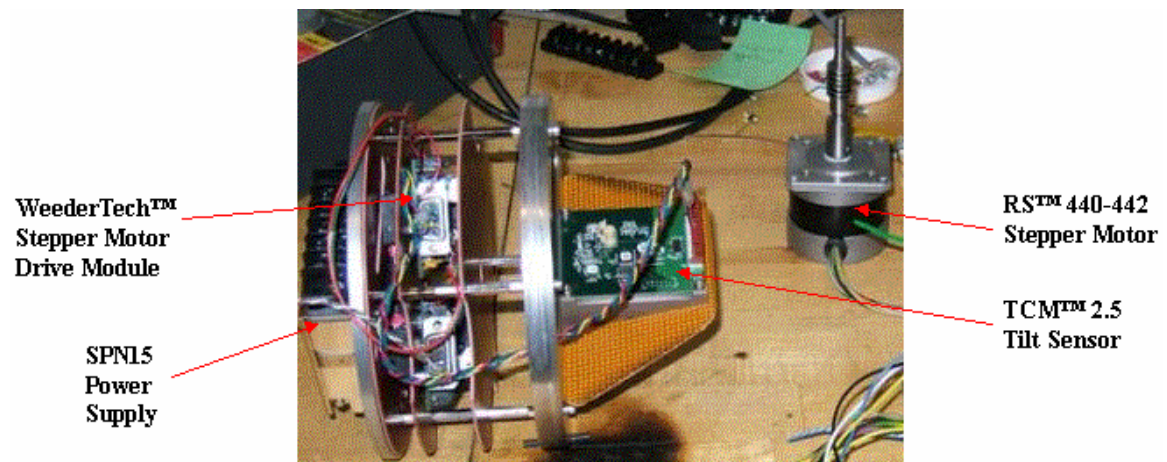


Figure 2.2.1: Instrument pod electronics stacking disc mount and stepper motor.

An overall system/communications diagram is illustrated in Figure 2.2.2. Note the six lines of communication/power that cross the dotted box are designated to the 6-pin underwater through hull connector in the Smart Tail.

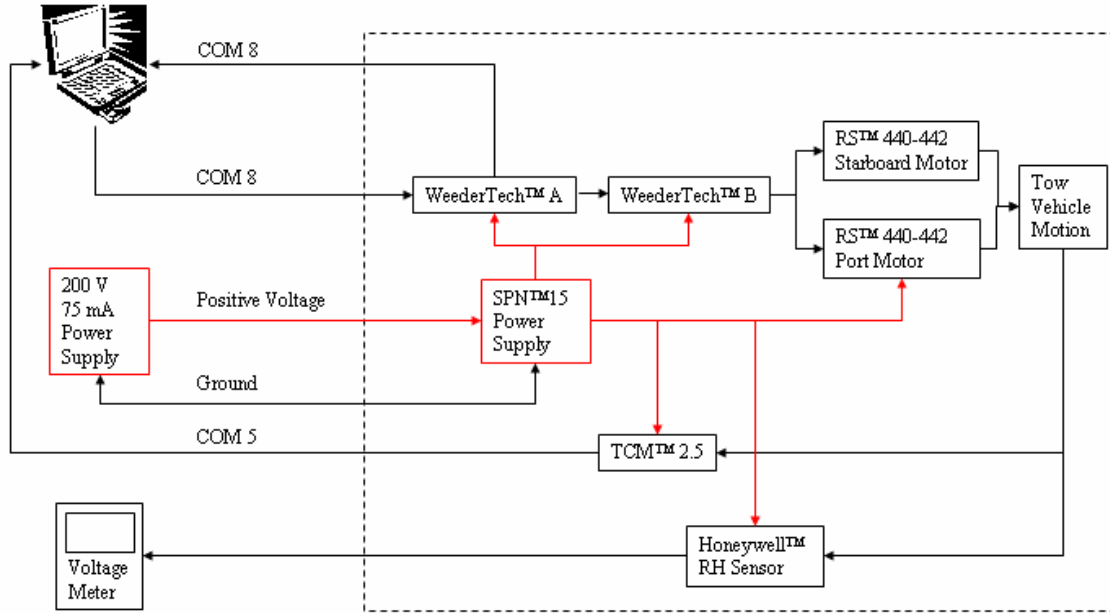


Figure 2.2.2: Overall electronics system diagram.

2.3 Testing Components

It was necessary to design and assemble the experimental setup for tow tank testing in the UNH Ocean Engineering tow tank. Since the Klein System 5000 towfish is too heavy for testing at the UNH facilities, a lightweight, reduced-length tow body was manufactured for testing purposes. The test body's length is 4.5 times its diameter. In order to reduce weight, the test body does not house a sonar transducer, however, it does contain an independently water-tight pressure sensor package. Figure 2.3.1 shows an exploded view of the towfish testing setup including the nose, reduced-length tow body, and Smart Tail. Note the K-wing™ is a depressor used in the field to increase hydrodynamic depression forces. This method is used to achieve desired towing depth with minimum length of cable (Latchman 1993).

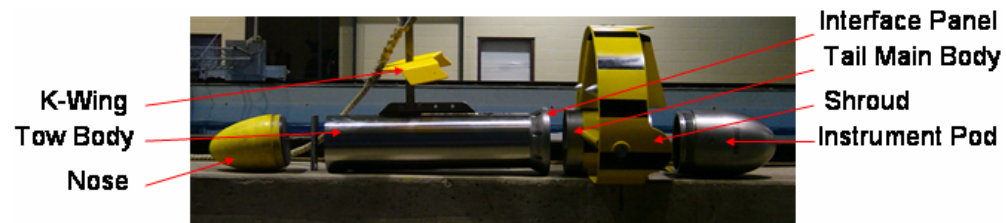


Figure 2.3.1: Exploded view of the towfish testing setup.

A device was required for attaching the towfish setup to the tow carriage that has the capability of meeting following objectives: must affix steadily to the carriage under full speed towing conditions, suspend the towfish below the water's surface and provide both minimum drag and maximum stiffness, while providing fine-adjustments in pitch, roll, and yaw. An assembly of parts, called the Tow Carriage Apparatus (TCA), was developed to meet these objectives. Major components of the TCA include: the towplate, clamps, leveling thumbscrews, tow shaft and fairings. Figure 2.3.2 and Figure 2.3.3 show a Pro Engineer™ 3-D solid model of the towfish setup as mounted in the UNH tow tank facilities (the Tufnose™ fairings were not included to prevent obscuring important details of the TCA).

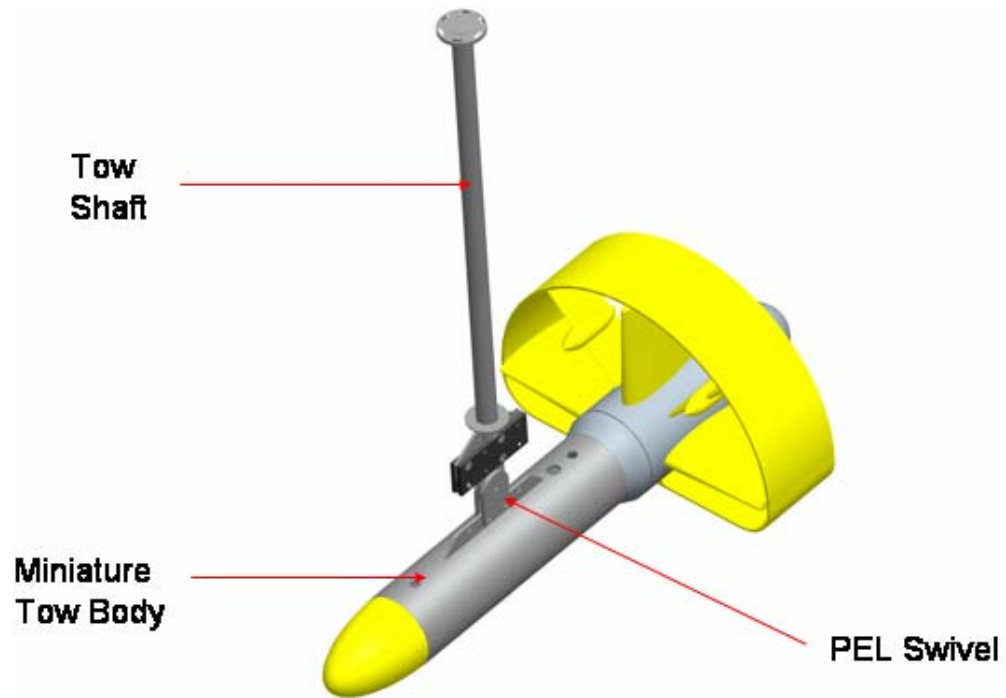


Figure 2.3.2: Towfish testing setup mounted to the PEL Swivel and Tow Shaft.

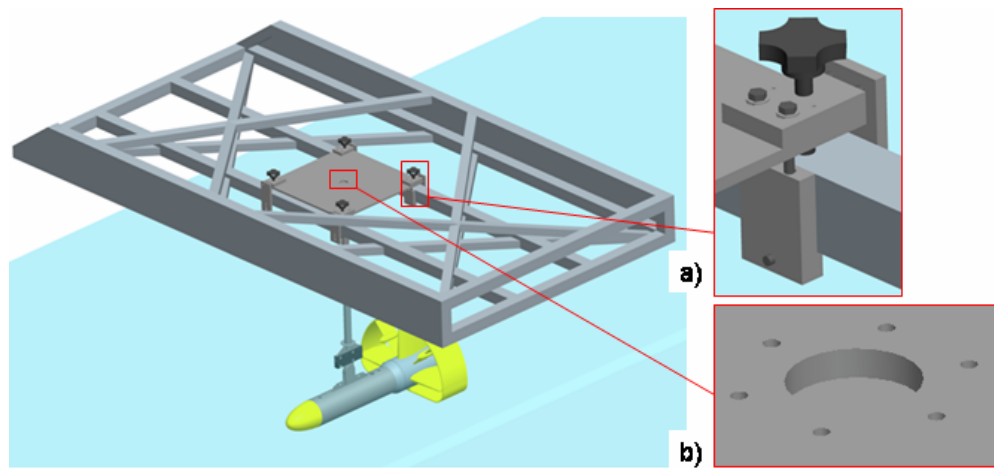


Figure 2.3.3: Tow Carriage Apparatus (TCA) mounted to the UNH tow carriage and towfish testing setup a) Clamping mechanism. b) Bolt circle and locating hole.

The towplate is a 26" x 26" x 1/2" thick plate of aluminum 6061 with a 3" x 4" x 3/4" thick aluminum plates welded to each corner. In the center of the plate is a 2" diameter locating hole with a 6-hole 1/4-20 bolt circle. There are four clamps, each located at the corners of the towplate. On each clamp, two aluminum blocks secure the towplate to the box-beam of the carriage in the x, y, and z directions by tightening three sets of 3/8" bolts. The leveling thumbscrews were designed to lift a 100 pound load with the ease of less than 10 foot pounds of torque applied to each thumbscrew. Calculations were made to find the thread size and diameter of thumbscrew needed. The calculations are included in Appendix A. The tow shaft is a T-304 stainless steel, 42.125" x 1.70" diameter rod with top and bottom welded-on mounting features, the top disk and the gusset. The top disk has a 0.05" raised boss that inserts into the towplate locating hole. Six slotted through holes surround the boss to allow 20 degrees of yaw adjustment. The gusset was constructed of 1/4" thick, 304 stainless steel and has four 3/8" through holes separated on 2" centers. The stainless steel cheek plates sandwich the gusset and are secured with four 3/8"-16 x 1" counter sunk bolts. A washer was slipped onto the rod before the top plate and gusset were welded onto their respective ends of the rod. The washer allows four interlocking Tufnose™ fairings to rotate freely about the shaft. The fairings reduce the drag coefficient of the cylindrical section of the tow shaft to a value of approximately 0.15 and prevent flow separation when towing at 6 knots (Appendix B & C).

Also designed for tank testing was the Paul E. Lavoie (PEL) Swivel device. It is a stainless steel joint that connects to the tow body and allows for rotational movement. It can be oriented parallel to the flow to allow a degree of freedom in pitch only or perpendicular to the flow to allow a degree of freedom in roll only. The PEL Swivel also has the capability of being locked to prevent movement.

CHAPTER 3

SENSOR CHARACTERIZATION

3.1 Sensor Error

The major advantage of TCM™2.5 Tilt Compensated 3-axis Compass Modules is that it utilizes Euler angles as the method of determining accurate orientation (PNI Corp.) However, tilt sensors like the TCM™ will give inaccurate angle measurement when subject to rectilinear acceleration. As the only source of feedback in the Smart Tail control loop, the TCM™ tilt sensor error may pose as the stabilization performance limiting agent. Sensor error experiments were performed in the Chase Ocean Engineering's electronics laboratory to characterize sensor error and filtering.

There were two main objectives to the sensor error experiments. The first objective was to evaluate the performance of the TCM™ 2.5 in contrast to its predecessor, the TCM™ 2. The tilt bulb sensing unit in the TCM™ 2 is a plausible source of error, due to inertial effects (also known as “sloshing”) of the fluid-filled transducer. The second objective was to quantify the tilt error as a function of rectilinear acceleration.

The sensor (TCM™2 TCM™ 2.5) or was mounted to a rolling cart that was oscillated by a motor-driven actuator shown in Figure 3.1.1.

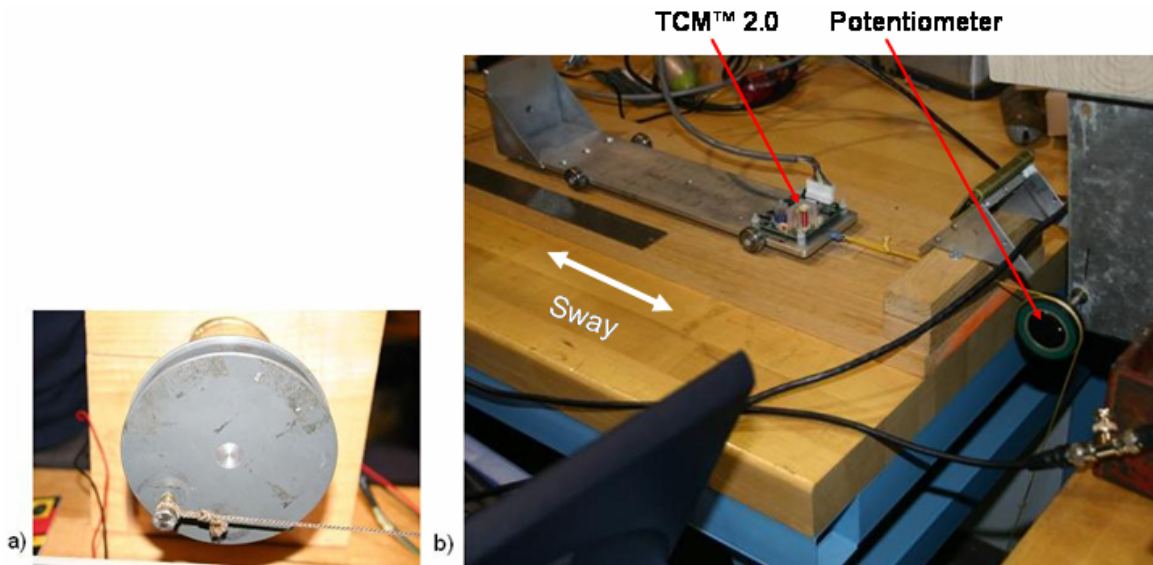


Figure 3.1.1: Testing setup for the sensor error experiment a) Oscillatory sway actuator b) Cart and potentiometer.

A cord that was attached to one end of the cart was wrapped around a potentiometer and then terminated by a flexible cord that was fixed to a support member of the lab bench. The potentiometer setup was used to measure the horizontal input excitation of the cart. The input was then compared to the roll sensed from the TCM™ 2.5 and TCM™ 2 to find the respective angular errors. Since the cart with the mounted sensor was run back and forth over a horizontal surface, any output value for roll from the sensor (other than zero) was an error that had been induced as a result of the horizontal motion of the cart. Both devices were sampled at 5 Hz.

The frequency of the back and forth oscillation (sway) of the cart was changed by applying a proportional DC voltage to the motor of the oscillating sway actuator. However, the frequency of the cart motion was not known in function form. Thus, a 128-point Fast Fourier Transform (FFT) was performed on both the tilt sensor data and the potentiometer data for several different excitation voltage trials. An example of the FFTs from the potentiometer and TCM™ 2.5 of the same oscillation trial is shown in Figure 3.1.2.

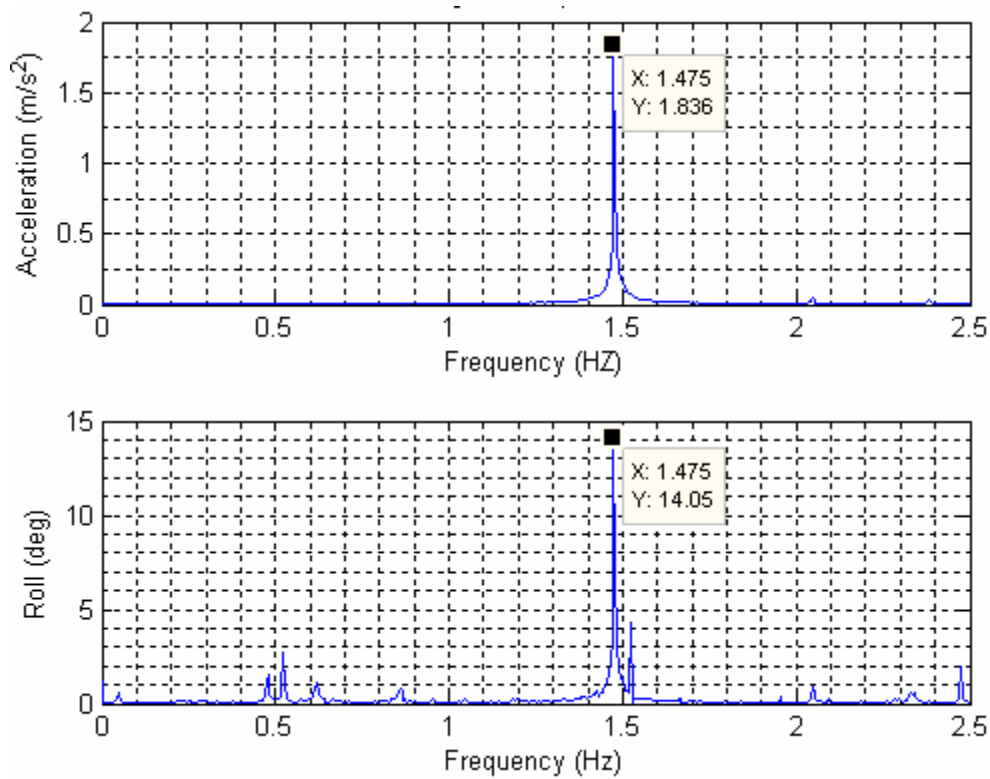


Figure 3.1.2: FFTs of the potentiometer and TCM™ 2.5 data from one trial of the oscillating cart experiment.

The peak value from the real component of an FFT gives two important values, the fundamental amplitude and frequency components of the signal. The fundamental frequency (peak) component of the voltage output from the potentiometer provides the input excitation frequency of the cart. The peak amplitude of the TCM™ roll data is the fundamental amplitude and therefore recorded as roll error for that frequency (in degrees). To find the rectilinear acceleration of the cart, the potentiometer raw data was converted to meters using the calibration curve fit (Appendix D) and a 2-point approximate derivative with respect to time was taken once for velocity and then again for acceleration. The peak values of roll error from the FFT were plotted vs. rectilinear acceleration to generate Figure 3.1.3.

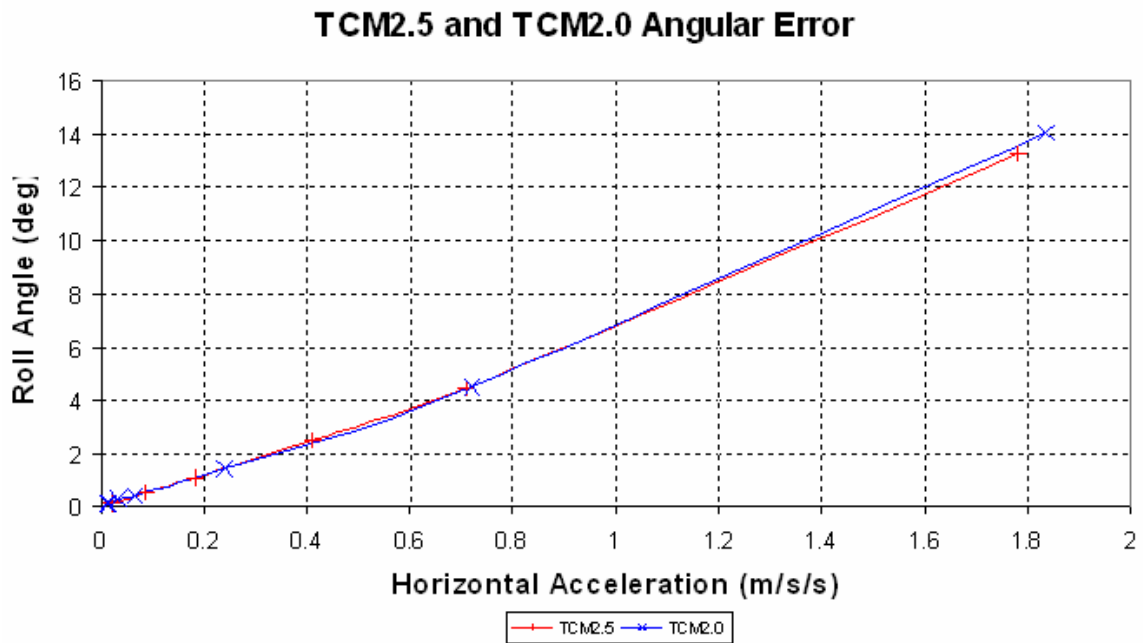


Figure 3.1.3: TCM™ 2.5 angular error as a function of horizontal acceleration.

Figure 3.1.3 shows that up to 1.8 m/s^2 , the difference in angular error between the TCM™ 2.0 and TCM™ 2.5 is negligible. Both sensors exhibited up to 14 degrees of error for this horizontal acceleration range.

3.2 Sensor Comparison

Results from the angular error experiment lead to further investigation of how the TCM™2.5 will perform during tow tank testing at UNH and how this performance compares with other commonly used tilt sensors in the marine industry. The tradeoff between sensing units is between cost, error, weight and volume. A comparative performance analysis of the TCM™ 2.5, TSS 335, and Octans III 3-axis tilt sensors (approximate costs of \$1200, \$30000, and \$75000, respectively) was investigated. Figure 3.2.1 shows the three sensors as they were mounted on the TCA.



Figure 3.2.1: TSS™ 335, TCM™ 2.5 and OCTANS™ III tilt sensors mounted to the Tow Carriage Assembly (TCA).

Figure 3.2.2 shows the pitch readings from each tilt sensor after the carriage was accelerated from zero to a constant velocity of 6 knots and then slowed down to a stop.

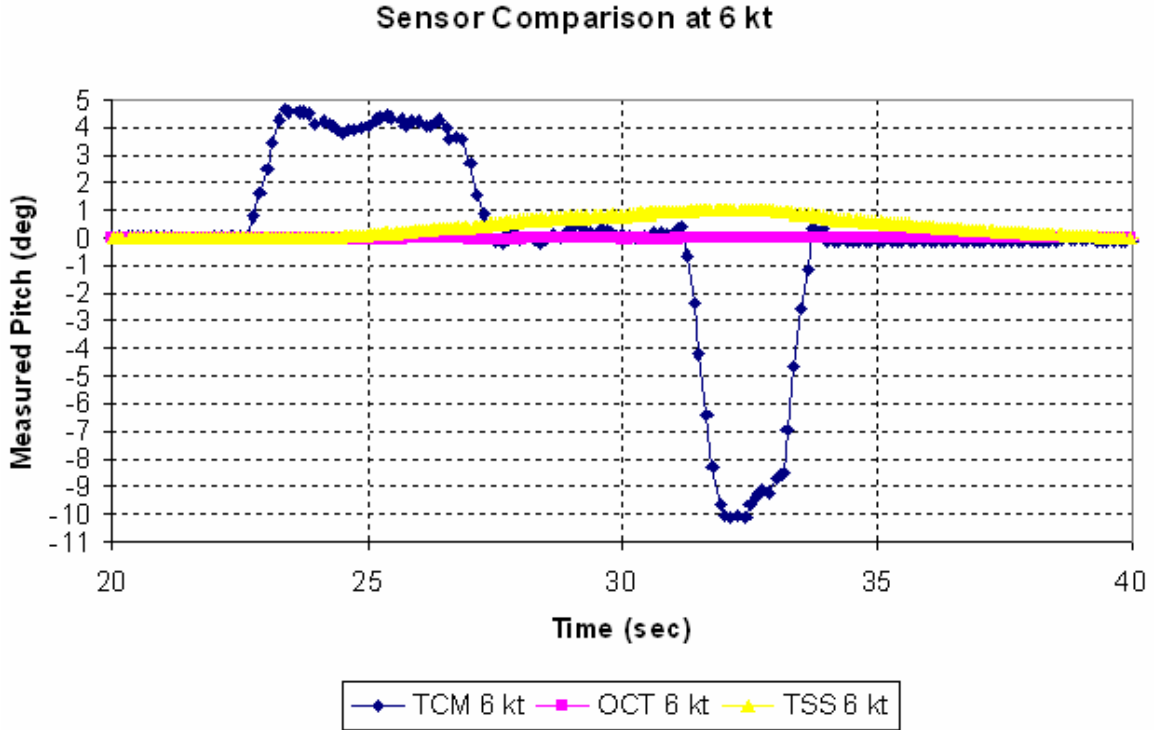


Figure 3.2.2: Results of the sensor comparison performance analysis at 6 kts.

The TCM™ 2.5 exhibited approximately 5 degrees of pitch error on the ramp up and 10 degrees error on the ramp down. The TSS™ 335 data exhibited 1 degree of pitch error over the entire tow period, and the OCTANS™ III exhibited negligible pitch error due to its insensitivity to surge.

3.3 Sensor Filter Characteristics

The TCM™2.5 tilt sensor has a digital damping (filter) option that can allow for a more stable reading. The digital damping filter time constants include values of 4, 8, 16, and 32. The sensor reading (output) values correspond to the following equation (PNI Corp)

$$Output = (1 - f(timeconst)) * current_measurement + f(timeconst) * old_measurements$$

where

$$f(\text{timeconst}) = 10^{\frac{\log(\frac{1}{2})}{\text{timeconst}}}.$$

An experimental setup was developed which used the oscillating actuator and potentiometer in a new configuration to characterize the amplitude response and phase delay as a function of frequency for the TCM™ 2.5 at different digital damping settings, as shown in Figure 3.3.1.

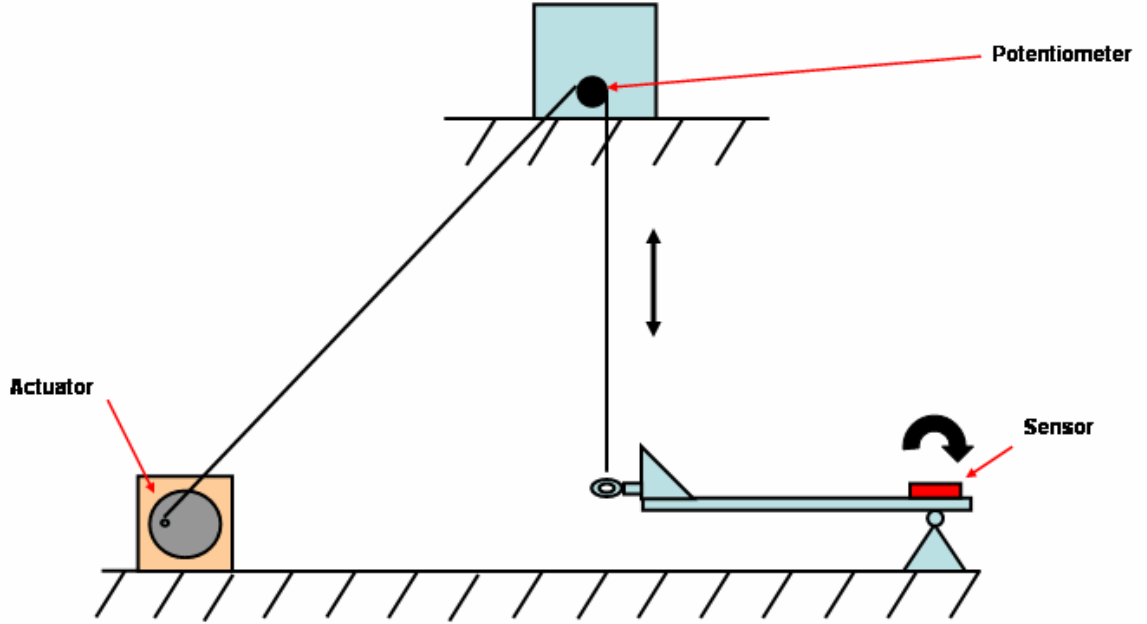


Figure 3.3.1: Experimental setup for TCM™ 2.5 filter characterization.

Again, Fast Fourier Transforms (FFT) were performed on both the tilt sensor data and the potentiometer data for several different actuator excitation voltages. The number of data points used in each FFT was formulated each time by the next highest power of 2, greater than or equal to the length of each data set with zero padding (typically 1024). Peak values were

extracted from FFTs of each trial. The fundamental amplitude of the TCM™ 2.5 was divided by the fundamental amplitude from potentiometer after the cart motion was calibrated to yield a unit-less amplitude ratio. Amplitude ratio was plotted as a function of the input frequency in Figure 3.3.2.

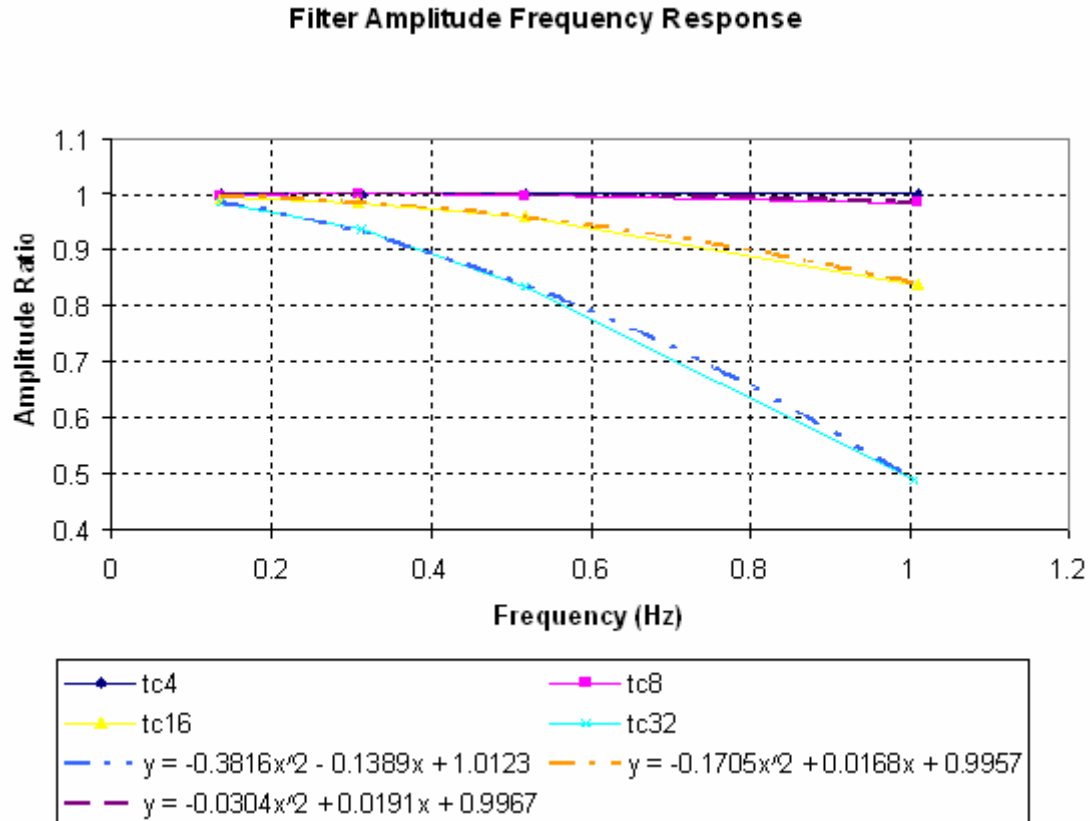


Figure 3.3.2: Effect of digital damping settings of the TCM™ 2.5 on output to input amplitude ratio as a function of frequency.

Matlab™ function *angle* was used to return the phase angle for each element in the complex form of FFT the arrays. Phase value were extracted from the new array at the position of the peak frequency in the corresponding real component of the FFT array for both the TCM™ 2.5 and potentiometer data. The difference between the phase value extracted for the

potentiometer minus that of the TCM™ 2.5 was designated as the phase delay. The phase delay for each digital damping setting was plotted as a function of frequency in Figure 3.3.3.

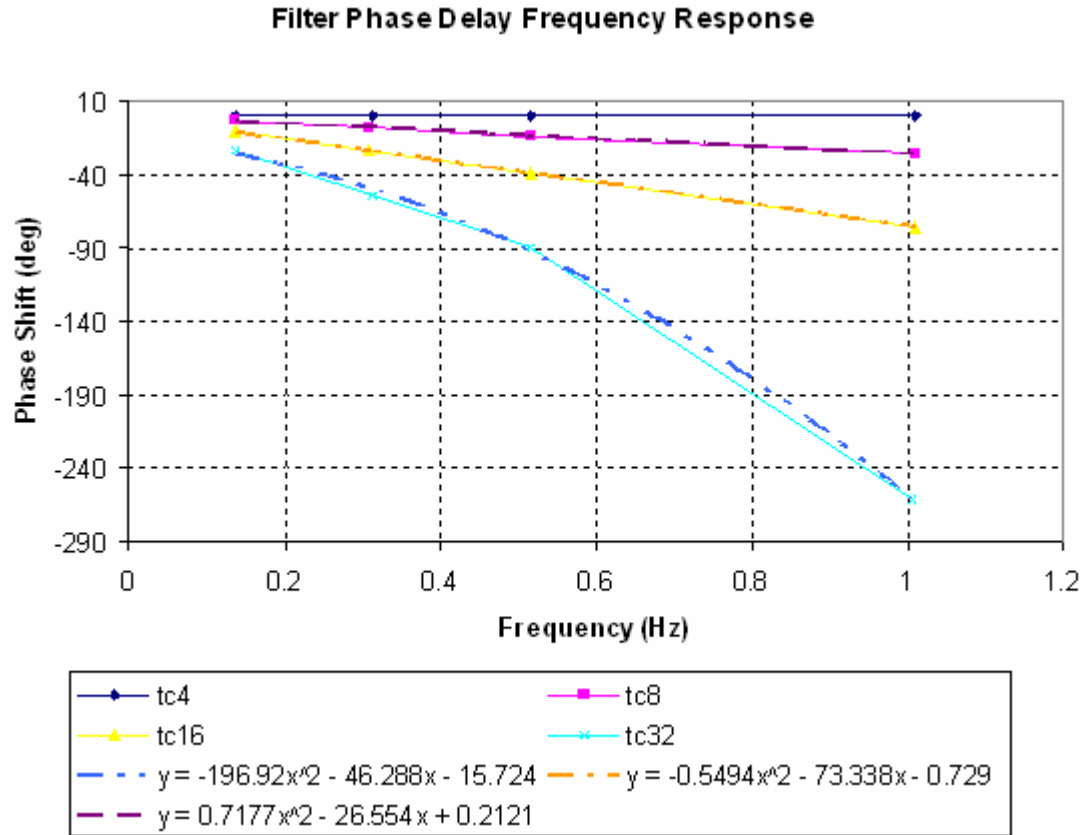


Figure 3.3.3: Effect of digital damping settings of the TCM™ 2.5 on phase delay as a function of frequency.

Note the -180 degrees of phase at approximately 0.8 Hz marks the stability margin for use of the TCM™2.5 on the *timeconstant* = 32 setting; closed-loop control using this setting is not possible at high frequencies.

CHAPTER 4

MOTOR CONTROL CHARACTERIZATION

4.1 **Motor Drive**

Two Weeder Technologies™ Stepper Motor Driver Modules (WTSMD) were installed into the Smart Tail for independent open-loop control of the starboard and port hybrid stepper motors. The WTSMD is a stackable RS-232 stepper motor driver card that advances the stepper motor a precise number of steps with an automatically generated s-curve acceleration/deceleration slope profile (“ramp mode”) or a host incremental, single-step mode (Appendix B). Figure 4.1.1 lists the command set for the WTSMD.

TITLE	COMMAND	DESCRIPTION
MOVE	M <i>pos</i>	Move stepper motor to a specific position (<i>pos</i>) at rate determined by VELOCITY using acceleration and deceleration curves. <i>pos</i> = 0 to 16,777,215. (Note 3)
HOME	H <i>dir index</i>	Move stepper motor in the specific direction (<i>dir</i>) at rate determined by VELOCITY using acceleration curve. Rotation will continue until limit switch activates index runoff and deceleration curve. <i>dir</i> = + or - <i>index</i> = 0 to 255. If <i>index</i> omitted, uses default of 0. (Note 3)
STEP	S <i>dir</i>	Move stepper motor one step in a specific direction (<i>dir</i>). <i>dir</i> = + or -. (Note 3)
VELOCITY	V <i>value</i>	Sets the pulse-per-second rate used in the MOVE or HOME function. <i>value</i> = 1 to 125, multiplied by 10. Default = 50 (500 pps). (Note 3, 4)
RAMP-RATE	R <i>value</i>	Sets the ramp rate used in the acceleration and deceleration curves. <i>value</i> = 1 to 255. Default = 50. (Note 3, 4)
POSITION	P <i>value</i>	Modifies the motor position counter. <i>value</i> = 0 to 16,777,215. (Note 3) If <i>value</i> is omitted, reads current position. Returns 0 to 16,777,215.
EXCITE	E <i>value</i>	Sets the driver excitation mode. <i>value</i> = 1 to 3. "1" being single phase, "2" being dual phase, 3 being half-step. Default = 1. (Note 3, 4)
IDLE	I <i>value</i>	Sets the idle current (via PWM) which is used at anytime the motor is at rest. <i>value</i> = 0 to 10. Default = 10 (100%). (Note 3, 4)
ERROR	?	This character will be returned after an invalid command or variable.
RESET	!	This character will be returned after a power-on reset, or brown-out.
<p>Note 1: All command strings sent to the data module should be preceded with the header character (see Table 1), and terminated with a carriage return. All responses from the data module will also appear in this format.</p> <p>Note 2: Any spaces shown above in the listing of the command strings are for clarity only. They should not be included in the actual transmission from the host, nor expected in a response from the data module.</p> <p>Note 3: After successful execution, this command will be echoed back to the host in the same format as received.</p> <p>Note 4: If <i>value</i> is omitted, reads the current setting which will be returned to the host in the same format as above.</p>		

Figure 4.1.1: Weeder Technologies™ Stepper Motor Drive Module command set (Weeder Tech™).

In the Smart Tail, the motor positions corresponding to the minimum and maximum elevator trajectory are 0 and 660 steps respectively, however, will be referred to in this document as – 330 and +330 steps from the reference position 0, which is the position of the elevators that is parallel to the towfish (neutral). The minimum and maximum motor positions correspond to ± 37 degree (Appendix D) elevator angle as illustrated in Figure 4.1.2.

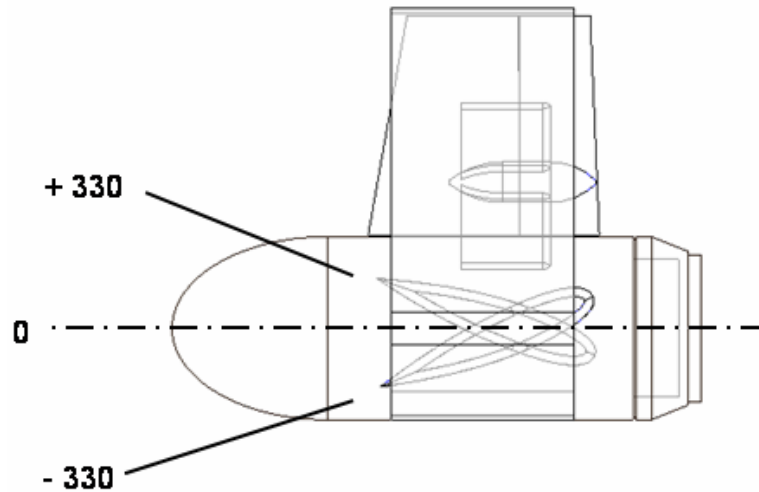


Figure 4.1.2: Position (in steps) reference for elevators (not to scale).

4.2 Operational Mode Performance

The WTSMD units can be queried for motor position using the P command, preceded with the header character assigned to the motor in query. The motor position can only be queried before and after the ramp mode command is executed and similarly for single-step mode since there was no provision for continuous feedback of the physical position of a stepper motor. A potentiometer was temporarily connected to the elevator's shaft to track the trajectory of the elevators for both operational modes. The experimental setup where the potentiometer is connected to the port side elevator is shown in Figure 4.2.1.



Figure 4.2.1: Potentiometer setup for elevator positioning.

Since the measurement of the output voltage from the potentiometer was asynchronous with the step commands, the trajectories of the elevators were sampled approximately 300 times faster than the motor step commands were issued. This was done to reduce noise in the trajectory measurement. The results from a 100 step command for both modes are shown in Figure 4.2.2.

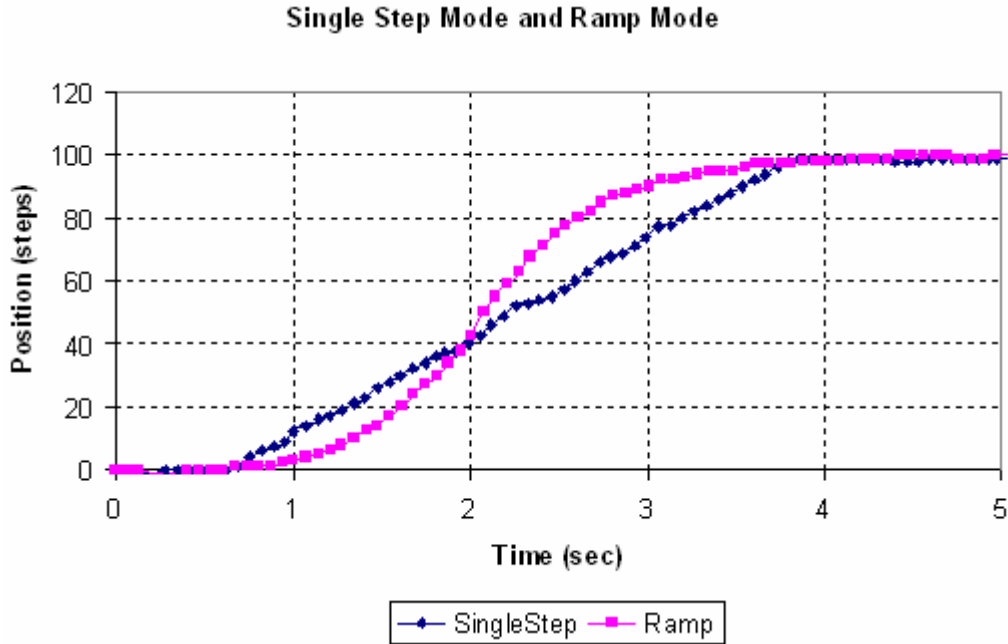


Figure 4.2.2: Single-step and ramp mode (R13, V50) position profiles for a 100 step command.

4.3 Command Timing

The time elapsed during command sequences of different lengths was also investigated using the potentiometer setup. Motor command timing is shown in Figure 4.3.1 for single-step and ramp mode of dual and single motor excitation. Executable software nicknamed SmartTail.exe (Appendix E) was written in order to send Weeder Tech™ defined “simultaneous” commands, which have 20 ms between command packets. The software was programmed to record the time taken to complete each command sequence.

Motor Command Timing for Two Different Modes

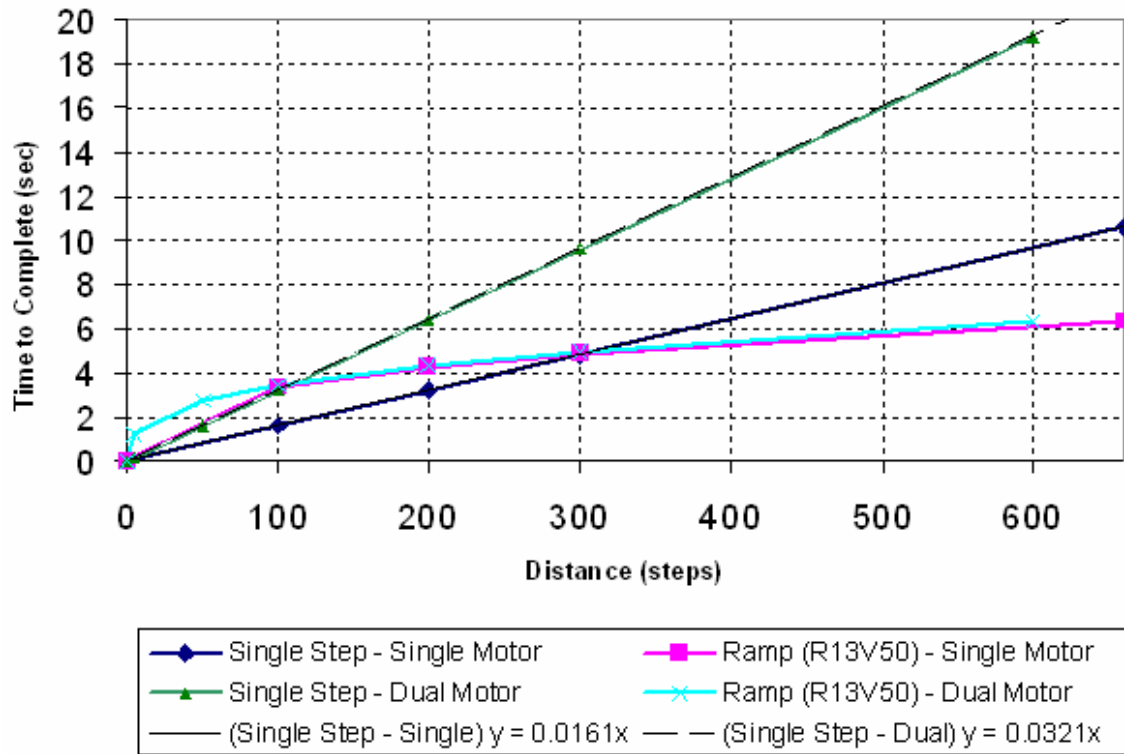


Figure 4.3.1: Motor command timing for single-step and ramp modes.

Figure 4.3.1 shows that for dual motor excitation, ramp mode (R13, V50 setting) is slower than single-step mode up to 100 steps as the number of steps in the command sequence increases, the single-step mode timing increases linearly to approximately 20 seconds at full range, while the ramp mode approaches 6 seconds for full range of elevator motion.

Ramp mode is intended to prevent motor stall during acceleration or position overrun during deceleration. In the event of motor stall, the WTSMD loses track of the motor position. Although ramp mode has the desirable and faster long-range motion, once a command is sent it cannot be interrupted. This is a major disadvantage for closed-loop control of a tow body,

making command sequencing unfavorable for high frequency response. Advantages of the single-step mode include faster command completion for up to 100 step moves and can be incremented at any amount. It also has the advantage that if the tilt value from the TCM™2.5 were to change rapidly it would be possible to avoid continuing to issue a command sequence that is no longer valid. For these reasons, single-step mode was chosen as the mode of operation for the SmartTail software, which was ultimately developed as the Smart Tail stabilization software package.

CHAPTER 5

TOW TANK TESTING

5.1 Experimental Setup

In order to examine towfish motion while underway, tow tank experiments were conducted at the University of New Hampshire's Chase Ocean Engineering Laboratory. There were three main objectives of this set of experiments. The first objective was to determine the towfish's transient characteristics of a step response in pitch and roll. The second objective was to evaluate the steady state characteristics, more specifically the steady state pitch and roll response of the towfish with constant non-zero elevator inputs at various tow speeds. The third objective was to assess the coupling which, in this case, is the effect that pitch has on roll and vice versa during steady state. The tow tank testing facilities are pictured in Figure 5.1.1.

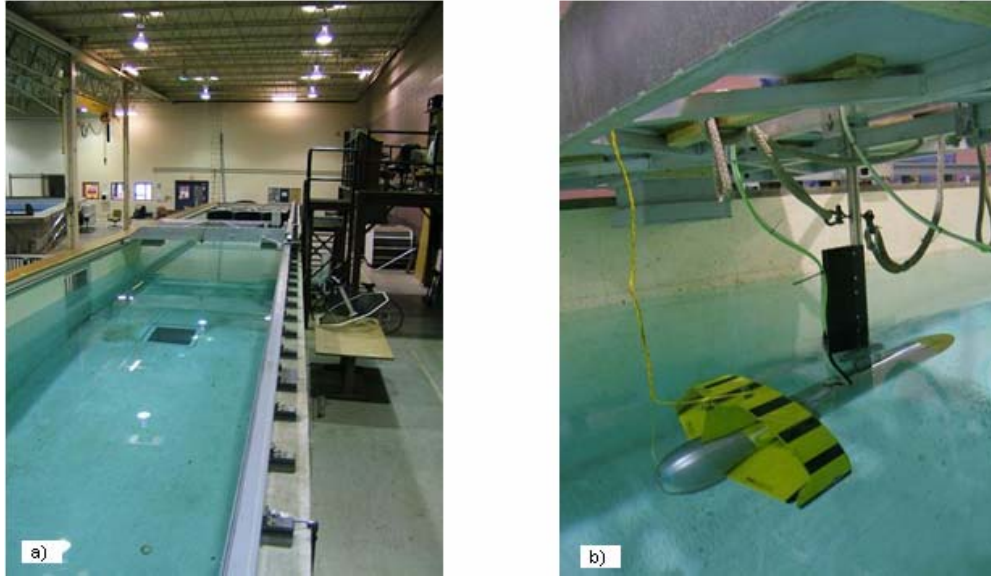


Figure 5.1.1 a) Tow tank testing facilities at University of New Hampshire's Chase Engineering Lab b) Towfish mounted to the Tow Carriage Assembly (TCA).

5.2 Pitch Testing

For the pitch testing, the towfish was attached to the TCA via the PEL Swivel with its one rotational degree of freedom oriented in the pitch plane. A shackle was attached to the tail's shroud with 1/8" aircraft cable extending to a quick release mechanism mounted to the TCA. In each speed trial, the cable was attached to the quick release at start-up, giving an initial pitch of approximately 10 degrees bow down. The elevators were then set into position. The tow carriage was accelerated up to a constant tow speed, and at that point, an operator riding atop of the carriage pulled the pin on the quick release that allowed the cable to go free. This procedure was repeated for 15 speed trials for each of the different 10 elevator positions. Speeds ranged from 0.5 to 6 knots with elevator positions ranging from -330 to +330 steps from zero (neutral).

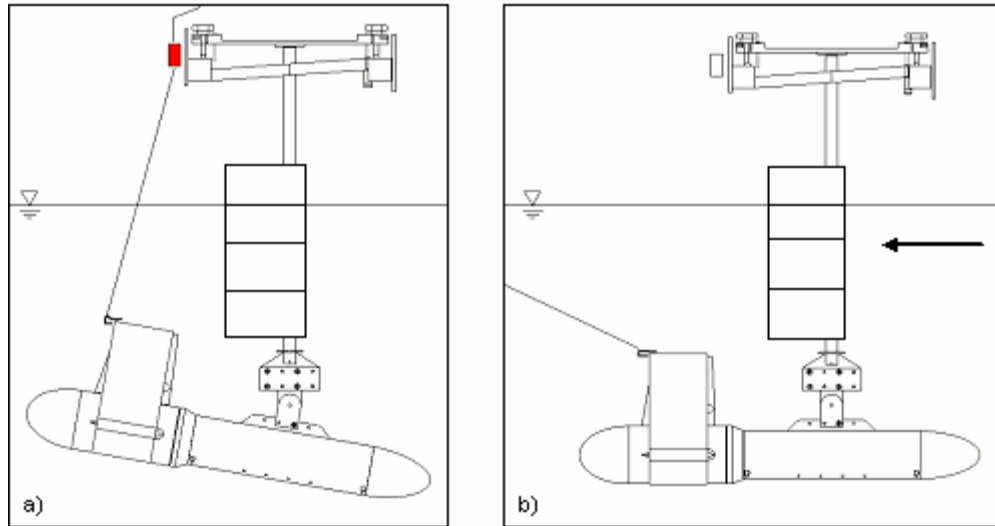


Figure 5.2.1: Pitch transient response experimental setup at a) pre-release condition b) post-release, steady state tow condition.

5.2.1 Transient Response

To determine the towfish's transient behavior, the elevators were set to the neutral position and the pitch data were recorded during speeds trials of 0.5, 1, 1.5, 2, 3 and 4 knots. 5 and 6 knot speed trials were not performed for the transient response experiment due to unsafe riding conditions for the operator at high speeds.

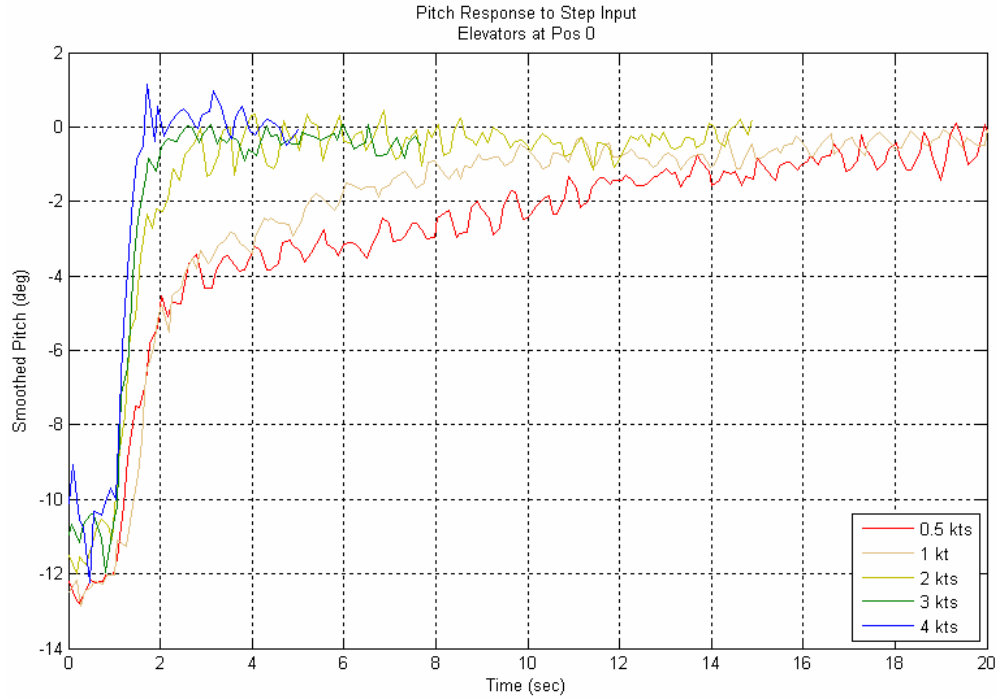


Figure 5.2.2: Transient pitch response starting at $t = 1$ second to an initial condition of -10 degrees.

Results in Figure 5.2.2 show the observed pitch response after release at $t = 1$ second; the plots were smoothed with a three point running average filter. The response appears to be first order at these tow speeds. The time constant was extracted from the 4 knot data as the time it takes to reach 63.2% of steady state. Results show that there is clearly a decrease in the time constant from 0.5 to 4 knots. Normal towing speeds for the sonar are 4 knots and above. Under these operating conditions, the towfish would respond no slower in pitch than a time constant of 0.3 seconds combined with a sampling time of 0.125 seconds.

5.2.2 Steady State Response

The steady state pitch experiments were carried out identically to the transient experiments except that the quick release pin pull was modified; the modification was so that it

was no longer required for an operator to ride the carriage. Instead, a cord was connected from the pin to the back tow tank wall, and as the carriage traveled far enough away from the wall the pin was released. Because of the constant cord length, for most trials the towfish was released while the carriage was still accelerating. This method enabled speed trials up to 6 knots while allowing enough time for the towfish to settle at steady state.

The 15 different speed trials were repeated for 10 different prescribed elevator positions of -330, -250, -170, -90, -60, -30, 0, +30, +130, and +330 steps. Because of the volume of trials performed, the data processing was semi-automated using a MatlabTM program. Raw data was read into MatlabTM and appeared as in Figure 5.2.3.

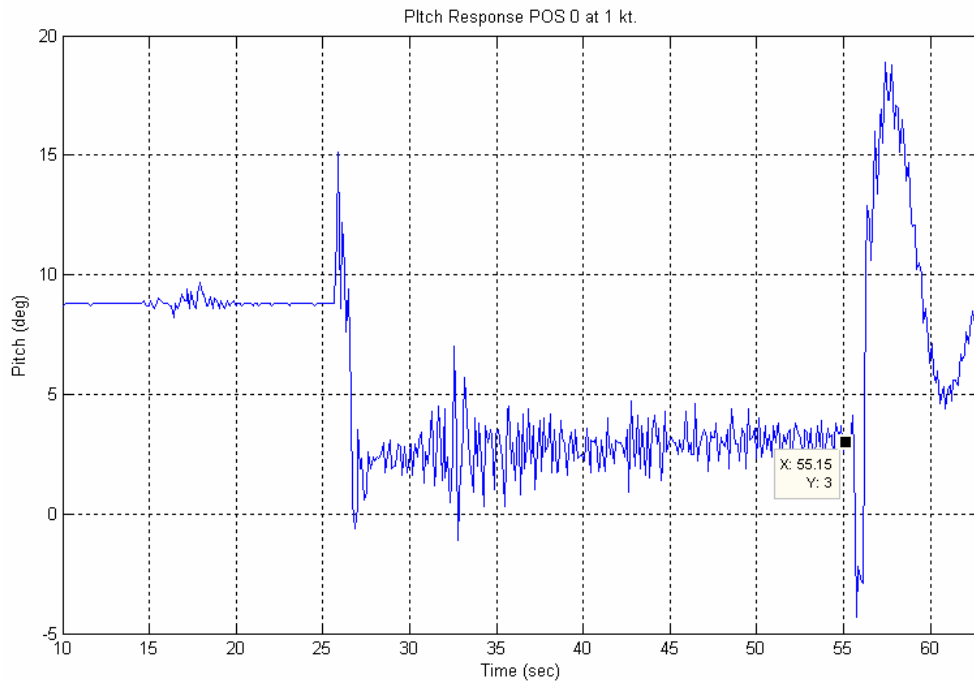


Figure 5.2.3: Raw pitch data as read into MatlabTM software.

To evaluate the steady state value of pitch, a point was handpicked on the flat area preceding the second sudden dip in each dataset. This is to be sure that the final pitch value was extracted before the carriage began to slow down. The selected point was entered into another Matlab[™] function, which averaged that point with the previous seven data points and returns the average (a one second average, given the 8 Hz sampling frequency). Those values were plotted against the tow speed to form Figure 5.2.4.

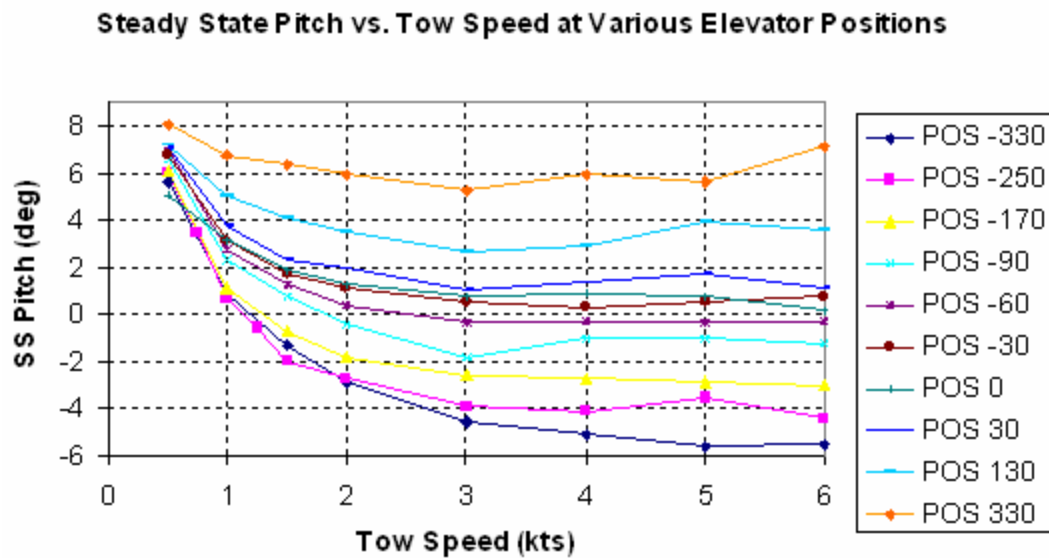


Figure 5.2.4: Steady state pitch vs. tow speed at various elevator positions.

It is expected that, if the towfish has neutral ballast and is towed with the elevators in the neutral position, the towfish should tow parallel to the flow. In this set of tow tank experiments, the towfish was loaded tail heavy in static water. This is a more common tow configuration in the field. The ballast condition indicates that the applied moment of the tail must overcome the moment generated by the center of gravity's displacement aft of the PEL Swivel.

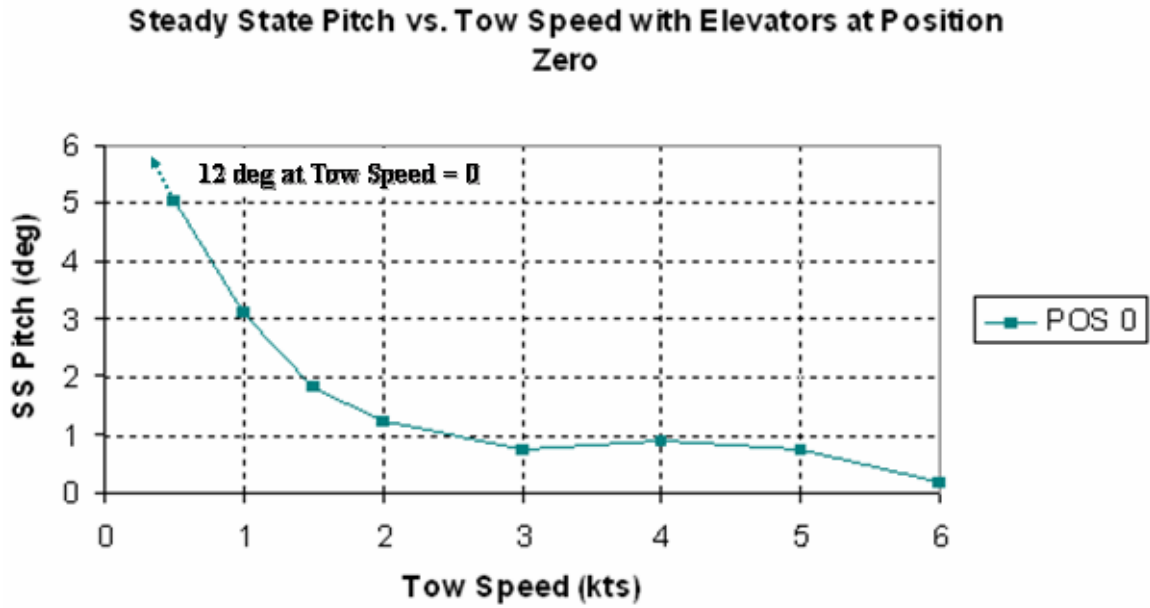


Figure 5.2.5: Steady state pitch vs. tow speed for elevator in neutral position case and static balance of 6 degrees bow up.

Figure 5.2.5 shows that the towfish, when initially balanced 12 degrees bow up (Appendix C), does not orient within one degree of parallel to the flow during steady state for tow speeds below 3 knots. This suggests that at these tow speeds the hydrodynamic righting cannot overcome the particular tail heavy, 12 degrees bow up initial attitude. This observation, and the fact that tow speeds for the Klein Series 5000 are 4 knots and above, took the focus away from further analysis of the 0.5 to 3 knot range.

Steady state pitch vs. elevator position is plotted for 3 to 6 knot speeds in Figure 5.2.6.

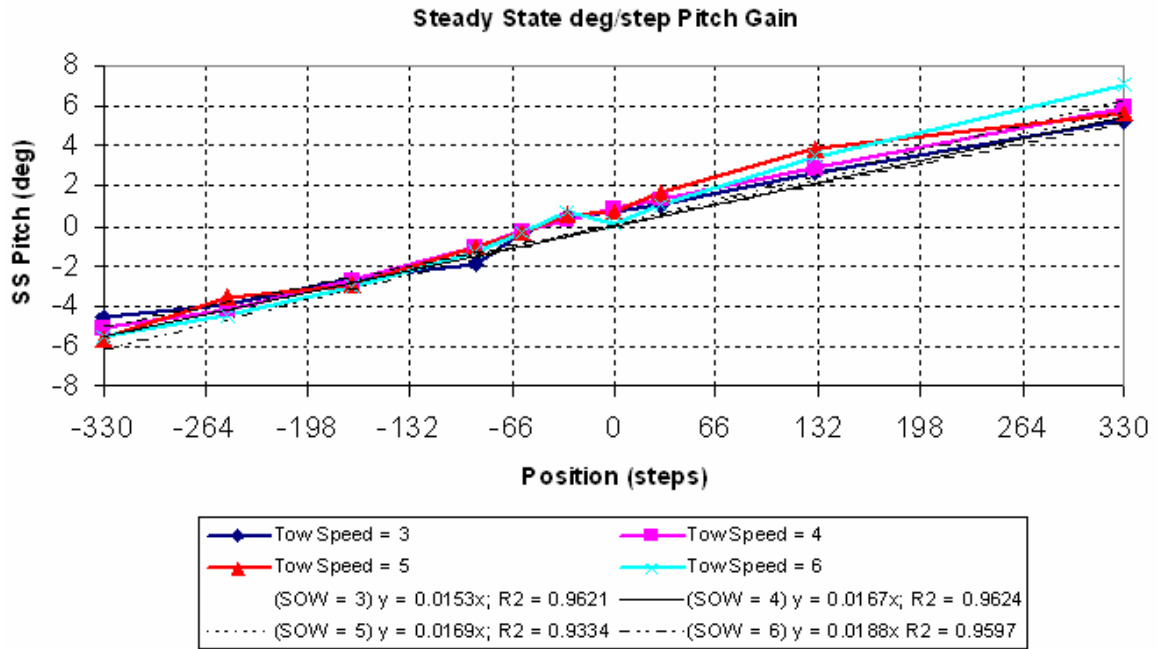


Figure 5.2.6: Steady state pitch vs. elevator position for 3 to 6 knot tow speeds.

The slope of the 4, 5 and 6 knot curves are presented in Table 5.2.1 with the corresponding range of motion that results from the maximum elevator sweep of 660 steps.

Tow Speed (kts)	Pitch Gain (deg/step)	Pitch Range (deg)
4	0.0167	11.02
5	0.0169	11.15
6	0.0188	12.41

Table 5.2.1: Steady state pitch/elevator position gain and towfish pitch range for tow speeds from 4 to 6 knots.

Table 5.2.1 shows that a 12.5% increase in the range of controllable towfish pitch occurs over the 4 to 6 knot tow speed range. However, since the typical tow speed is from 5 to 10 knots,

the 6 knot value for gain (deg/step) was chosen to approximate the gain, independent of tow speed.

5.3 Roll Testing

Roll testing was conducted similar to the pitch testing, although, the PEL Swivel was oriented perpendicular to the flow for a degree of freedom in the roll plane and the towfish was ballast to have the center of mass under the PEL Swivel. The shackle with connecting cord was attached to the port side of the tail's shroud, and the number of speed trials conducted was decreased. After reviewing the pitch data, it was decided to omit speed trials under 1.5 knots and to reduce the number of trials between 1.5 and 6 knots. Figure 5.3.1 shows the roll step response after the data was smoothed by a three point running average.

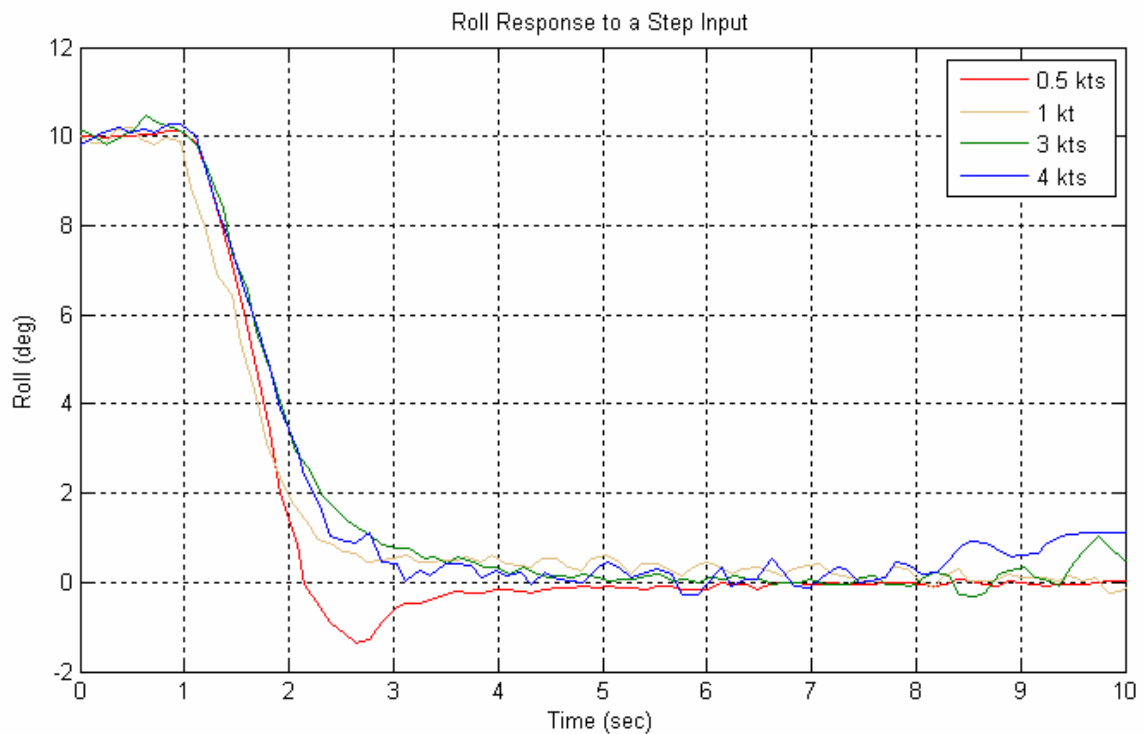


Figure 5.3.1: Transient roll response to an initial condition.

The steady state gain and time constant for pitch and roll are presented in Table 5.3.1.

4 kts and above	K_{ss} (deg/step)	τ (sec)
Pitch	0.0188	0.25
Roll	0.0948	0.6

Table 5.3.1: Steady state gain and time constant results for pitch and roll.

The towfish time constant, sampling rate, and motor command sequence timing are together considered the control update rate for the Smart Tail closed-loop control system. The slew rate (degrees/second) is dominated by motor command sequence timing, which is much slower than the towfish time constant found shown in Table 5.3.1.

5.4 Steady State Coupling

Isolated towfish roll is produced by a symmetric but opposite offset in the starboard and port elevators about the neutral position. When the port and starboard elevators are offset about a position other than zero, the towfish experiences both pitch and roll. For example, if the starboard elevator is set to zero and the port is set to +60 steps, the effective pitch would be equivalent to the pitch produced from setting both elevators to +30 steps. In addition, roll is caused by the 60 step difference between the two elevator positions. In this way, the towfish experiences steady state coupling.

A test case of speed trials was done to verify this assertion. Four, 5 and 6 knot speed trials were performed for each of the two configurations: +180 in port; 0 in starboard and +90 in port; +90 in starboard. The towfish was constrained to only allow rotation in pitch by the PEL Swivel.

Tow Speed	S.S. Pitch (deg) +180/0	S.S. Pitch (deg) +90/+90
4	2.91	3.63
5	3.3	2.87
6	3.66	3.37

Table 5.4.1: Effect of coupling at steady state with swivel degree of freedom in pitch.

Table 5.4.1 shows that the +180/0 and +90/+90 cases have comparable pitch values at steady state. The +180/0 case may have been effected by the torque in the roll direction impacting the pitch degree of freedom of the PEL Swivel.

5.5 Elevator Loading

An additional tow tank experiment was conducted to investigate the applied lift force on the elevators at tow speeds up to 6 knots at 9 degrees of pitch, which is the maximum value of pitch expected. This information is useful for the prediction of motor stall during the performance of the Smart Tail active control. Airline cable was attached from the Smart Tail to a strain gauge that was mounted on the tow carriage. The cable was fastened to a length that forced 9 degrees of pitch, bow down, as shown in Figure 5.5.1.

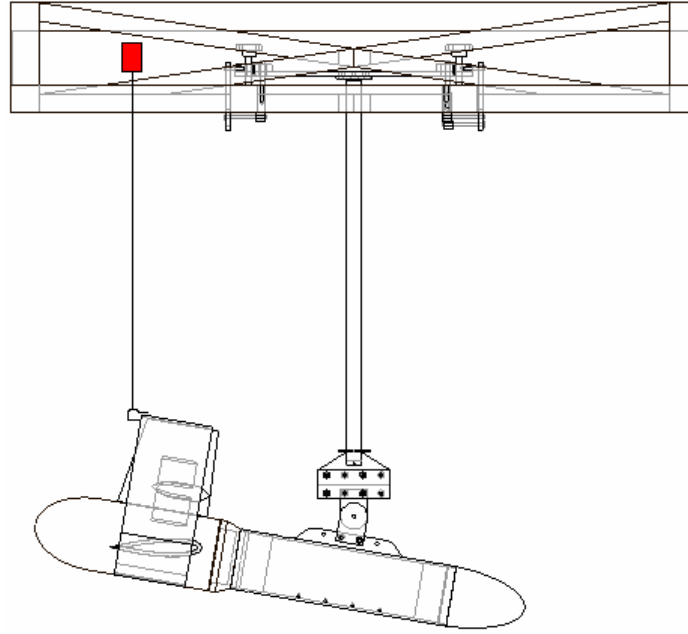


Figure 5.5.1: Elevator loading experimental setup with elevators positioned parallel to flow.

In order to determine the net load on the elevators, two sets of speed trials were performed. The first set of trials was completed with the elevators set at position zero, which was parallel with the tow body. The second set of trials was completed with the elevators set at position - 77 steps, which corresponded to an angle that was parallel to the flow. The net load on the blades was calculated by subtracting the load at steady state from trials with the elevators parallel to the body minus the corresponding values from trials with the elevators parallel to the flow. These values were plotted as a function of tow speed in Figure 5.5.2.

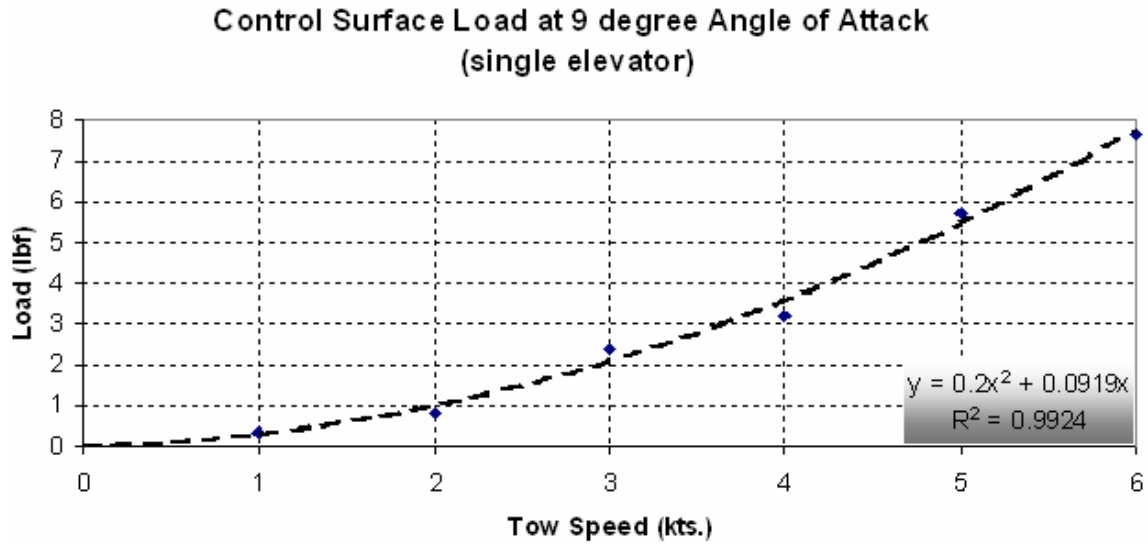


Figure 5.5.2: Results for elevator loading up to 6 knots tow speed.

Results from the elevator loading test show that the load on the elevators is proportional to tow speed squared, as expected. The maximum steady-state load experienced on a single elevator at 6 knots was approximately 8 lbs out of a total force (for the neutral case) of approximately 40 lbs per elevator. The torque induced by this value does not exceed the 11 ft-lb motor stall torque limit on the elevator shaft.

CHAPTER 6

FIELD TESTING

6.1 Testing Objectives

A one day cruise was conducted on the Research Vessel Gulf Challenger in May of 2006. The objective was to acquire the magnitude and frequency information of the towfish pitch and roll motion during tow while observing variables such as speed through water, tow cable tension, direction of tow and towfish depth. The tow took place at approximately 42° 59' N, 70° 34' W, near the Isles of Shoals, which is 7 miles off the coast of NH.



Figure 6.1.1 Research Vessel Gulf Challenger off Portsmouth Harbor.

6.2 Magnitude of Towfish Response

For the first part of the tow, the PEL Swivel device was attached to the towfish to offer freedom of rotation in pitch between the towfish and the tow cable termination. The towfish was towed for 50 minutes, retrieved to lock the PEL Swivel and then put back in the water where it was towed for approximately 30 minutes. The high magnitude pitch spikes (marked by dashed green line) in Figure 6.2.1 resulted from retrieval and re-deploying when the PEL Swivel was switched from the unlocked to the locked state. With the PEL Swivel unlocked, the magnitude of the pitch response ranged from ± 10 degrees. After the PEL Swivel was locked, the pitch response increased to ± 20 degrees, although, it later reduced to ± 5 degrees after the vessel made a major change in course at $t = 66$ minutes in Figure 6.2.1.

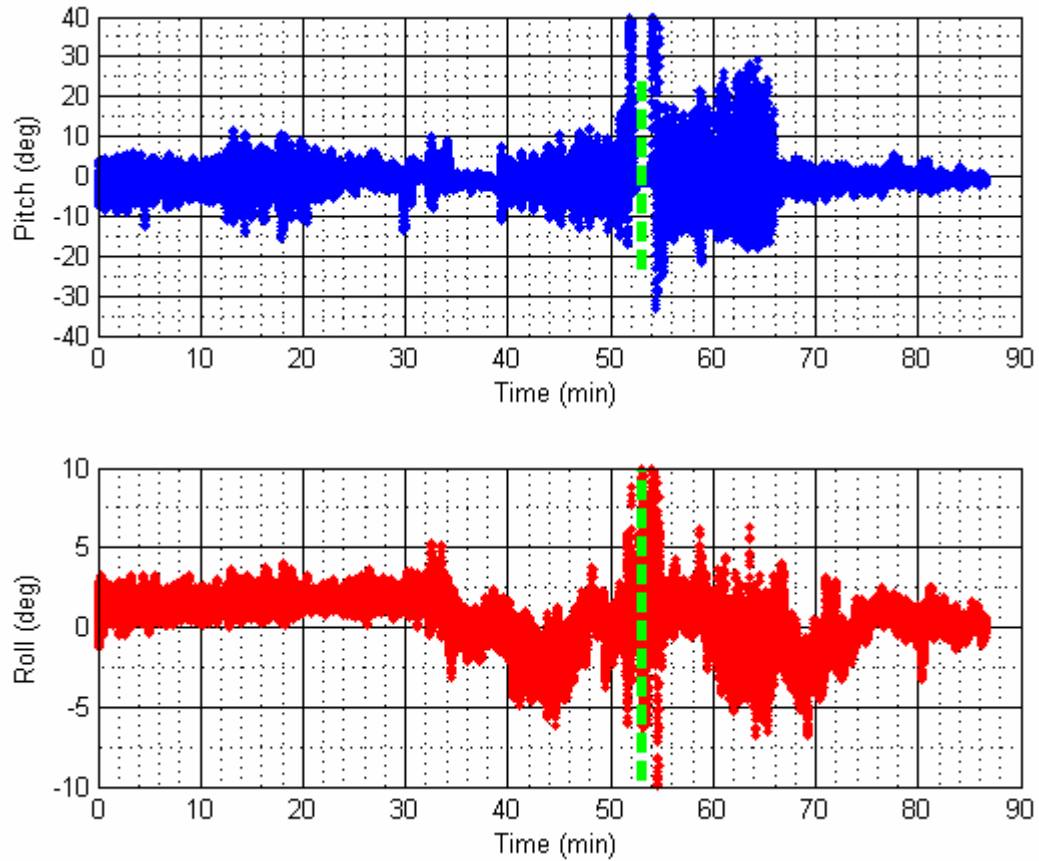


Figure 6.2.1: Pitch and roll magnitude results from R/V Gulf Challenger tow.

The tradeoff for using the PEL Swivel was either a very large pitch response or a very small pitch response depending on the tow direction (relative to the local sea), or a mediocre pitch response for all tow directions. Roll response stayed within ± 5 degrees during tow, unaffected by the use of the PEL swivel or tow direction. The largest roll values were observed as the vessel was turning at $t = 46$ minutes and $t = 66$ minutes.

Results from the field test show that using the PEL Swivel unlocked kept the towfish pitch within ± 12 degrees. This and the negligible effect that the swivel had on towfish roll response gave reason to implement the device in future field tests.

6.3 Frequency Content in Towfish Response

Fast Fourier Transform (FFT) techniques can be used to extract frequency components from the field-testing dataset. A sliding FFT was performed (by the MatlabTM function *spectrogram*) on the pitch and roll data to create a spectrogram. A spectrogram is a 3-dimensional representation of Power Spectral Density (PSD) as a function of frequency (y-axis) and time (x-axis). The resulting spectrogram from the field-testing data for roll and pitch is plotted in Figure 6.3.1 and Figure 6.3.2. There is one section of the spectrogram that should be disregarded. This includes features in the pitch and roll spectrograms between the 50 and 60 minute marks, when the towfish was retrieved and then re-deployed.

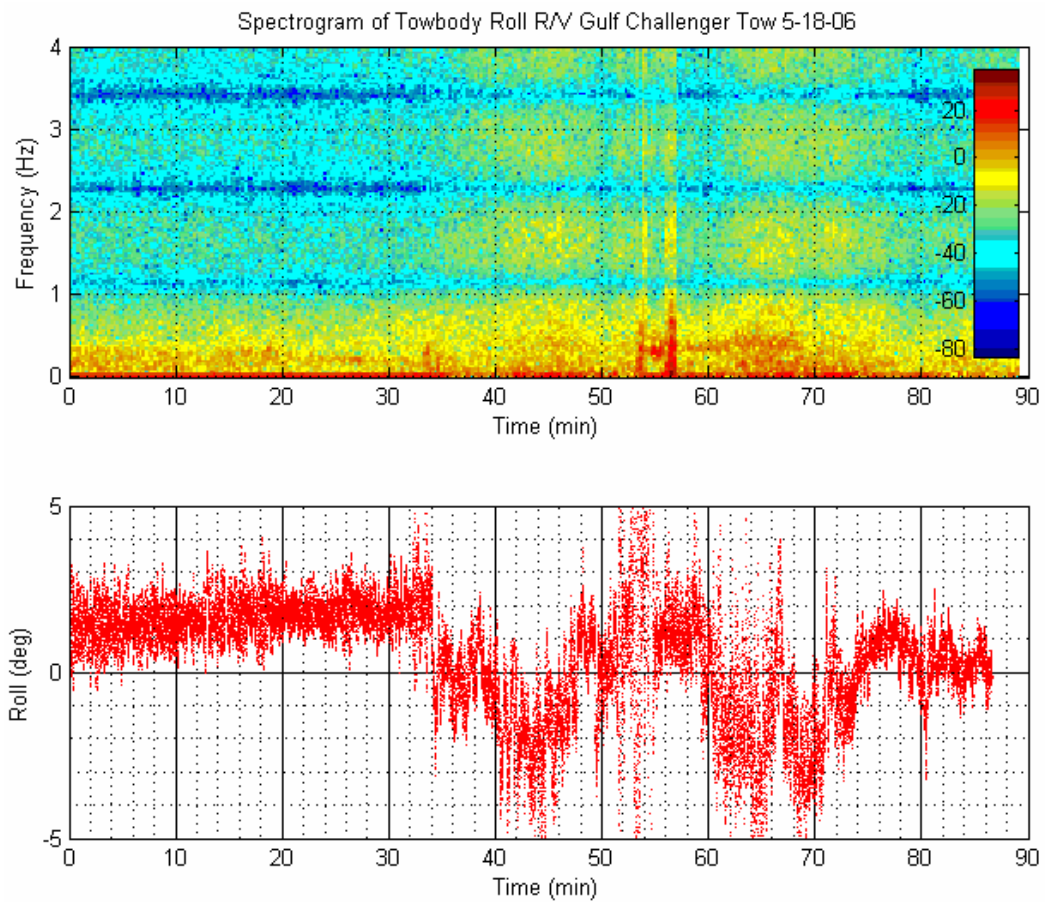


Figure 6.3.1: Roll spectrogram (color scale is Power Spectral Density in dB) in the top plot and roll data from field testing in the bottom plot (red).

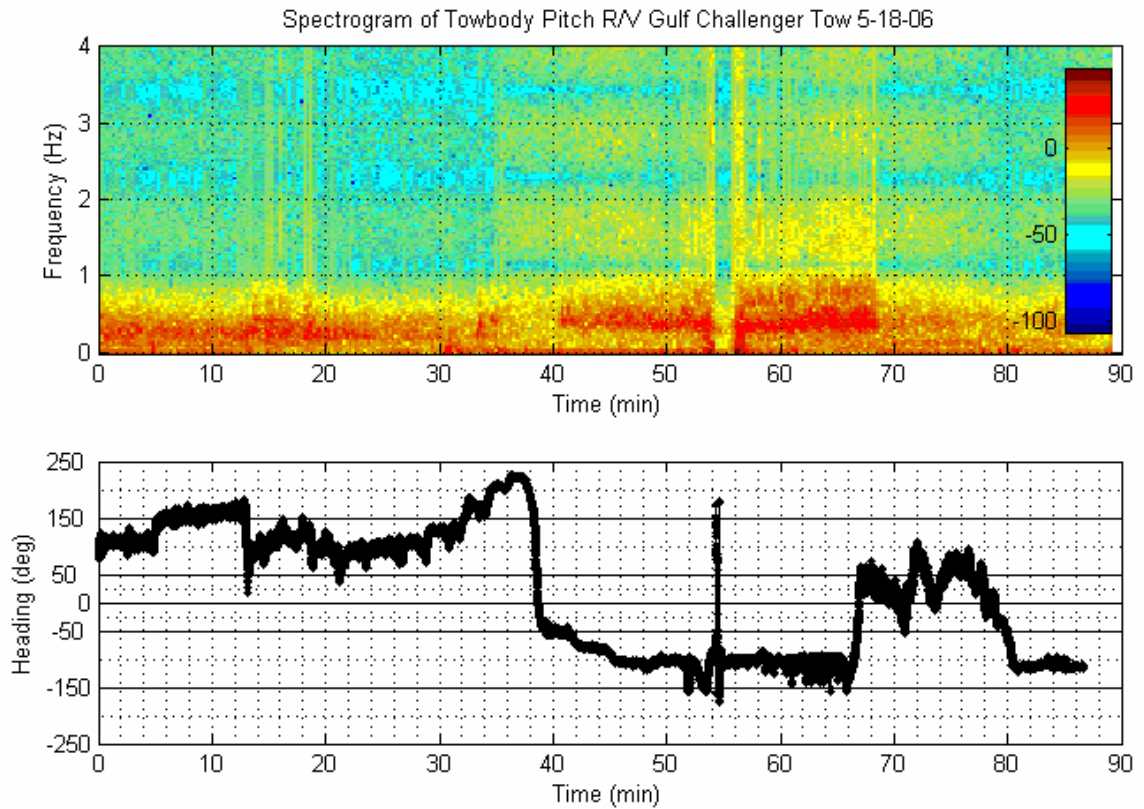


Figure 6.3.2: Pitch spectrogram (color scale is Power Spectral Density in dB) in the top plot compared with major changes in direction of tow during field testing in the bottom plot (black).

A 256-point computation window was used with 50% overlap. That is, the first 256-point FFT was computed on the dataset starting at $t = 0$ as well as each successive 256 points in time (with 50% of the points used from the previous set) until the entire 87 minutes of data were analyzed. From the results in Figure 6.3.1 and Figure 6.3.2 it is important to note that that the frequency response was no greater than 1 Hz for pitch and 0.5 Hz for roll.

6.4 Test Variable Observations

Various test variables were monitored while towing in order to provide insight as to what the major contributors were to changes in towfish motion. This was later used to make simplifying assumptions for mathematical modeling. These observations are plotted in Figure 6.4.1.

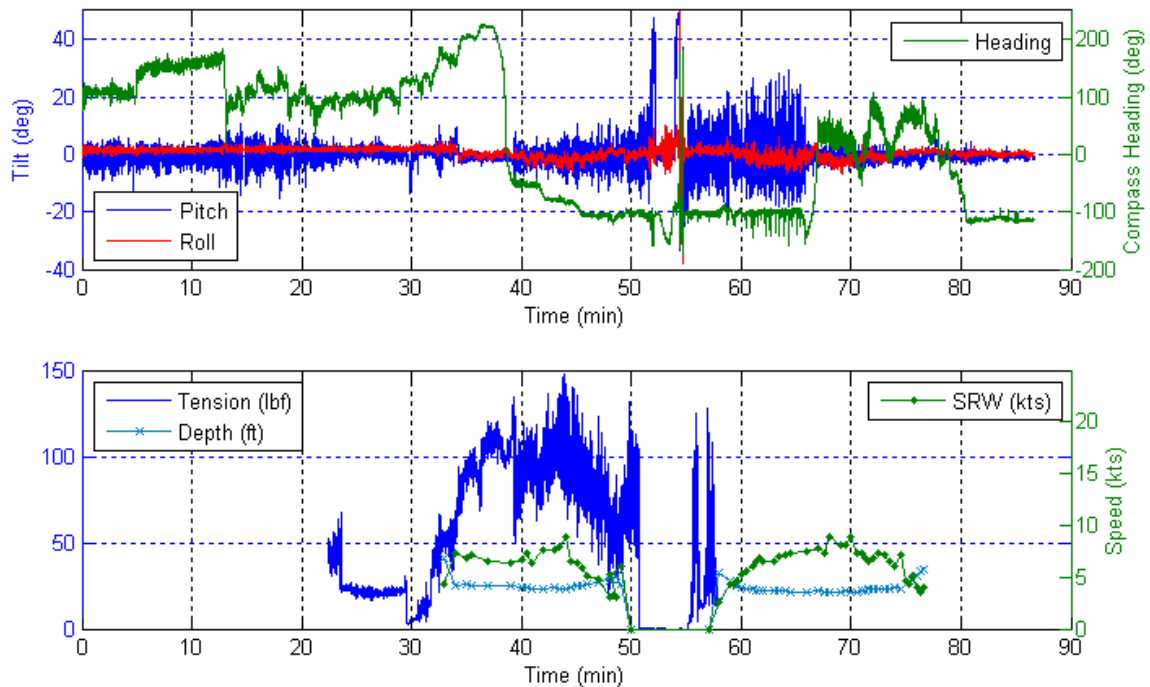


Figure 6.4.1 Observations after free tow from R/V Gulf Challenger

Figure 6.4.1 shows that as the vessel began to change course after $t = 30$ minutes and the speed through water increased. As a result, the towfish's cable tension increased and its depth decreased. A similar trend occurred after $t = 65$ minutes, although the load cell data stopped due to software failure. The observations show that when the vessel changed direction in a field of surface waves the magnitude and frequency at which the vessel exerted tension on the tow cable changed. These changes in tension, in turn, particularly influenced the towfish

pitch and to a much lesser extent towfish roll. The towfish roll was more a characteristic of the vessel turning rather than the vessel heading relative to the field of surface waves.

CHAPTER 7

MATHEMATICAL MODELING AND SIMULATION

7.1 Modeling the Plant

Dominant characteristics of the tow vehicle motion were incorporated into a mathematical model that was developed based on first principles. Although more complex models exist, the test tank facilities at UNH are currently not adequate for model parameter characterization (i.e. hydrodynamic coefficients, torque on the vehicle from the tow cable, etc). A robust controller can accommodate for model errors while meeting the stabilization performance criteria.

The following equation of motion, developed from Newton's laws, was used to describe the dominant characteristics of the plant.

$$T = J\ddot{\theta} + b\dot{\theta} + k\theta$$

Equation 7.1.1

Where T is the resultant torque from the combined drag force acting as a righting moment that keeps the vehicle parallel to the flow, the torque from the static ballast condition of the vehicle, and the lift force (normal to the flow) input torque from the control surfaces. Here J is the moment of inertia, b is a damping constant, k is a spring constant,

and θ describes the rotation of the vehicle relative to vertical.

Tank testing in Chapter 5 showed that at higher tow speeds the effect of viscous damping was much greater than the effect of the inertia. That observation allowed second-order oscillating effects to be neglected. Thus, Equation 7.1.1 was simplified to the following

$$T = b\dot{\theta} + k\theta . \quad \text{Equation 7.1.2}$$

At a constant tow speed, it was assumed that the static ballast and righting moment from the static components in the towfish do not vary and the lift force input torque is proportional to the pitch or roll elevator configuration. The transfer function is as follows:

$$\frac{\theta(s)}{X(s)} = \frac{K_{ss}}{\tau s + 1} \quad \text{Equation 7.1.3}$$

Where $\theta(s)$ is the output vehicle pitch or roll in degrees, $X(s)$ is the plant input elevator position pitch or roll configuration in steps, K_{ss} is the steady state gain in deg/step and τ is the time constant in seconds.

7.1.1 Simulating the Plant

The transfer function in Equation 7.1.3 was applied to pitch and programmed into a Matlab™ Simulink workspace as shown in Figure 7.1.1.

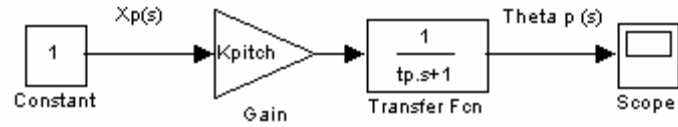


Figure 7.1.1: Plant model of pitch in Simulink™ workspace.

The simulation was run with K_{pitch} and τ_p extracted from Table 5.3.1 and is compared to tank testing results in Figure 7.1.2.

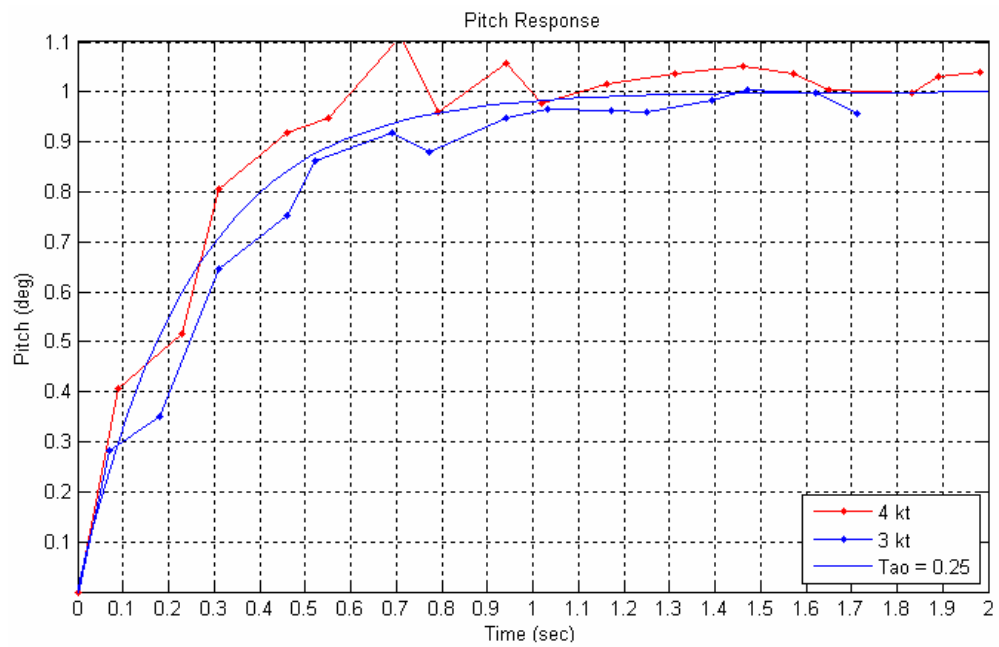


Figure 7.1.2: Pitch step response simulation results as compared to 3 and 4 knot tow tank test data.

Similarly, the SimulinkTM model for roll is shown in Figure 7.1.3.

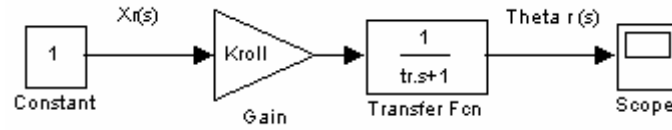


Figure 7.1.3: Plant model of roll in SimulinkTM workspace.

The simulation was run with K_{roll} and τ_r extracted from Table 5.3.1 and is compared to tank testing results in Figure 7.1.4.

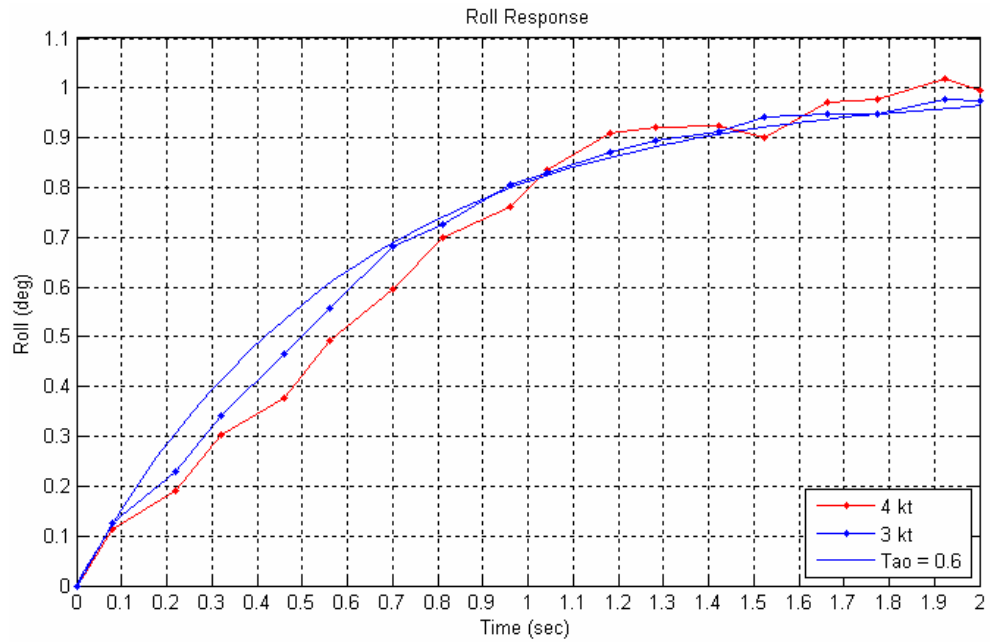


Figure 7.1.4: Roll step response simulation results as compared to 3 and 4 knot tow tank test data.

7.1.2 Coupling Pitch and Roll

Steady state coupling, as described in Section 5.3 of this document, was applied to the Simulink™ model in Figure 7.1.5.

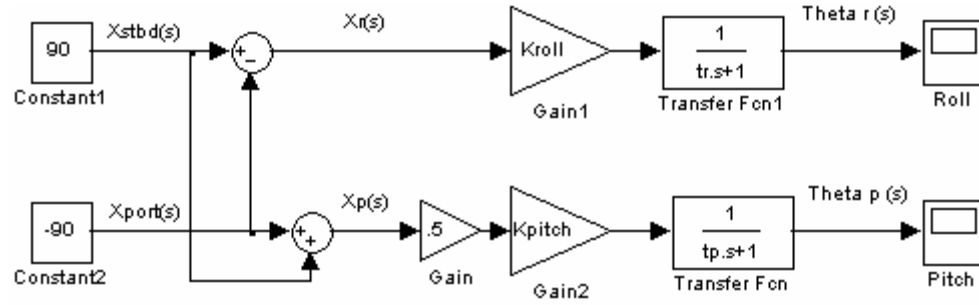


Figure 7.1.5: Coupled model of the plant in Simulink™ workspace.

The model shows that the elevator roll configuration, $X_r(s)$, is the difference between the starboard and port elevator positions and the elevator pitch configuration, $X_p(s)$, is the sum of the starboard and port positions, divided by two.

7.2 Modeling the Motors

The common equations of motion (Franklin, Powell, and Enami-Naeini) used for a DC motor are the following

$$K_t i_a = J\ddot{\theta} + b\dot{\theta} \quad \text{Equation 7.2.1}$$

Where

$$T = K_t i_a \quad \text{Equation 7.2.2}$$

T is the applied torque on the rotor that is proportional to the armature current, J is the rotor's moment of inertia, and b is a viscous friction coefficient. After taking the Laplace Transform, combining the above equations, and neglecting the effect of inductance results to the following equation.

$$\frac{\Theta(s)}{V_a(s)} = \frac{K}{s(\tau s + 1)} \quad \text{Equation 7.2.3}$$

where

$$K = \frac{K_t}{bR_a + K_t K_e} \quad \text{Equation 7.2.4}$$

$$\tau = \frac{R_a J}{bR_a + K_t K_e}$$

Here K_t is the torque constant, K_e is the electric constant, and R_a is the resistance in the armature circuit. These values, however, do not need to be defined because both K and τ were experimentally determined.

7.2.1 Simulating the Motors

The transfer function in Equation 7.2.3 was put into a Matlab™ Simulink workspace as shown in Figure 7.2.1.

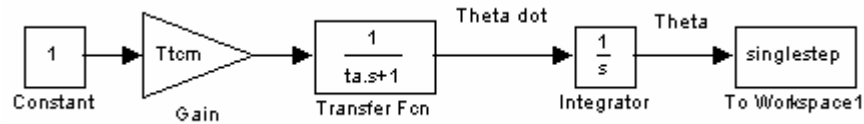


Figure 7.2.1: Stepper motor model in Simulink™ workspace.

The simulation was run with T_{cm} at the 8 Hz sampling frequency of the TCM™ 2.5 and τ_a extracted from the slope of the single step, dual motor excitation data series and is compared to lab testing results in Figure 7.2.2.

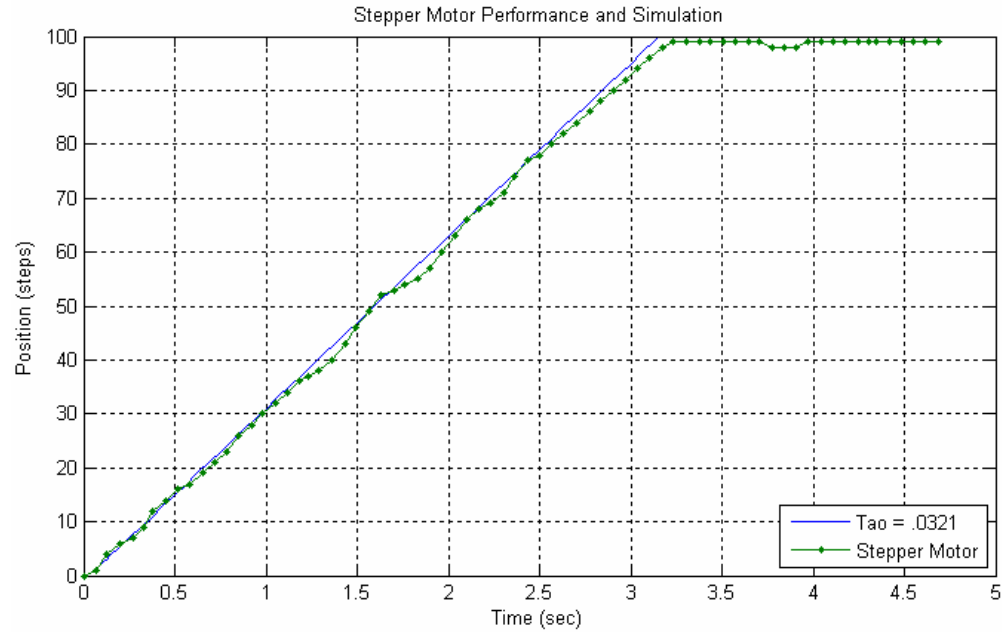


Figure 7.2.2: Comparison of simulation and stepper motor performance after 100 single-step commands.

7.2.2 Adding the Motors into the System Model

Figure 7.1.5 showed the coupled model of the plant with a single input of the position of the starboard elevator and separate input for the position of the port elevator. The model for the stepper motors was added into the system model of the plant by connecting the output of each stepper motor model to the $X_{\text{stbd}}(s)$ and $X_{\text{port}}(s)$ inputs. This is shown in Figure 7.2.3.

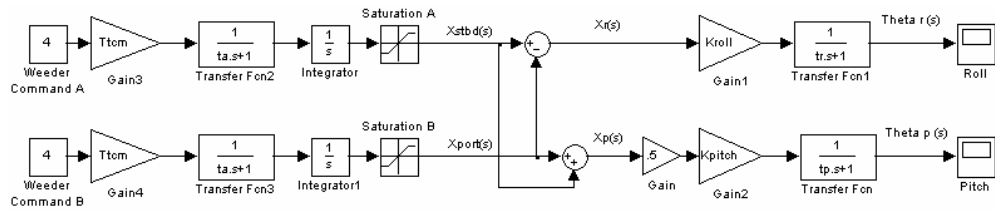


Figure 7.2.3: System model including motor control.

Saturation limits of +330 steps to -330 steps were added to the model to account for the physical limitations of the tail that stop the elevators from moving past these positions and are referred to as the “range of control”.

CHAPTER 8

CONTROLLER DESIGN

8.1 **Feedback and Decoupling**

The final Simulink™ model developed in Chapter 7 were modified for feedback control by placing two negative feedback loops from the pitch and roll outputs and connecting them into the stepper motor Command A and Command B inputs. A zero-order-hold was added to each feedback path in order to simulate the 8 Hz sampling frequency of the TCM™ 2.5 tilt sensor.

In addition, steady state decoupling was accommodated for in the command input. This is to ensure that if towfish roll is desired, a roll command can be sent through the Weeder™ boards so that no towfish pitch results, and vice versa. Decoupling was applied to the system model. The towfish system is displayed in terms of path gains (Fussell 2005), as shown in Figure 8.1.1.

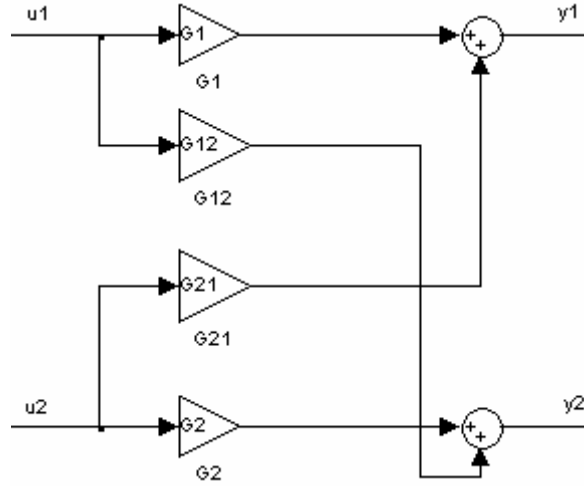


Figure 8.1.1: System coupling in terms of path gains.

The gain G_1 is the product of all the system gains in the path from the first input u_1 to the first output y_1 . The gain G_{21} is the product of gains from u_2 to y_1 . The gain G_{12} is the product of gains from u_1 to y_2 . The gain G_2 is the product of gains from u_2 to y_2 . Equation 8.1.1 shows the system gains are organized into a matrix \mathbf{T} .

$$\mathbf{y} = \mathbf{T}\mathbf{u}$$

where

$$\mathbf{T} = \begin{bmatrix} G_1 & G_{21} \\ G_{12} & G_2 \end{bmatrix}$$

Equation 8.1.1

$$\mathbf{y} = \begin{bmatrix} y_1 \\ y_2 \end{bmatrix}$$

$$\mathbf{u} = \begin{bmatrix} u_1 \\ u_2 \end{bmatrix}$$

The equation was solved for the system inputs u_1 and u_2 and is shown as follows,

$$\mathbf{u} = \mathbf{T}^{-1} \mathbf{y} .$$

Equation 8.1.2

The towfish system path gains are:

$$\begin{aligned} G_1 &= T_{tcm} \cdot K_{roll} \\ G_2 &= \frac{T_{tcm} \cdot K_{pitch}}{2} \\ G_{12} &= \frac{T_{tcm} \cdot K_{pitch}}{2} \\ G_{21} &= -T_{tcm} \cdot K_{roll} \end{aligned} .$$

Equation 8.1.3

Solving for \mathbf{T}^{-1} gives the following

$$\mathbf{T}^{-1} = \begin{bmatrix} \frac{1}{2 \cdot T_{tcm} \cdot K_{roll}} & \frac{1}{T_{tcm} \cdot K_{pitch}} \\ -\frac{1}{2 \cdot T_{tcm} \cdot K_{roll}} & \frac{1}{T_{tcm} \cdot K_{pitch}} \end{bmatrix} .$$

Equation 8.1.4

For simulation, the \mathbf{T}^{-1} matrix was incorporated into a state-space block that was placed ahead of the system model developed in Chapter 7. For this state-space block, local parameters were defined as such:

$$\begin{aligned} \dot{x} &= \mathbf{A}x + \mathbf{B}u \\ y &= \mathbf{C}x + \mathbf{D}u \end{aligned}$$

Equation 8.1.5

where,

$$\begin{aligned}
\mathbf{A} &= [0] \\
\mathbf{B} &= [0 \quad 0] \\
\mathbf{C} &= \begin{bmatrix} 0 \\ 0 \end{bmatrix} \\
\mathbf{D} &= \begin{bmatrix} \frac{1}{2 \cdot T_{tcm} \cdot K_{roll}} & \frac{1}{T_{tcm} \cdot K_{pitch}} \\ -\frac{1}{2 \cdot T_{tcm} \cdot K_{roll}} & \frac{1}{T_{tcm} \cdot K_{pitch}} \end{bmatrix}
\end{aligned}
\tag{Equation 8.1.6}$$

which gave the equations:

$$\begin{aligned}
y_1 &= \frac{1}{2 \cdot T_{tcm} \cdot K_{roll}} \cdot u_1 + \frac{1}{T_{tcm} \cdot K_{pitch}} \cdot u_2 \\
y_2 &= -\frac{1}{2 \cdot T_{tcm} \cdot K_{roll}} \cdot u_1 + \frac{1}{T_{tcm} \cdot K_{pitch}} \cdot u_2
\end{aligned}
\tag{Equation 8.1.7}$$

Again, input and output variables shown in Equation 8.1.7 are defined locally for the state-space De-Coupler block in the Matlab SimulinkTM workspace. The addition of this block to the system model is shown in Figure 8.1.2.

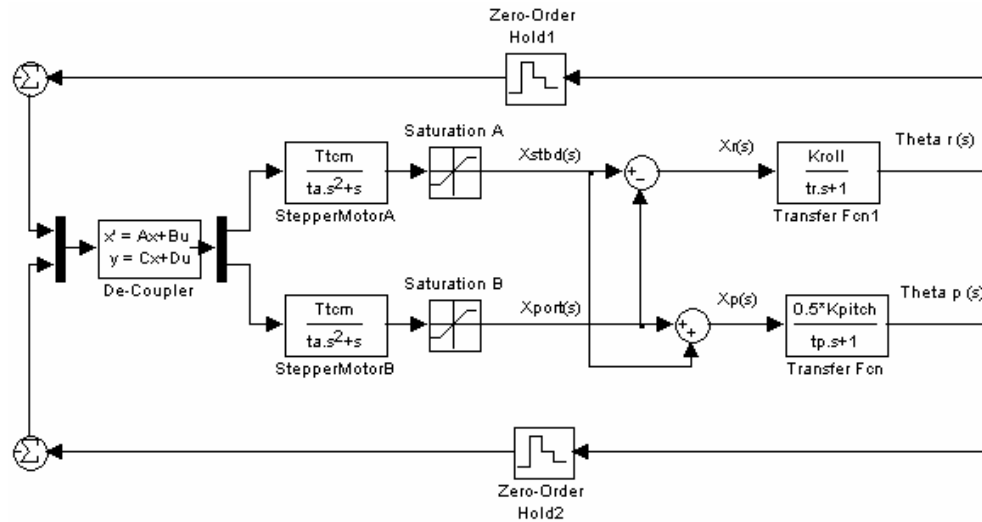


Figure 8.1.2: Decoupled system model with negative feedback.

A simple check was made with the new model to see if the towfish stabilizes after it is given an initial condition in pitch and in roll. The simulation was also used to see if the De-Coupler works effectively. The simulation was run and the results are plotted in Figure 8.1.3 and Figure 8.1.4. The elevator positions are shown on the left and the towfish's response on the right.

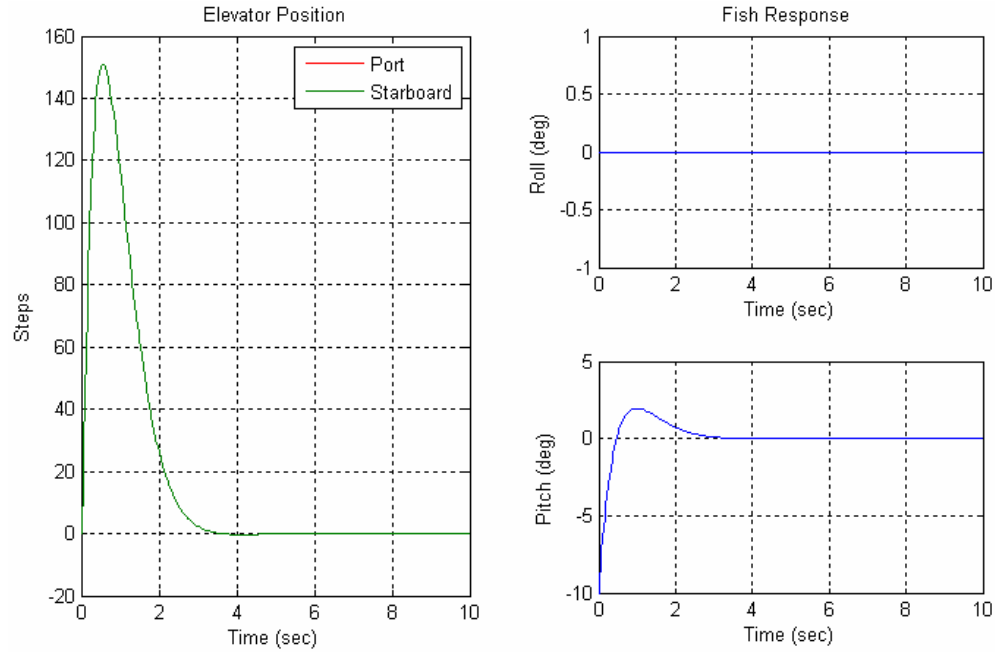


Figure 8.1.3: Decoupled system response with -10 degree pitch initial condition.

The simulation in Figure 8.1.3 shows that the towfish settled within 4 seconds after an initial condition of -10 degrees in pitch. Zero roll resulted from the pitch command input. Although the addition of the De-Coupler was not the complete controller implemented in the Smart Tail, the time required for the towfish to settle in the simulation leads one to expect that the towfish should be readily controlled for low frequency pitch disturbances.

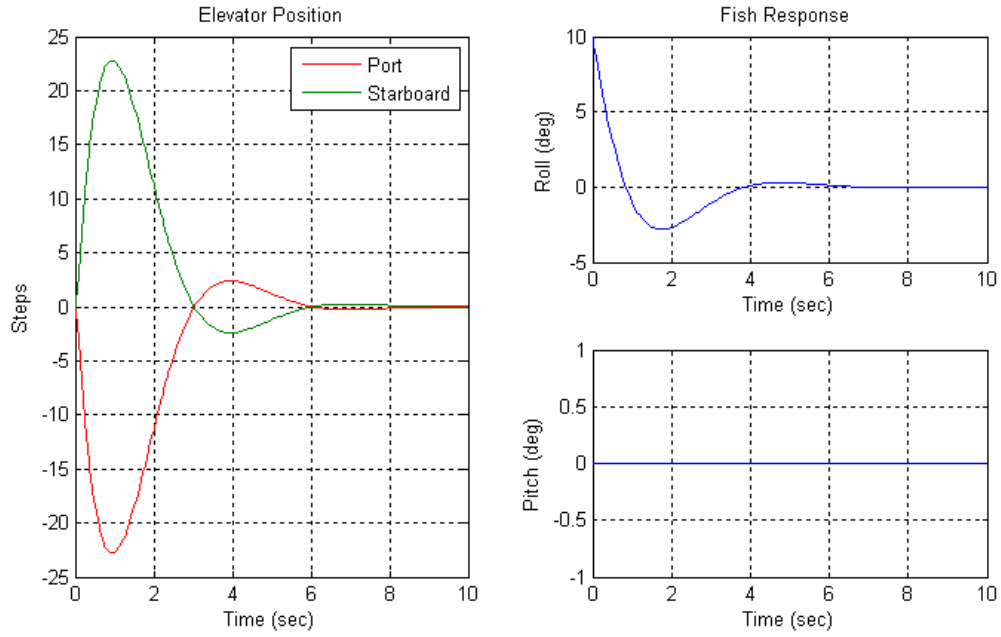


Figure 8.1.4: Decoupled system response with 10 degree roll initial condition.

The simulation in Figure 8.1.4 shows that the towfish settled within 6 seconds after an initial condition of 10 degrees in roll. Zero pitch resulted from roll command input. Although the addition of the De-Coupler was not the complete controller implemented in the Smart Tail, the time required for the towfish to settle in the simulation leads one to expect that the towfish should be readily controlled for low frequency roll disturbances.

8.2 Controller Type

For simplified models, a robust controller is needed to maintain adequate stability margins and performance levels in the presence of model errors (Brogan 1991). Proportional, Integral, Derivative (PID) controllers can be tuned to give suitable performance based exclusively on the knowledge of dominant system time constants. Therefore, this type of controller was considered. A PID Controller (with approximate derivative) block was placed in

the feedback paths of the system model in the Simulink™ workspace. A method was devised to tune the controller's proportional, integral, and derivative feedback gains: K_p , K_i , and K_d .

The integral gain, K_i , was set to zero for both the pitch and roll due to the presence of a free integrator in the model. Thus, the controller is a PD controller. In order to tune K_p and K_d for the multiple-input, multiple-output (MIMO) system, the model was broken up into two single-input, single-output (SISO) systems, one for pitch and the other for roll.

The characteristic equation for each SISO was derived and then discretized. The root locus vs. K_p was plotted in the z-plane to find the critical gain. Similar to the Ziegler-Nichols tuning rules for PID controllers (Ogata 2004), the value of K_p was set to half the critical value, and the characteristic equation was then rearranged to plot the root locus vs. K_d . A value of K_d was chosen where the damping ratio was at the (industry defined) desirable value of 0.707.

8.3 Pitch as a Single-input, Single-output System

The system model was transformed to a SISO system by isolating pitch as the output and designating the input to be, u_2 , in front of the De-Coupler. This is shown in Figure 8.3.1.

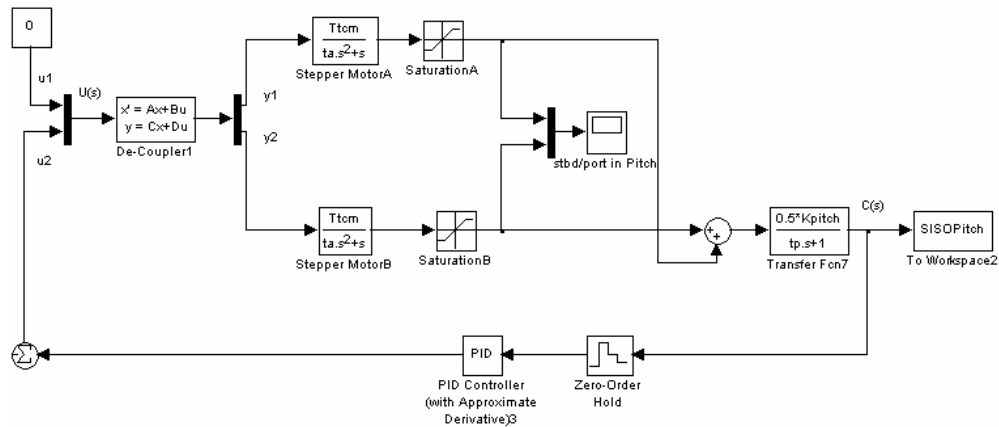


Figure 8.3.1: SISO pitch system model.

For the SISO pitch model, the roll input u_1 was set to zero and the equations of the de-coupler became:

$$\begin{aligned} y_1 &= \frac{1}{T_{tcm} \cdot K_{pitch}} \cdot u_2 \\ y_2 &= \frac{1}{T_{tcm} \cdot K_{pitch}} \cdot u_2 \end{aligned} \quad \text{Equation 8.3.1}$$

The continuous time open loop transfer function of the block diagram in Figure 8.3.1 was reduced to:

$$\begin{aligned} \frac{C(s)}{U(s)} &= \left[\left(\frac{1}{T_{tcm} \cdot K_{pitch}} \cdot \frac{T_{tcm}}{t_a s^2 + s} \right) + \left(\frac{1}{T_{tcm} \cdot K_{pitch}} \cdot \frac{T_{tcm}}{t_a s^2 + s} \right) \right] \cdot \left(\frac{K_{pitch}}{2 \cdot (t_p s + 1)} \right) \cdot (K_{d_pitch} s + K_{p_pitch}) \\ &= \frac{K_{d_pitch} s + K_{p_pitch}}{t_a t_p s^3 + (t_a + t_p) s^2 + s} \end{aligned} \quad \text{Equation 8.3.2}$$

Since the root locus was plotted with Matlab™, the characteristic equation needs to take the form

$$0 = 1 + K \frac{num}{den}$$

where *num* is the numerator polynomial and *den* is the denominator polynomial (Ogata 2004).

With the PD controller added, the characteristic equation of the closed-loop transfer function was the following,

$$0 = 1 + K_{p_pitch} \frac{1}{(t_a \cdot t_p)s^3 + (t_a + t_p)s^2 + (1 + K_{d_pitch})s} . \quad \text{Equation 8.3.3}$$

K_{d_pitch} was set to zero in order to investigate the effects of proportional feedback gain on the system dynamics. The following open-loop transfer function entered into MatlabTM was,

$$\frac{num(s)}{den(s)} = \frac{1}{(t_a \cdot t_p)s^3 + (t_a + t_p)s^2 + s} . \quad \text{Equation 8.3.4}$$

Values for t_a and t_p were plugged in to Equation 8.3.4 and the discrete equation was generated (by the MatlabTM function *c2d*) with the zero-order-hold method and a sampling period of 0.125 seconds.

$$\frac{num(z)}{den(z)} = \frac{.01677z^2 + .02935z + .002056}{z^3 - 1.627z^2 + 0.6392z - .01235} \quad \text{Equation 8.3.5}$$

This was used to generate the root locus vs. K_{p_pitch} plot shown in Figure 8.3.2 and the Bode diagram in Figure 8.3.3.

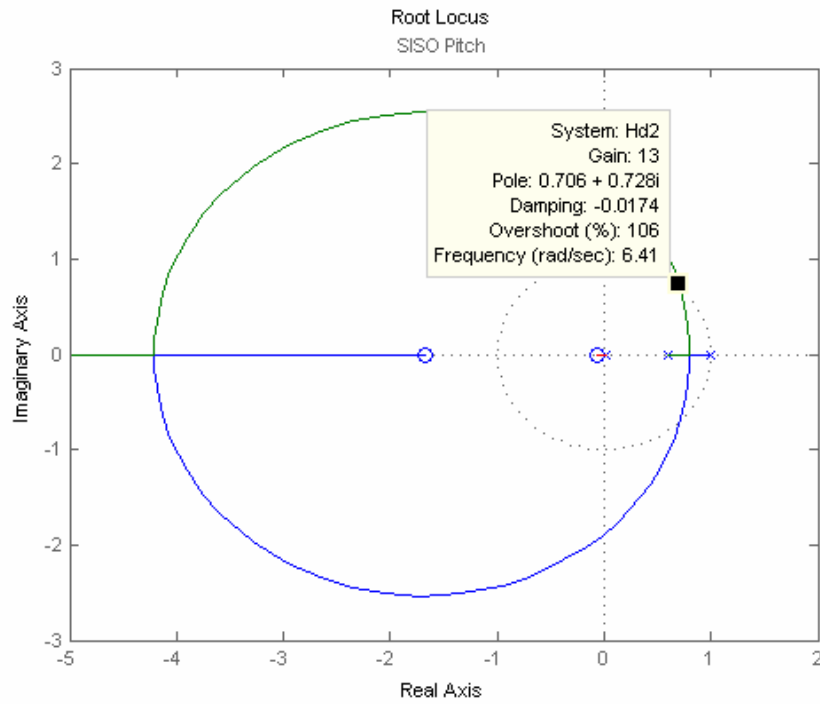


Figure 8.3.2: Root Locus vs. K_{p_pitch} in the z-plane for the SISO pitch model.

The data-tip in Figure 8.3.2 shows that the critical period is 6.41 rad/sec (≈ 1 Hz) and the critical gain is 13.

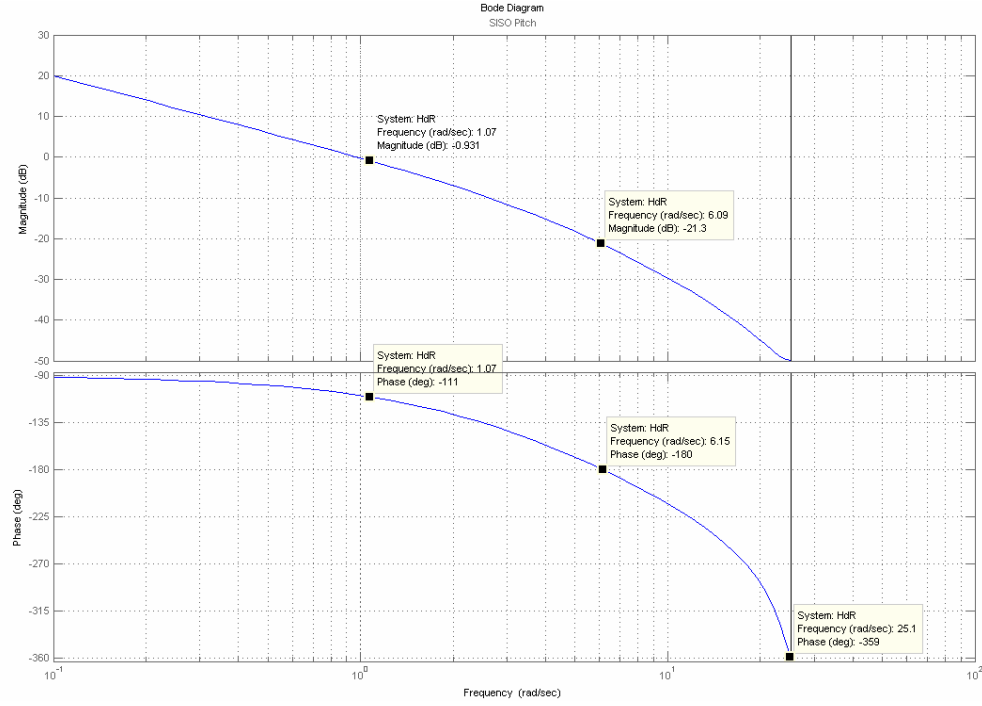


Figure 8.3.3: Bode plot for the K_{p_pitch} in the SISO pitch model with K_{d_pitch} set to zero.

The Bode diagram in Figure 8.3.3 shows the system to have -180 degrees to -360 degrees of phase in frequencies from approximately 6 rad/sec to 25 rad/sec (≈ 1 Hz to 4 Hz). This suggests that, at the very best, the towfish can only be stable for disturbance periods larger than 1 second. The proportional feedback gain and phase margins are both positive at values equal to 21.3 dB and 69 degrees, respectively.

To look at the root locus vs. K_{d_pitch} , Equation 8.3.3 was rearranged as follows,

$$0 = 1 + K_{d_pitch} \frac{s}{(t_a \cdot t_p)s^3 + (t_a + t_p)s^2 + s + K_{p_pitch}}. \quad \text{Equation 8.3.6}$$

After descretizing, the characteristic equation is

$$\frac{C(z)}{U(z)} = \frac{0.3z^2 - 0.2199z - .08007}{z^3 - 1.38z^2 + 0.7036z - .01235} \quad \text{Equation 8.3.7}$$

K_{p_pitch} was set to half of the critical value extracted from the plot in Figure 8.3.2. The root locus vs. K_{d_pitch} plot and Bode diagram generated from Equation 8.3.7 are shown in Figure 8.3.4 and Figure 8.3.5, respectively.

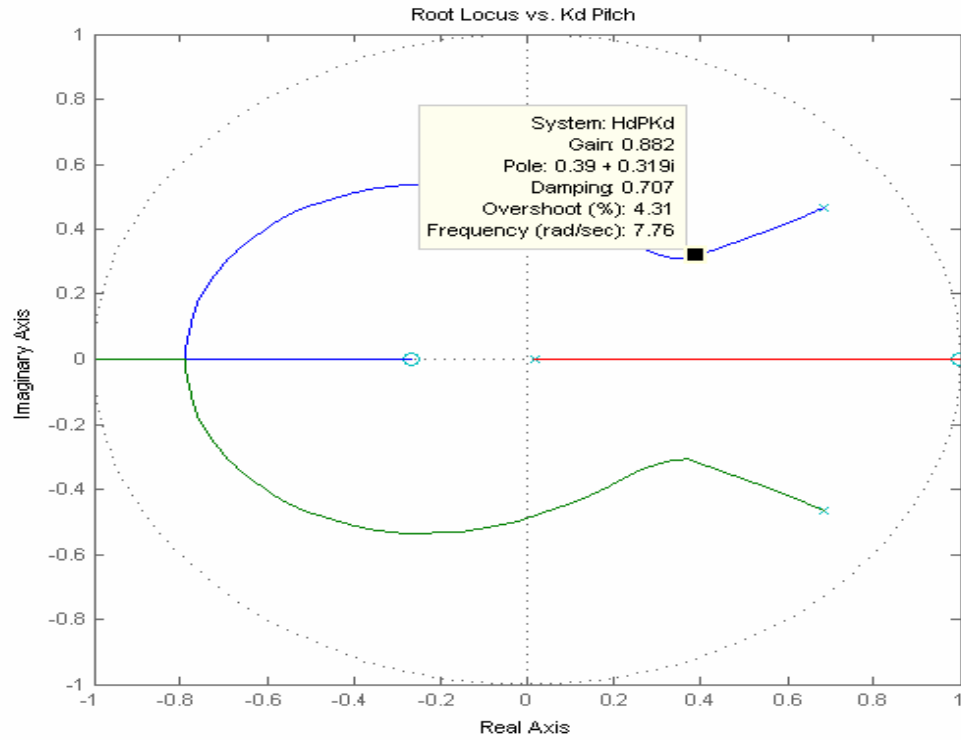


Figure 8.3.4: Root Locus vs. K_{d_pitch} in z-plane of SISO pitch model with K_{p_pitch} set to half of the critical proportional feedback gain.

The data-tip in Figure 8.3.4 shows that when K_{d_pitch} is 0.808 the system has a damping ratio of 0.707.

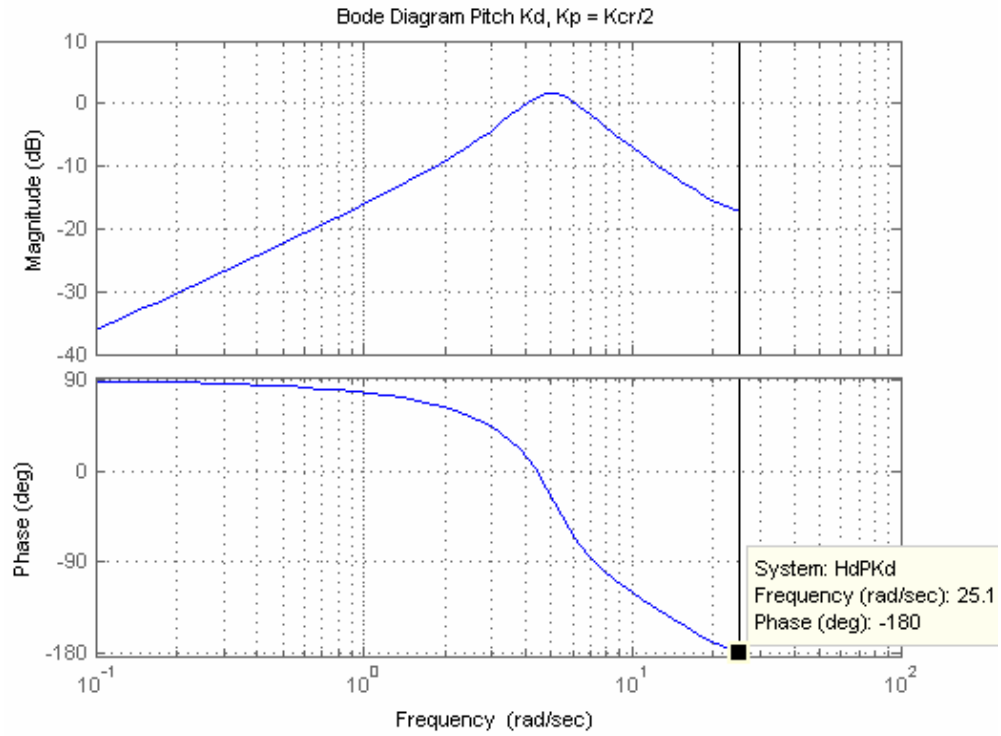


Figure 8.3.5: Bode Diagram for K_d _pitch of the SISO pitch model with K_p _pitch set to half of the critical proportional feedback gain.

The Bode diagram in Figure 8.3.5 shows that for all frequencies less than 25 rad/sec (≈ 4 Hz) the frequency response has less than 180 degrees of phase. The system phase margin has improved to approximately 120 degrees at the expense of the gain margin, which has decreased to approximately 17 dB.

8.4 Roll as a Single-input, Single-output System

The system model was transformed to another SISO system by isolating roll as the output and designating the input to be, u_1 , in front of the De-Coupler. This is shown in Figure 8.4.1.

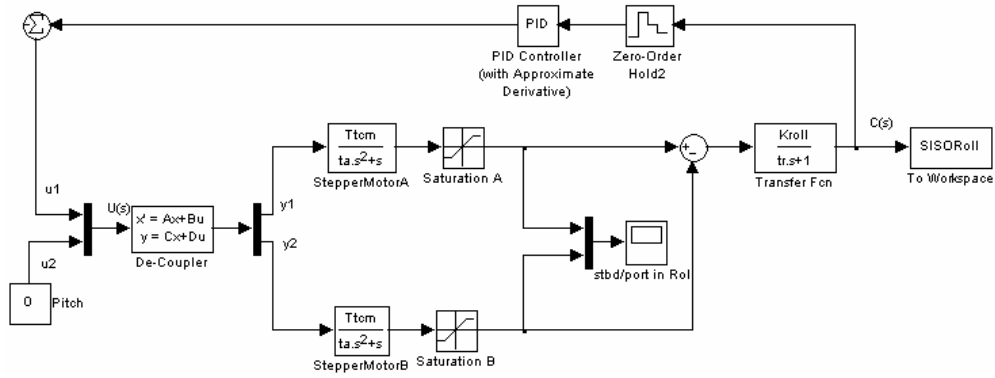


Figure 8.4.1: SISO roll system model.

For the SISO roll model, the pitch input u_2 was set to zero and the equations of the de-coupler became:

$$\begin{aligned} y_1 &= \frac{1}{2 \cdot T_{tcm} \cdot K_{roll}} \cdot u_1 \\ y_2 &= -\frac{1}{2 \cdot T_{tcm} \cdot K_{roll}} \cdot u_1 \end{aligned} \quad \text{Equation 8.4.1}$$

The continuous time open loop transfer function of the block diagram in Figure 8.4.1 was reduced to:

$$\frac{C(s)}{U(s)} = \left[\left(\frac{1}{2 \cdot T_{tcm} \cdot K_{roll}} \cdot \frac{T_{tcm}}{t_a s^2 + s} \right) - \left(-\frac{1}{2 \cdot T_{tcm} \cdot K_{roll}} \cdot \frac{T_{tcm}}{t_a s^2 + s} \right) \right] \cdot \left(\frac{K_{roll}}{t_r s + 1} \right) \cdot (K_{d_roll} s + K_p)$$

$$= \frac{K_{d_roll}s + K_p}{t_a t_r s^3 + (t_a + t_r)s^2 + s} \quad \text{Equation 8.4.2}$$

The characteristic equation for the closed-loop transfer function takes the form:

$$0 = 1 + K_{p_roll} \frac{1}{(t_a \cdot t_r)s^3 + (t_a + t_r)s^2 + (1 + K_{d_roll})s} \quad \text{Equation 8.4.3}$$

Analogous to the pitch SISO, the derivative feedback gain K_{d_roll} was set to zero as follows,

$$\frac{num(s)}{den(s)} = \frac{1}{(t_a \cdot t_r)s^3 + (t_a + t_r)s^2 + s} \cdot \frac{1 - e^{-Ts}}{s} \quad \text{Equation 8.4.4}$$

and then discretized to the form

$$\frac{num(z)}{den(z)} = \frac{.007561z^2 + .01439z + .001082}{z^3 - 1.832z^2 + 0.8488z - .01653} \quad \text{Equation 8.4.5}$$

This equation was used to generate the root locus vs. K_{p_roll} plot shown in Figure 8.4.2 and the Bode diagram in Figure 8.4.3.

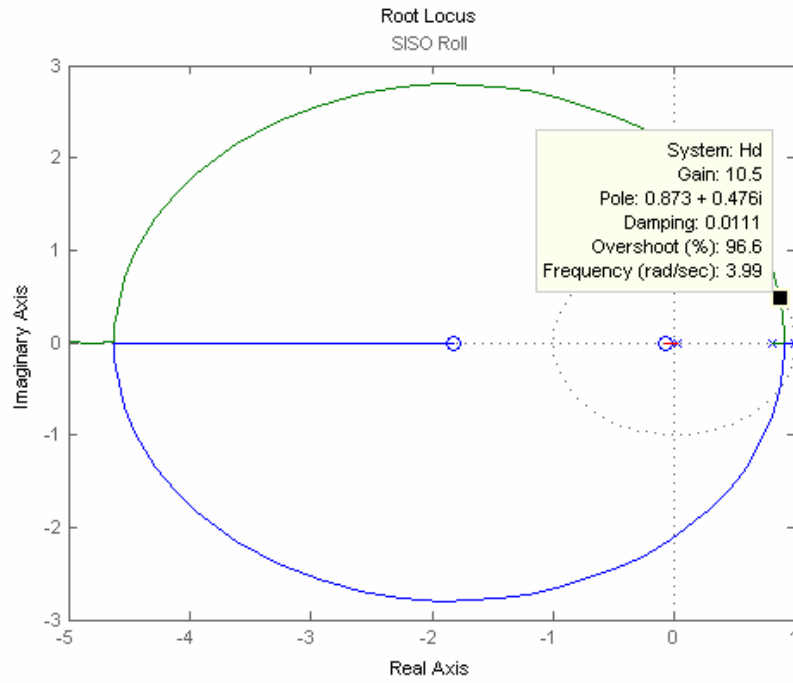


Figure 8.4.2: Root Locus vs. K_{p_roll} in z-plane of SISO roll model with K_{d_roll} set to zero.

The data-tip in Figure 8.4.2 shows that the critical period is 3.99 rad/sec (≈ 0.64 Hz) and the critical gain is 10.5.

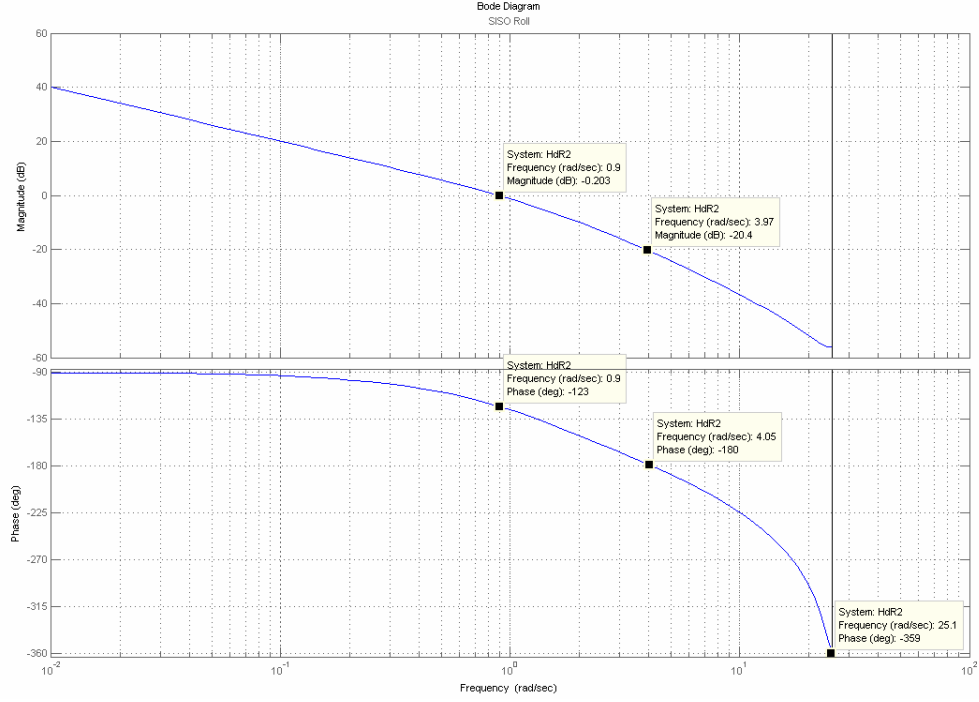


Figure 8.4.3: Bode plot for K_{p_roll} in the SISO roll model with K_{d_roll} set to zero.

The Bode plot in Figure 8.4.3 shows the system to have -180 degrees to -360 degrees of phase in frequencies from approximately 4 rad/sec to 25 rad/sec, (≈ 0.64 Hz to 4 Hz). This suggests that, at the very best, the towfish can only be stable in roll for disturbance periods longer than 1.5 seconds. The system gain and phase margins are both positive at values equal to 20.4 dB and 57 degrees, respectively.

To look at the root locus vs. K_{d_roll} , Equation 8.4.3 was rearranged as follows,

$$0 = 1 + K_{d_roll} \frac{s}{(t_a \cdot t_r)s^3 + (t_a + t_r)s^2 + s + K_{p_roll}}. \quad \text{Equation 8.4.6}$$

After discretizing, the characteristic equation is

$$\frac{C(z)}{U(z)} = \frac{0.1422z^2 - 0.101z - .04121}{z^3 - 1.739z^2 + 0.8758z - .01653} \quad \text{Equation 8.4.7}$$

K_{p_roll} was set to half of the critical value extracted from the plot in Figure 8.4.2. The root locus vs. K_{d_roll} plot and Bode diagram generated from Equation 8.4.7 are shown in Figure 8.4.4 and Figure 8.4.5, respectively.

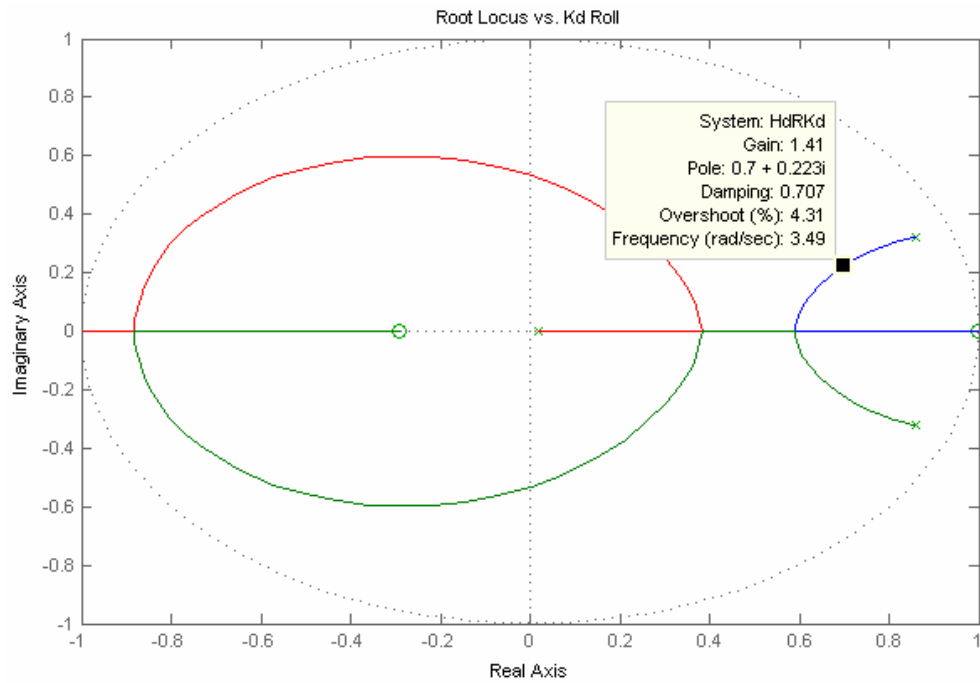


Figure 8.4.4: Root locus vs. K_{d_roll} (in the z-plane) for the SISO roll system with K_{p_roll} set to half critical proportional feedback gain.

The data-tip in Figure 8.3.4 shows that when K_{d_roll} is 1.41 the system has a damping ratio of 0.707.

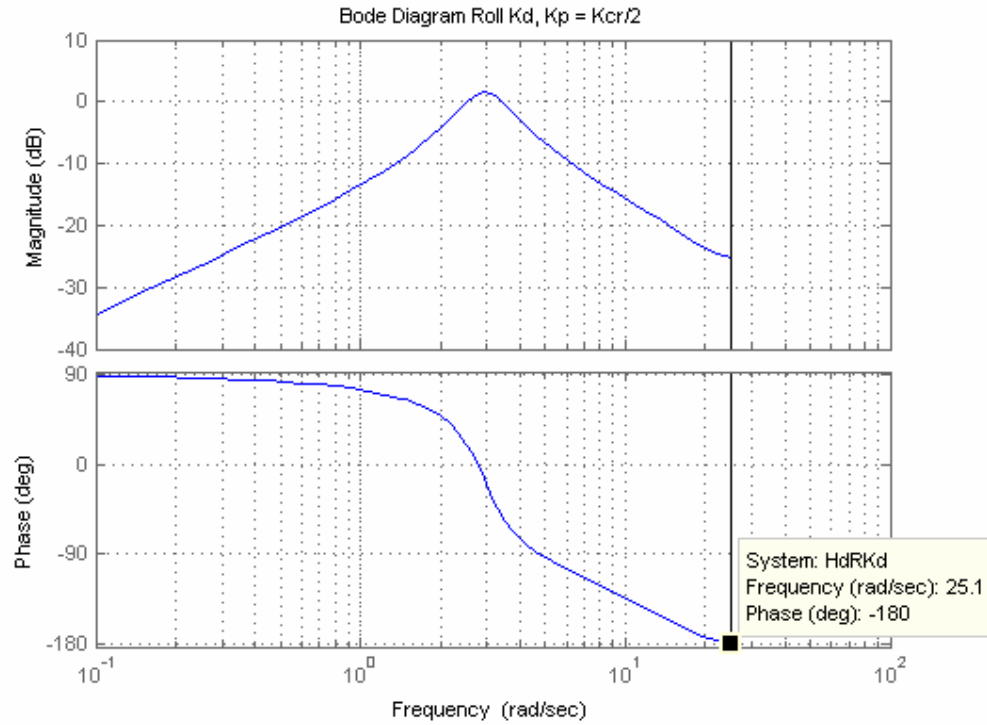


Figure 8.4.5: Bode Diagram for Kd_roll of the SISO roll model with Kp_roll set to half of the critical proportional feedback gain.

Figure 8.4.5 shows that the phase margin has improved by approximately 160 degrees with the addition of derivative feedback and the system is stable for all frequencies less than 25 rad/sec (≈ 4 Hz). The gain margin increased to approximately 25 dB.

8.5 Controller Parameters in the Overall Loop

Two versions of the controller were finalized for field testing. The primary version of interest, Version 1, uses the gains from the controller established from the tuning method as outlined in the previous section. Another version, Version 0, is a modification of the derivative feedback gains. Table 8.5.1 shows the final choice for the Version 1 proportional and derivative feedback gain values.

	Kp V1	Kd V1
Pitch	6.5	0.882
Roll	5.25	1.41

Table 8.5.1: Controller parameters selected for Version 1 (V1) implementation.

These values plugged into Equations 8.3.2 and 8.4.2 give the following respective transfer functions

$$\frac{C(s)}{U(s)} = \frac{0.88s + 6.5}{0.008s^3 + 0.282s^2 + s} \quad \text{Equation 8.5.1}$$

$$\frac{C(z)}{U(z)} = \frac{0.379z^2 - 0.011z - 0.056}{z^3 - 1.627z^2 + 0.639z - 0.012} \quad \text{Equation 8.5.2}$$

for pitch and

$$\frac{C(s)}{U(s)} = \frac{1.41s + 5.25}{0.019s^3 + 0.632s^2 + s} \quad \text{Equation 8.5.3}$$

$$\frac{C(z)}{U(z)} = \frac{0.242z^2 - 0.069z - 0.052}{z^3 - 1.832z^2 + 0.849z - 0.017} \quad \text{Equation 8.5.4}$$

for roll.

The Bode Diagrams for each of these equations can now be plotted for the overall loop gain of pitch and roll.

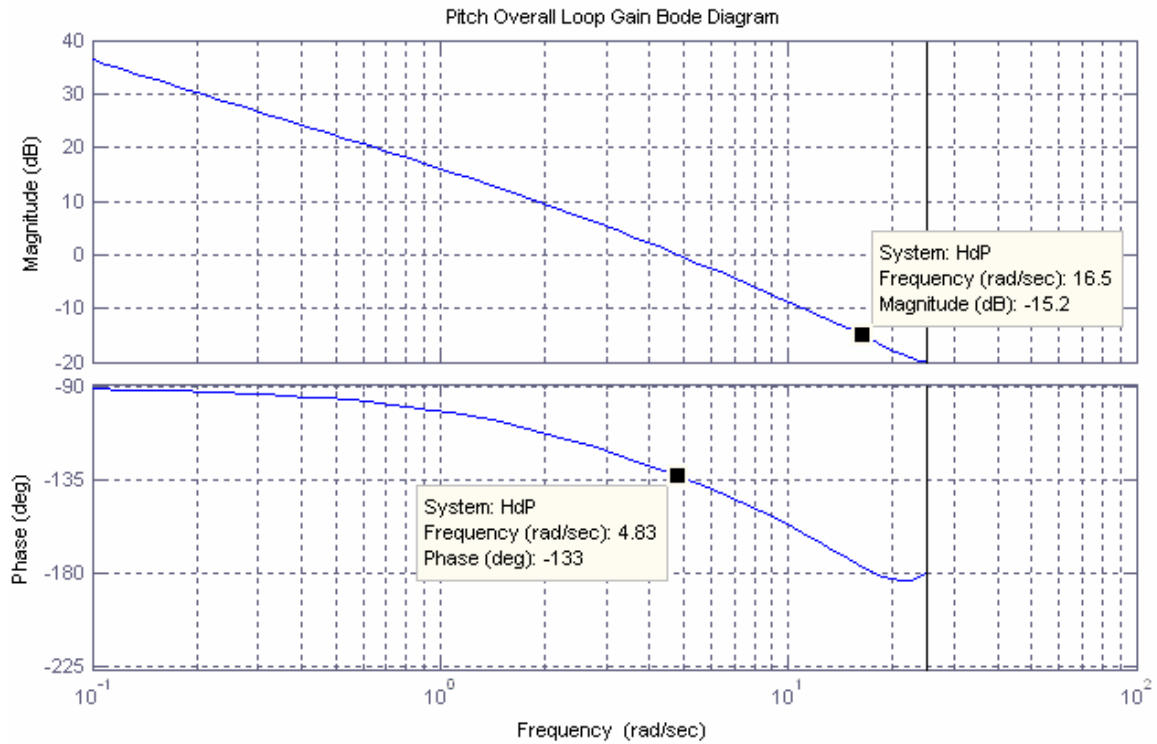


Figure 8.5.1: Bode Diagram for overall loop gain of the SISO pitch Version 1 model.

The overall loop gain Bode Diagram for pitch Version 1 shows approximately 15 dB of gain margin at a frequency of 16.5 radians/second (≈ 2.6 Hz) and 47 degrees of phase margin at a frequency of 4.83 radians/second (≈ 0.77 Hz). Adequate disturbance rejection performance is denoted by the frequency value at the 20 dB magnitude mark. This is the frequency at which the Smart Tail is expected to provide sufficient corrective action to disturbances. The 20 dB mark on the plot above indicates that the Smart Tail with Version 1 control can stabilize disturbance periods greater than 11 seconds in pitch.

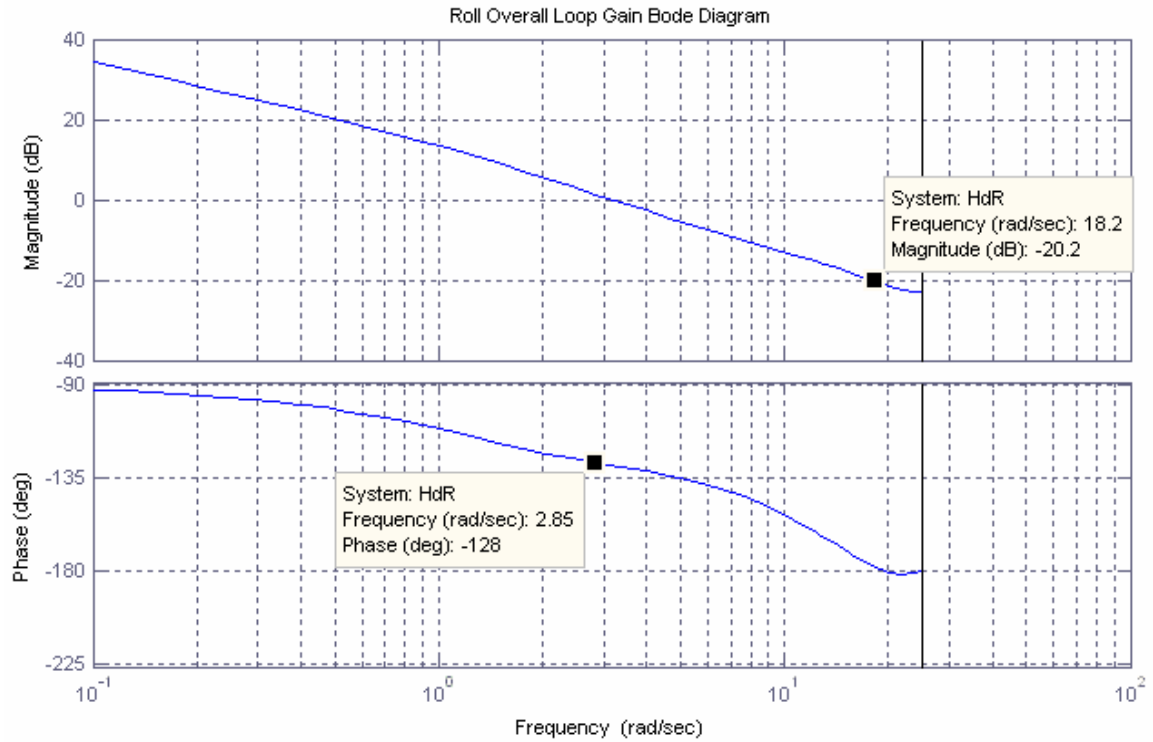


Figure 8.5.2: Bode Diagram for the overall loop gain of the roll Version 1 SISO model.

The overall loop gain Bode Diagram for roll Version 1 shows approximately 20 dB of gain margin at a frequency of 18.2 radians/second (≈ 2.9 Hz) and 52 degrees of phase margin at a frequency of 2.85 radians/sec (≈ 0.45 Hz). The 20 dB mark on the plot above indicates that the Smart Tail with Version 1 control can stabilize disturbance periods greater than 13 seconds in roll.

Controller parameters were adjusted to form Version 0 of the controller. Table 8.5.2 shows the final choice for the Version 0 proportional and derivative feedback gain values.

	Kp V0	Kd V0
Pitch	6.5	0.25
Roll	5.25	0.275

Table 8.5.2: Controller parameters selected for Version 0 (V0) implementation.

The Bode Diagrams for each of these equations can now be plotted for the overall loop gain of pitch and roll.

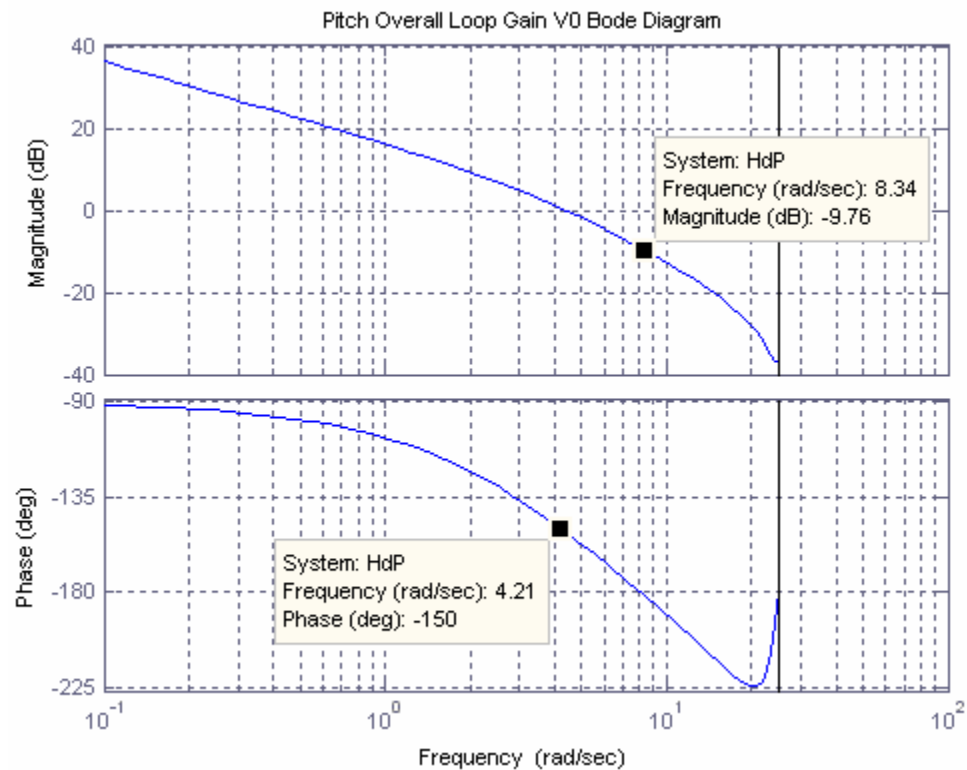


Figure 8.5.3: Bode Diagram for overall loop gain of the SISO pitch Version 0 model.

The overall loop gain Bode Diagram for pitch Version 0 shows approximately 9.8 dB of gain margin at a frequency of 8.4 radians/second (≈ 1.4 Hz) and 30 degrees of phase margin at a frequency of 4.21 radians/second (≈ 0.67 Hz). The 20 dB mark on the plot above indicates

that the Smart Tail with Version 0 control can stabilize disturbance periods greater than 11 seconds in pitch.

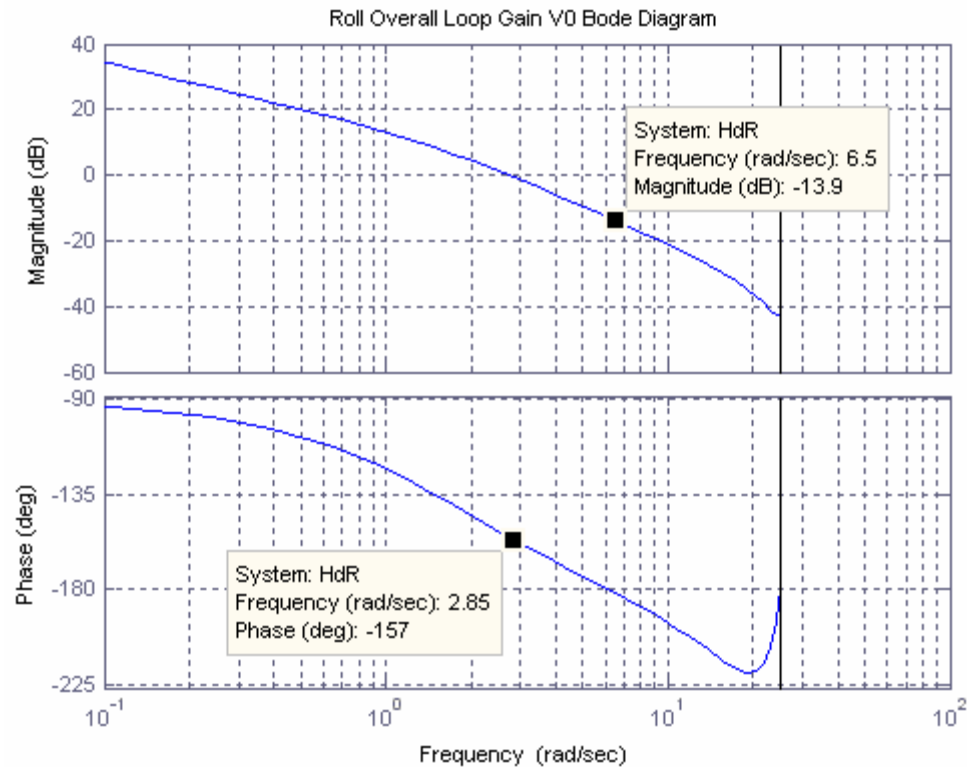


Figure 8.5.4: Bode Diagram for overall loop gain of the SISO pitch Version 0 model.

The overall loop gain Bode Diagram for roll Version 0 shows approximately 14 dB of gain margin at a frequency of 6.5 radians/second (≈ 1.03 Hz) and 23 degrees of phase margin, at a frequency of 2.85 radians/sec (≈ 0.45 Hz). The phase margin for this version is on the small side of the (industry defined) general rule of 30 degrees of phase margin; however, the controller was implemented regardless. The 20 dB mark on the plot above indicates that the Smart Tail with Version 0 control can stabilize disturbance periods greater than 16 seconds in pitch.

8.6 Test Inputs

The parameters from Version 1 of the SISO controller tuning were plugged into the final working MIMO model shown in Figure 8.6.1. A saturation limit of ± 5 steps and a rounding function was added to the De-Coupler block output. This simulates the integer format of the command given to the Weeder™ boards at the maximum rate of 5 steps per communications heartbeat (8 Hz).

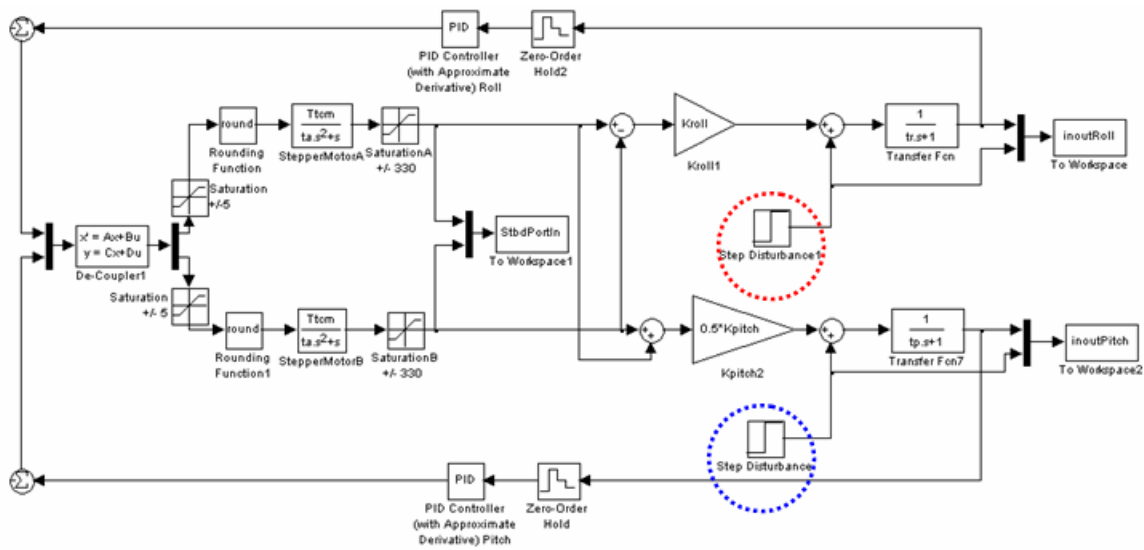


Figure 8.6.1: Multiple-input, multiple-output (MIMO) system model with feedback control. Location of pitch and roll disturbance are indicated by blue and red circles, respectively.

In order to anticipate an infinite variety of possible inputs, the simulation was used to examine how the model reacts to aperiodic and periodic signals (Brogan 1991) with the following test inputs:

1. Step Functions
2. Ramp Functions

3. Sinusoids.

In the simulations, near maximum amplitude and frequency conditions are examined. The method used was to place the disturbance input before the plant in Figure 8.6.1. The elevator corrective action and towfish response was then observed and is presented in the following six figures.

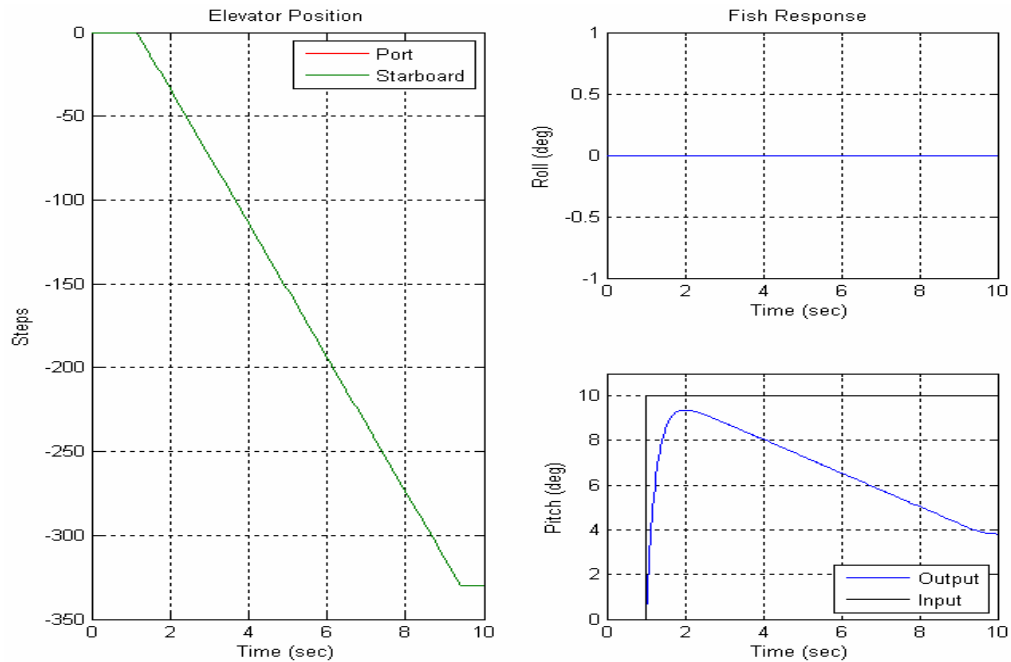


Figure 8.6.2: Simulated system response to a 10 degree pitch step disturbance with PD control.

Figure 8.6.2 shows the system response to a 10 degree pitch step-input, starting at $t = 1$ second. After 10 seconds the towfish was within 4 degrees of horizontal. This simulation implies that the towfish pitch can be stabilized at low frequencies, so long as the corrective elevator action is within the range of control.

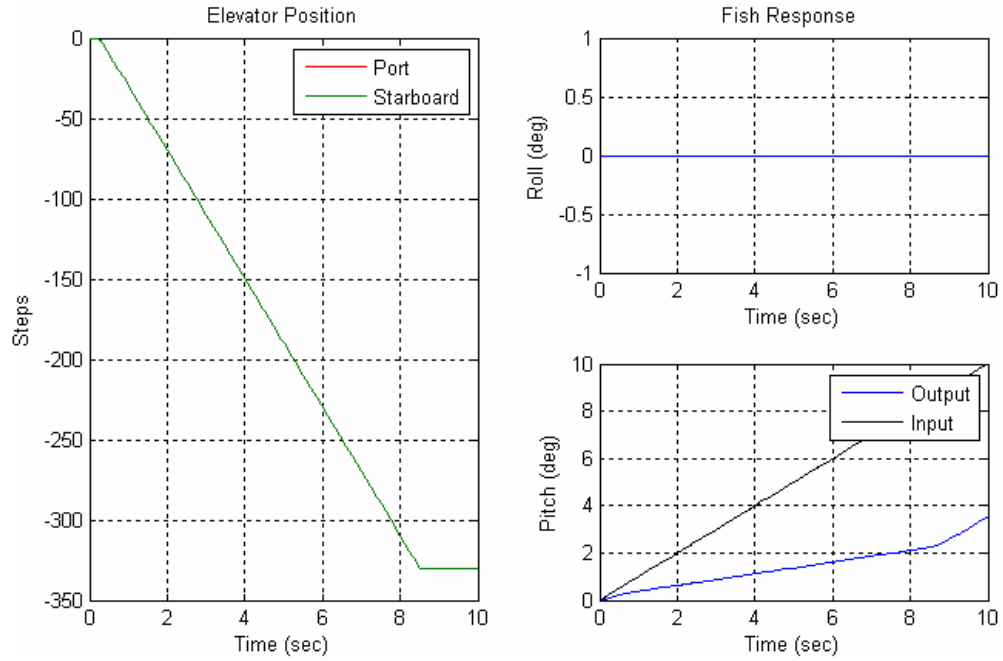


Figure 8.6.3: Simulated system response to a pitch ramp disturbance with PD control.

Figure 8.6.3 shows the system response to a 1 deg/sec pitch ramp-input, starting at $t = 0$ seconds. For the first 10 seconds the towfish remained within 4 degrees of horizontal. This simulation implies that the Smart Tail may have difficulty stabilizing the towfish under a prolonged pitch rate disturbance due to the range of control limits and magnitude of response induced per step of elevator corrective action (i.e. the degrees/step gain found in Chapter 5).

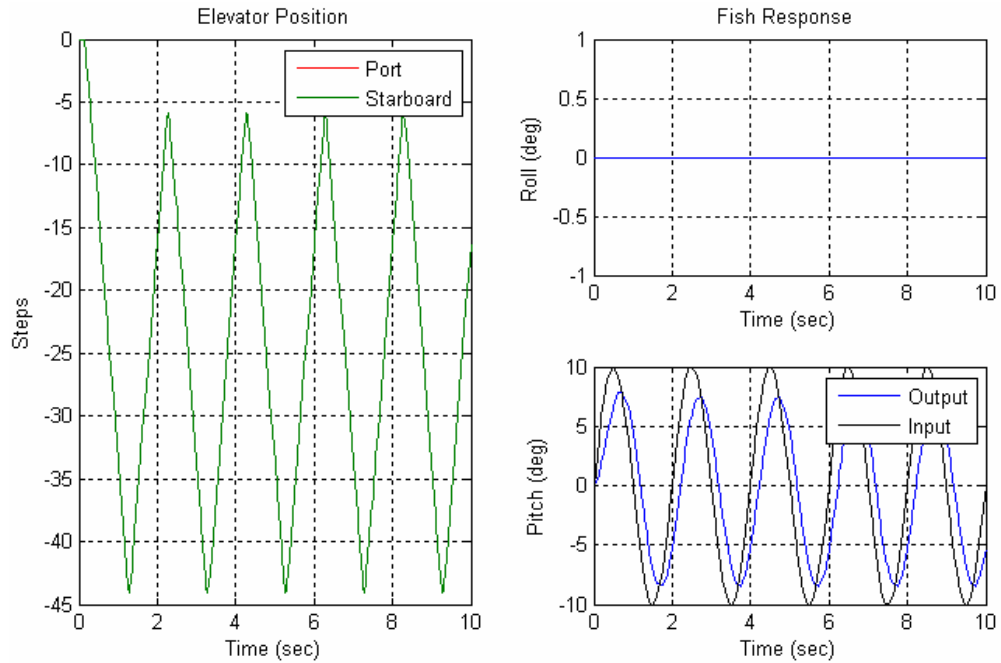


Figure 8.6.4: Simulated system response to a 0.5 Hz pitch sinusoid disturbance with PD control.

Figure 8.6.4 shows the system response to a 0.5 Hz, 10 degree pitch sinusoid-input. The towfish reduced the amplitude of the input to 7 degrees from horizontal. As indicated by the Bode Diagram for overall pitch loop gain, the controller can reduce but not eliminate vehicle response to high frequency pitch disturbances.

Similarly, the system response to roll is examined.

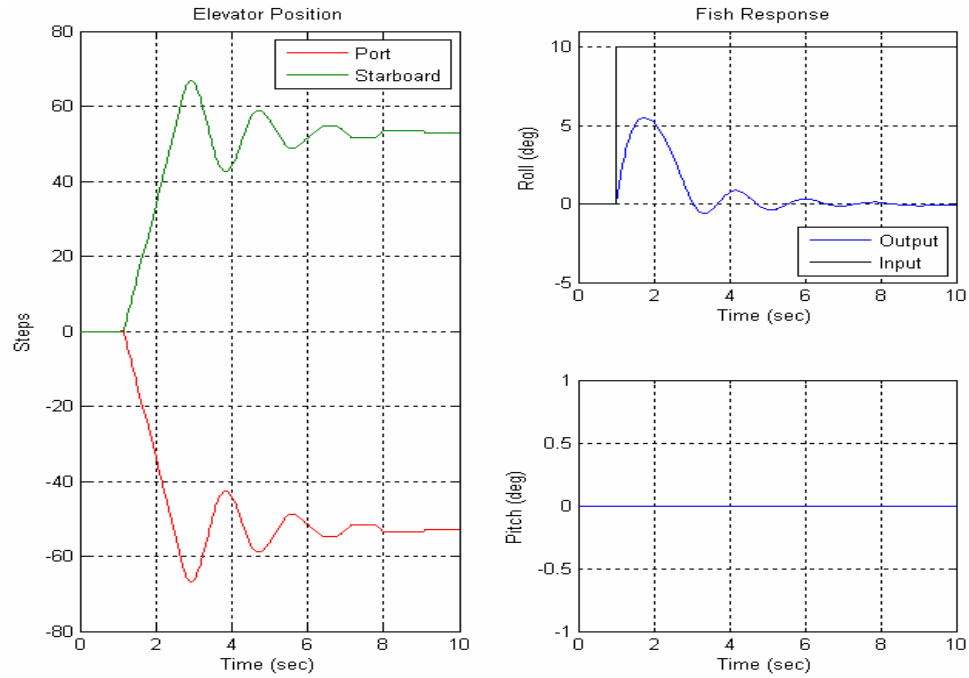


Figure 8.6.5: Simulated system response to a 10 degree roll step disturbance with PD control.

Figure 8.6.5 shows the system response to a 10 degree roll step-input, starting at $t = 1$ second. The system settled within 2 degrees of horizontal after 5 seconds. This simulation implies that the towfish roll can be stabilized at low frequencies, so long as the corrective elevator action is within the range of control.

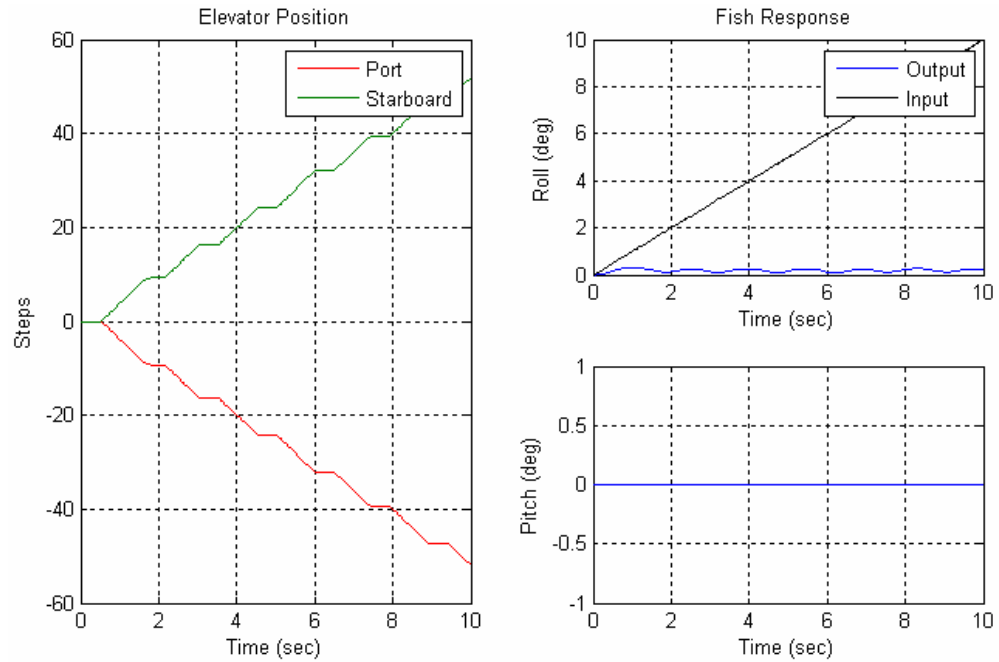


Figure 8.6.6: Simulated system response to a roll ramp disturbance with PD control.

Figure 8.6.6 shows the system response to a 1 deg/sec roll ramp-input, starting at $t = 0$ seconds. For the entire 10 seconds of the simulation, the towfish remained within 1 degree of horizontal. This means that for the first 10 seconds of the simulation, the magnitude of roll response induced per step of elevator corrective action is enough to stabilize the ramp disturbance. After a prolonged period of time, this simulation implies that the Smart Tail may have difficulty stabilizing the towfish under a roll rate disturbance due to the range of control limits.

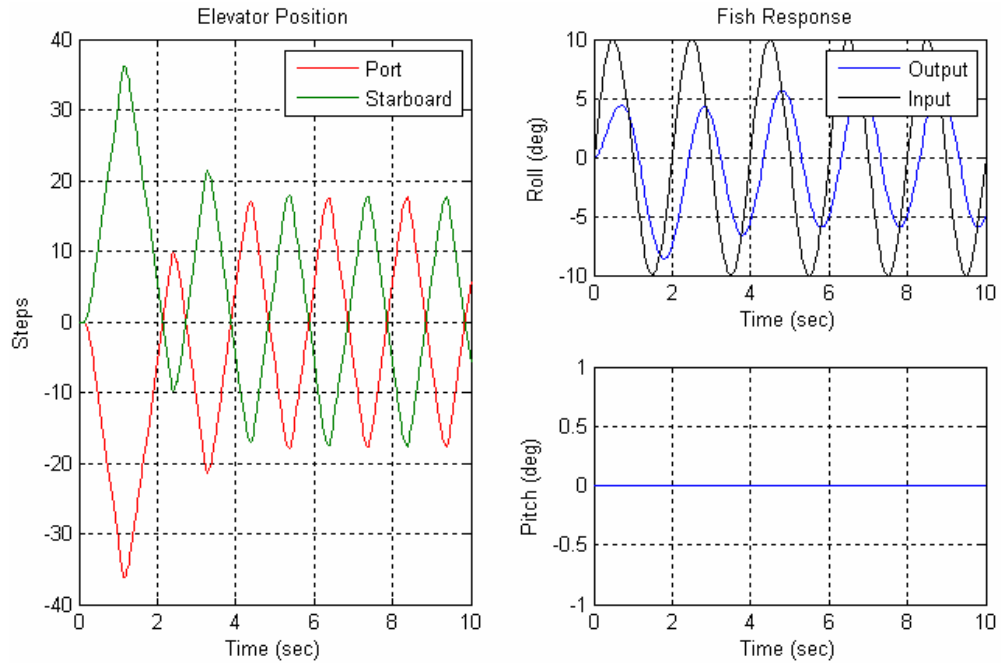


Figure 8.6.7: Simulated system response to a 0.5 Hz roll sinusoid disturbance with PD control.

Figure 8.6.7 shows the system response to a 0.5 Hz, 10 degree roll sinusoid-input. The towfish reduced the amplitude of the input to 6 degrees from horizontal after 3 seconds. Again, as indicated by the Bode Diagram for overall roll loop gain, the controller can reduce but not eliminate vehicle response to high frequency roll disturbances.

CHAPTER 9

CONTROLLER PERFORMANCE EVALUATION

9.1 Field Observations

Two surveys were conducted to evaluate the performance of Smart Tail. The first survey was on October 19, 2006 and the second was on October 24th, 2006. Observations of tow cable tension, towfish depth, and speed through water (SRW) were collected to provide a record of possible differences that may have existed between the two surveys.

The same sensors were used to record the test variables as were used in the preliminary field testing of the Smart Tail in May of 2006. The speed through water and pressure were sampled at 1 Hz and the tow cable tension was sampled at 15 Hz. The cable tension was down-sampled to 1 Hz using the *decimate* MatlabTM function. New time vectors were constructed for each entire time series at one second increments, on the integer values. The depth and speed through water measurements were interpolated using the *interp* MatlabTM function to align those measurements to the new time base. Tension and depth were plotted as a function of speed through water and trend lines were fitted to each dataset, as shown in Figure 9.1.1.

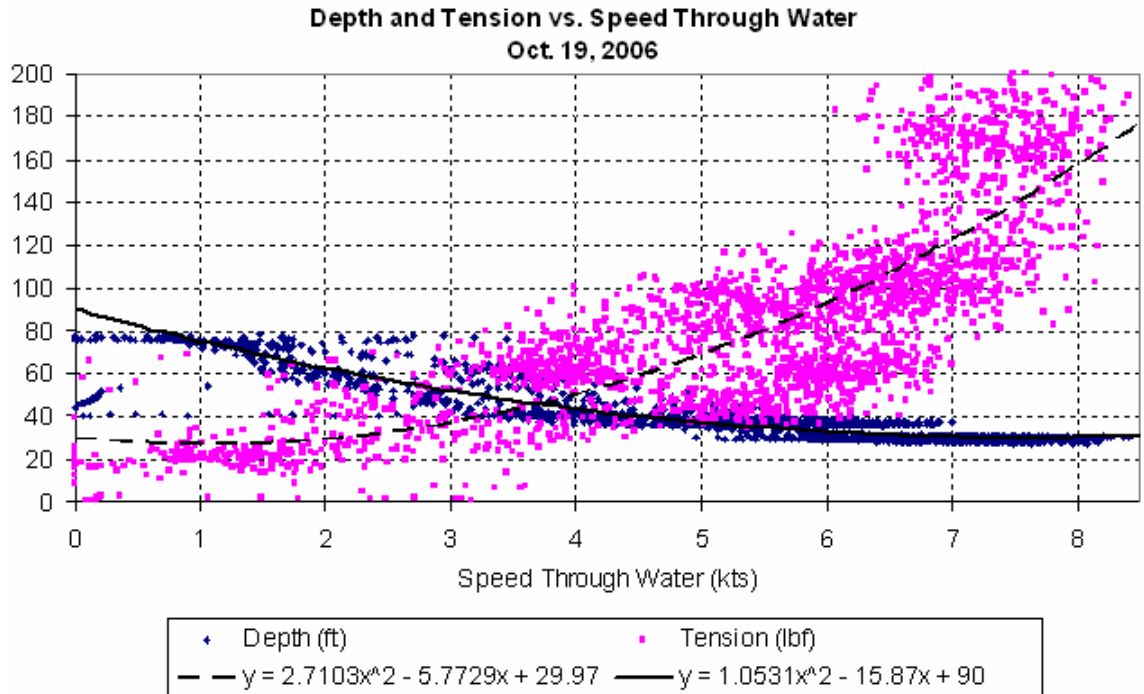


Figure 9.1.1: Depth and tension as a function of speed through water for the October 19th, 2006 survey.

The tow cable tension essentially varied quadratically with the tow speed. At the highest speed, the sensor that was deployed to measure speed through water was observed to rise and skip along the surface. That is that most probable cause for some of the tow cable tension values to appear elevated in the speed range of 7 to 8 knots.

The October 19th survey was conducted in open ocean like conditions, (at about 43° 04' N, 70° 30' W) approximately 6 miles off of the coast of Maine. The October 24th survey was conducted in two different conditions, first in the river mouth near Portsmouth harbor (at about 43° 03' N, 70° 42' W), New Hampshire and later in open ocean like conditions, (at about 43° 0' N, 70° 39' W) approximately 6 miles off the coast of New Hampshire. Trend lines from each survey during the river mouth and open ocean conditions are plotted in Figure 9.1.2.

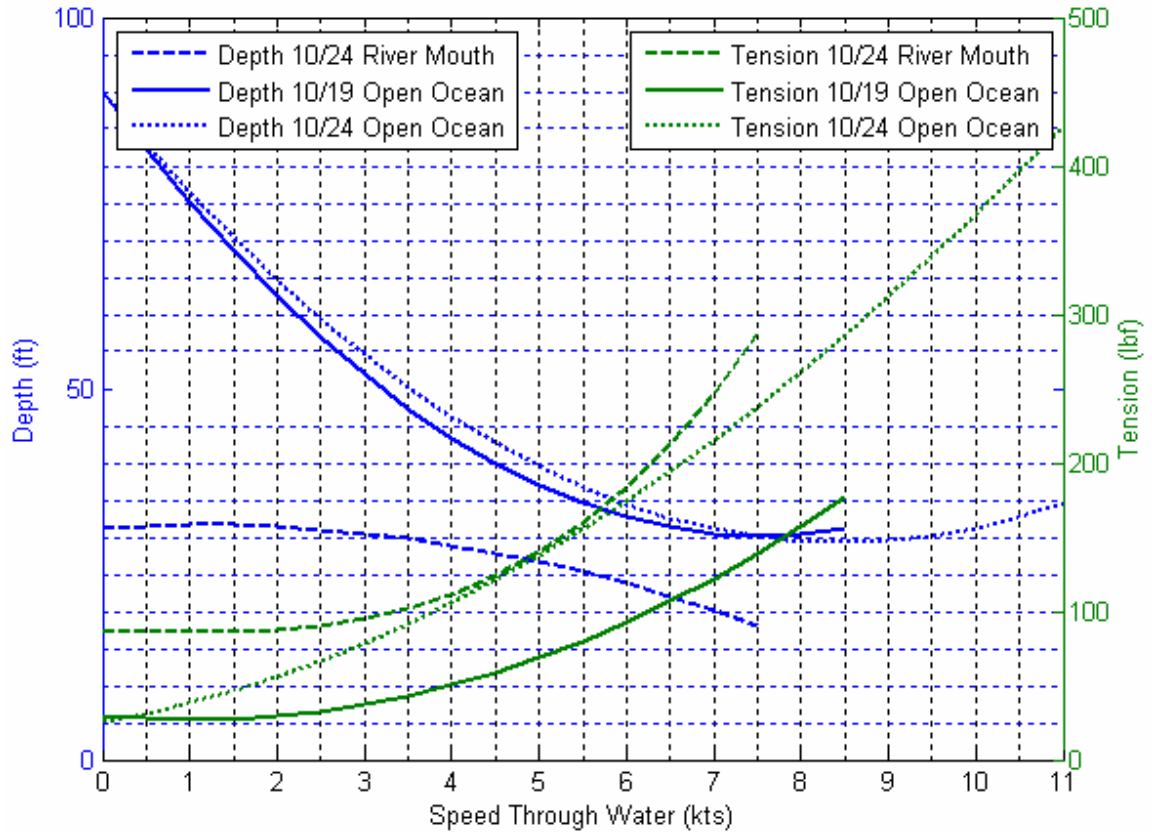


Figure 9.1.2: Comparison of depth and tension vs. speed through water trend lines from Oct. 19th, 2006 and Oct. 24th, 2006 surveys.

In general, the trend lines show that as the speed through water increases, the depth decreases and the tension increases. These trends are in accordance with commonly known physics of tow bodies. The differences in the depth curves at zero speed indicate the best fit values of the different amounts of cable out when operating in the River Mouth as opposed to operating in the Open Ocean.

9.2 Magnitude of Towfish Response

The magnitude of towfish response with and without control was analyzed by selecting three sections of data, sections A, B, and C from the October 19th survey. This survey was conducted with and without control Version 0 active during various portions of the survey. Sections A and B were selected without active control, and the port and starboard elevators locked in the neutral position. Section C was under active control using Version 0, where proportional feedback gain is set to half the critical values defined in Chapter 8 and the derivative feedback gains are around one quarter of the respective critically damped values. Each section is 270 seconds in length and was selected during periods when the mean speed through water and tension were reasonably constant. Figure 9.2.1 shows the juxtaposition of the towfish pitch and roll response for all three sections.

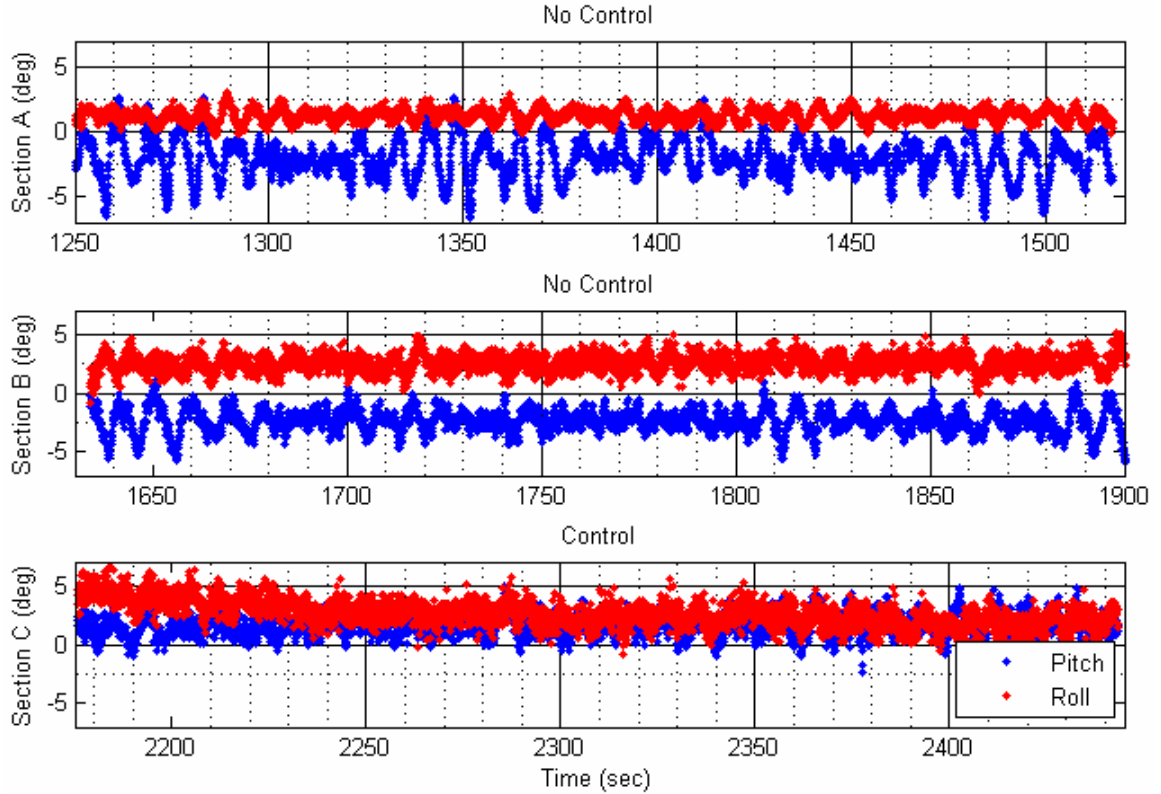


Figure 9.2.1: Sections A, B, and C from the October 19th, 2006 survey. Section C is with control Version 0 active.

All three sections were extracted from data taken when the vessel was on the same heading and with the same amount of tow cable out. Section B is closest in time preceding the control being turned from inactive to active and is therefore indicative of what the towfish response might have been in Section C if the control had remained inactive. The largest difference between the plots in Figure 9.2.1 is the change in mean value and standard deviation of the towfish pitch. The sections are analyzed further to investigate how the major forcing function, cable tension, differed from section to section and at what speed the towfish had been towed.

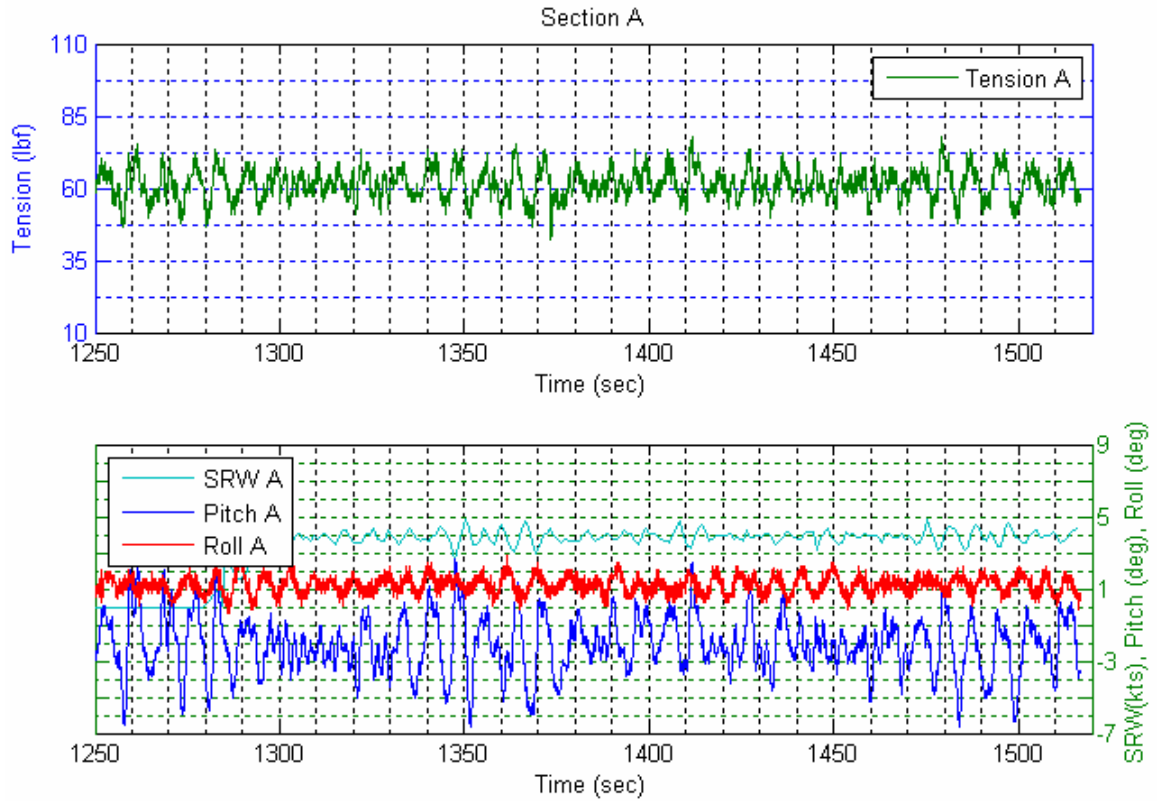


Figure 9.2.2: Section A of the October 19th, 2006 survey.

Figure 9.2.2 shows that section A was extracted from the dataset where the vessel was traveling at a mean speed through water of 3.65 kts and the mean tension applied to the cable was approximately 60 lbf. The tension plot appears to vary sinusoidally with a similar pattern exhibited in the corresponding towfish pitch response. A variation of approximately 25 lbs in the modulated waveform for tension corresponds to a variation of 9 degrees of pitch, with peak amplitudes at 1260, 1360 and 1490 seconds.

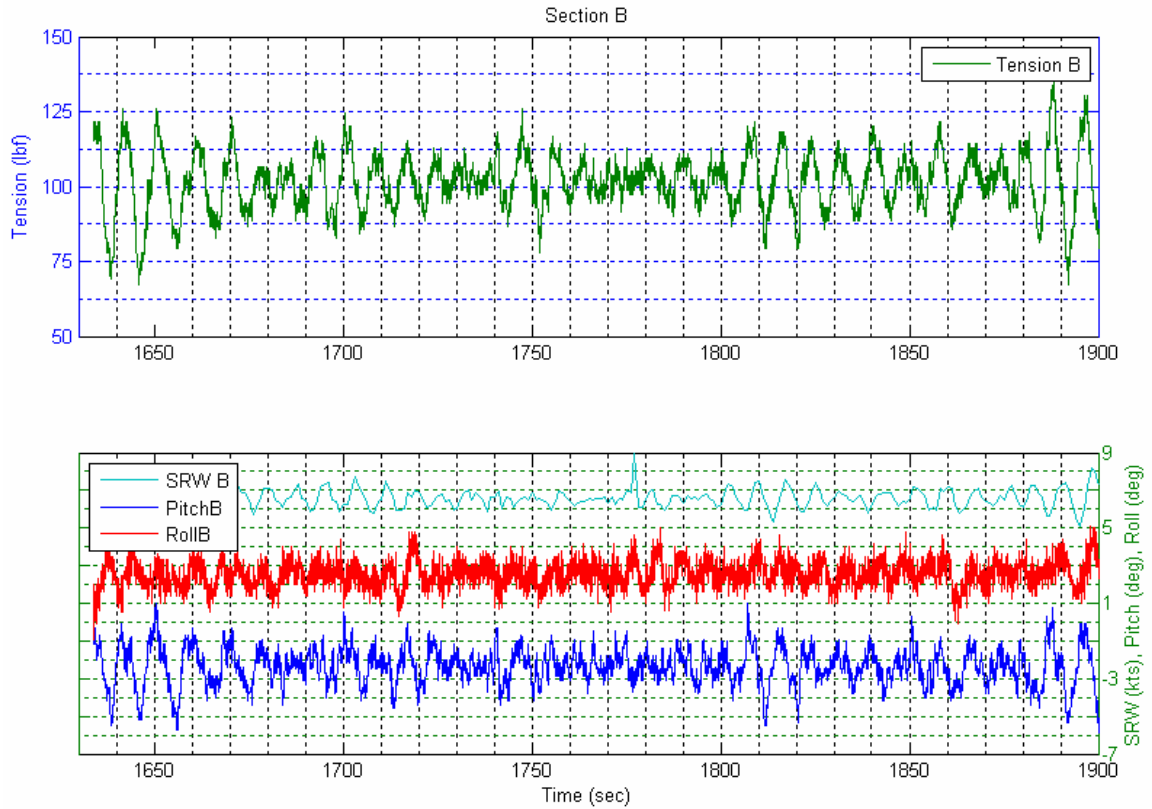


Figure 9.2.3: Section B of the October 19th, 2006 survey.

Figure 9.2.3 shows the mean speed through water and mean tension for Section B were 6.57 kts and 101 lbs, respectively. Like Section A, corresponding temporal patterns appear in the tow cable tension and in the towfish pitch response. A maximum variation of approximately 50 lbs in the tension corresponds to a variation of 7 degrees of towfish pitch response, with peak amplitudes at 1640, 1700, 1750, 1810 and 1900 seconds.

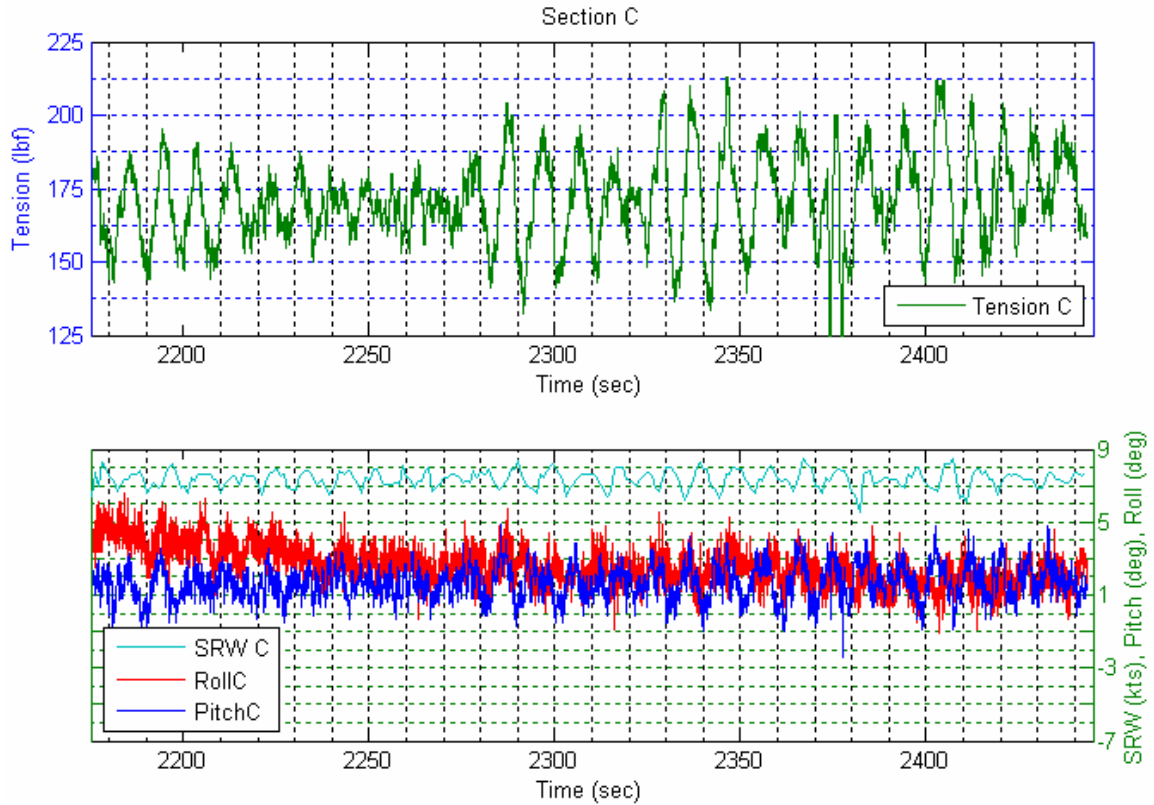


Figure 9.2.4: Section C of the October 19th, 2006 survey.

Figure 9.2.3 shows the mean speed through water and mean tension for Section C were 7.36 kts and 171 lbs, respectively. Again, the tension readings in Section C show sinusoidal variations with low frequency amplitude modulation, however, with active control, the pitch time series does not show signs of motion that corresponds in time with the variation in tow cable tension. The mean pitch in Section C is closer to zero than in Sections A and B which presumably is a result of the control effort. The mean roll of Section C approaches zero after 50 seconds of the control effort. Table 9.2.1 shows the mean and standard deviation of all of the variables observed in each section.

	Mean _A	σ_A	Mean _B	σ_B	Mean _C	σ_C
Tension (lbf)	61.31	5.17	101.72	9.70	170.85	15.28
Depth (ft.)	40.64	0.42	29.19	0.24	30.34	0.20
SRW (kts.)	3.65	0.90	6.57	0.55	7.36	0.47
Pitch (deg)	-2.05	1.58	-2.38	1.01	1.66	0.93
Roll (deg)	1.26	0.49	2.55	0.73	2.62	1.11

Table 9.2.1: Mean and standard deviation values for variables observed in Sections A, B and C of the October 19th survey.

The results show a close relation between the variations in speed through water and pitch for 10 second periods. The peak to peak variation in reported (observed) pitch during sections B and C are comparable with the expected horizontal acceleration induced pitch error in the TCMTM2.5, assuming the observed changes in vessel speed were causing the towfish to surge. The wave history for that survey from the nearest Gulf of Maine Ocean Observing System (GoMOOS) buoy B – Western Maine Shelf was 8 second period with 2.6 ft. height at 12 pm (for Section A) and 8 second period with 2.2 ft. height at 1 pm (for Sections B and C).

9.3 Low Frequency Performance

Sections of data were extracted from the October 24th, 2006 survey during conditions of dynamic speed, tension and heading to observe overall low frequency controller performance in the open ocean setting. Throughout this chapter, cable tension has been used to infer the forcing function for towfish pitch. Although high frequency compass heading content cannot be considered a source of forcing function information for roll, major changes in compass heading, as measured from the towfish, typically result from major changes in course made good of the boat, and therefore can be used to determine when a large change in roll is expected. From the data observed, major changes in speed always effected tow cable

tension which in turn affects the pitch of the towbody. Mean speed through water for this data segment was a constant of 6.5 kts. The wave history for GoMOOS buoy B – Western Maine Shelf was 2.1 second period with 0.9 ft. height at 10 am, 3.2 second period with 1.0 ft. height at 11 am, and 8.0 second period with 1.3 ft. height at 12 pm.

First, a reference data set is extracted and shown in Figure 9.3.1.

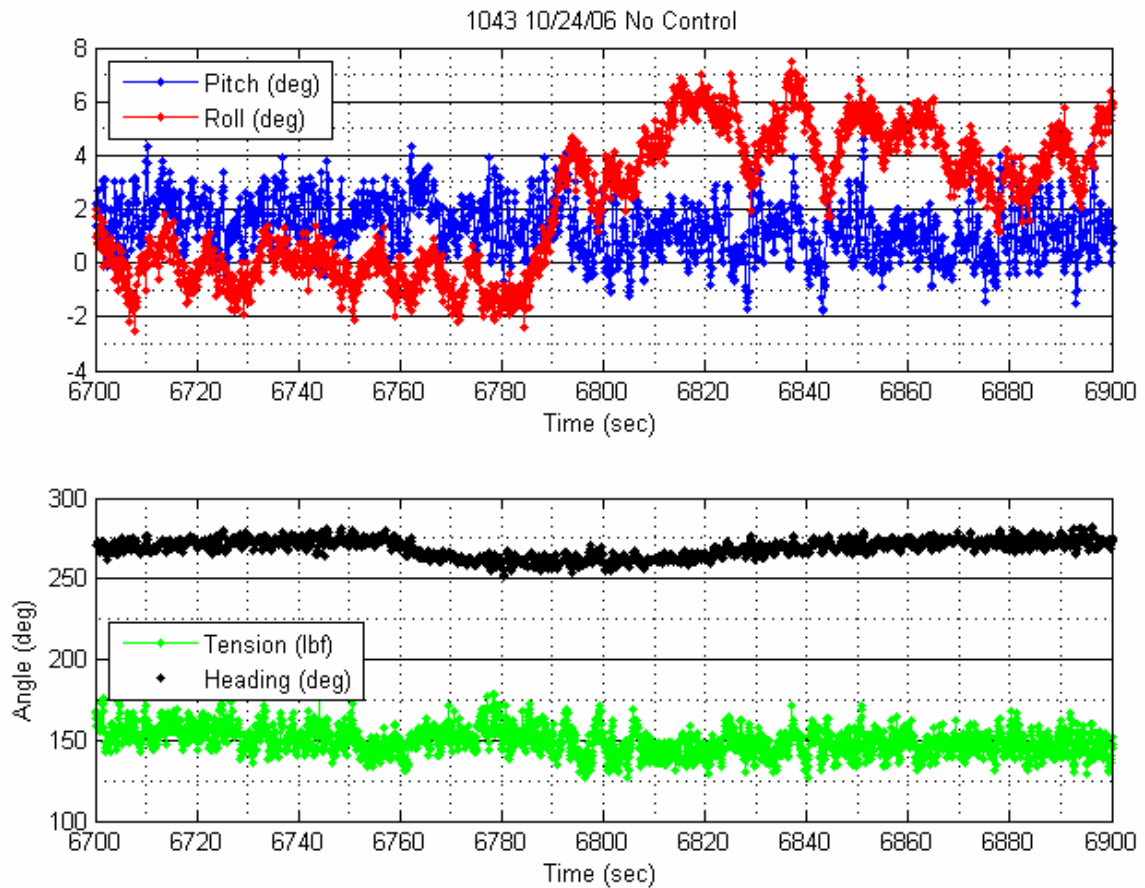


Figure 9.3.1: A reference data set from the October 24th data set, post 10:43 am with no control active.

Figure 9.3.1 shows while towing at 6.5 knots, 20 lbf and a change in heading of approximately 50 degrees can cause an increase in roll of 7 degrees.

A section of data starting at 10:57 am of the October 24th, 2006 survey is examined. To interpret the data set, note that the TCM™2..5 was mounted in the Smart Tail such that positive pitch was tail down and positive roll was starboard down. To correct a positive pitch, both elevators must move (downward) in a negative direction and vice versa. Correct a positive roll, the port elevator (Position B) must move in the positive elevator direction and the starboard elevator must move in a negative elevator direction (Position A). Figure 9.3.2 shows control was activated at $t = 7330$ seconds, marked by the dashed blue line.

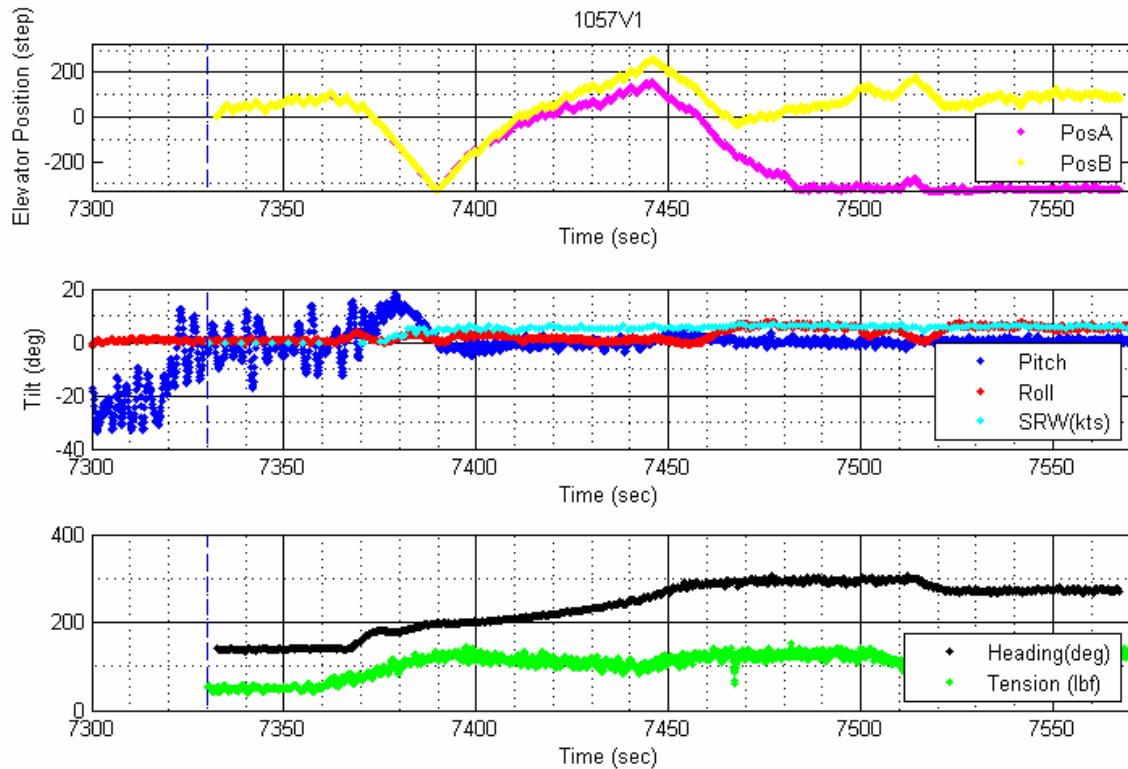


Figure 9.3.2 Section of data from 10:57 am on October 24th, 2006 survey with control Version 1 active.

The towfish was fully lowered into the water by $t = 7300$ seconds. The boat started to speed up after $t = 7375$ seconds. As the boat increased in speed, the elevator positions became

more negative to counter the positive pitch. When the pitch crossed zero from positive to negative, the elevators change direction and move in a positive direction. The elevators responded with the appropriate corrective action at the zero crossing of towfish pitch. However, the data indicated that the low frequency corrective action was not based on the change in slope of the overall pitch motion. The design of the PD controller developed in Chapter 8 was intended to implement corrective action based on a combination of the sign of the pitch and the sign of the feedback signal's smooth derivative, which is evident in the simulations.

The first 100 seconds of Figure 9.3.2 indicate that both starboard and port elevators were moving in the same manner, which indicated that large pitch corrections took precedence over roll commands. After the first 100 seconds of the 10:57 am data section, as shown in Figure 9.3.3, the port and starboard elevator positions start to diverge which indicates that the controller has begun to issue commands that were intended to correct the roll of the towfish.

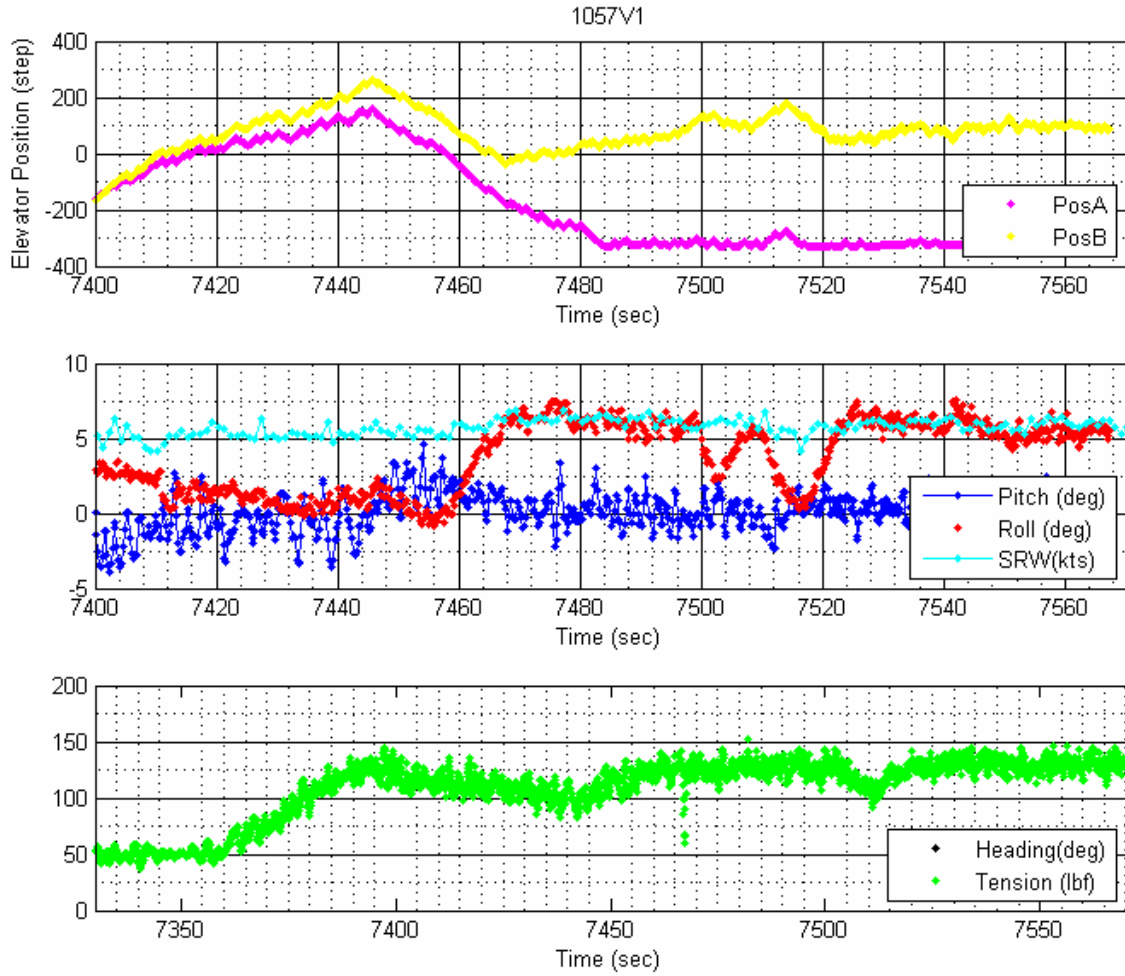


Figure 9.3.3: 100 seconds after control active on 10:57 am
data set from Oct. 24th, 2006 with Version 1 control.

At the start of the data set in Figure 9.3.3, positive value of roll causes the difference between position B and position A to increase. Elevator Position B is greater than Position A, which was the appropriate corrective action of a positive towfish roll. At $t = 7460$, the difference between Position B and Position A is approximately 50 steps to correct a 2.5 degree roll and increases to approximately 200 step difference by $t = 7500$ to correct a 6 degree roll. According to the plant steady state gain in Table 5.3.1, 50 and 200 step differences correspond to a 4.74 degree and 18.96 degree respective correction for 4 knots tow speed and above. This

indicates that either the actual plant gain for roll was lower than expected, the Weeder™ motor control cards lost track of the elevator positions, or a combination of both.

At $t = 7485$ the position of elevator A can no longer decrease due to the -330 step software limit on the range of motion. This is an example of how the available range of roll control may be limited by a portion of the elevator control range allocated to pitch correction. Note that the mean speed through water for this section was approximately 6 kts.

Another section of data was analyzed from a later time of the same survey with Version 0 of the software activated. Startup conditions are shown in Figure 9.3.4.

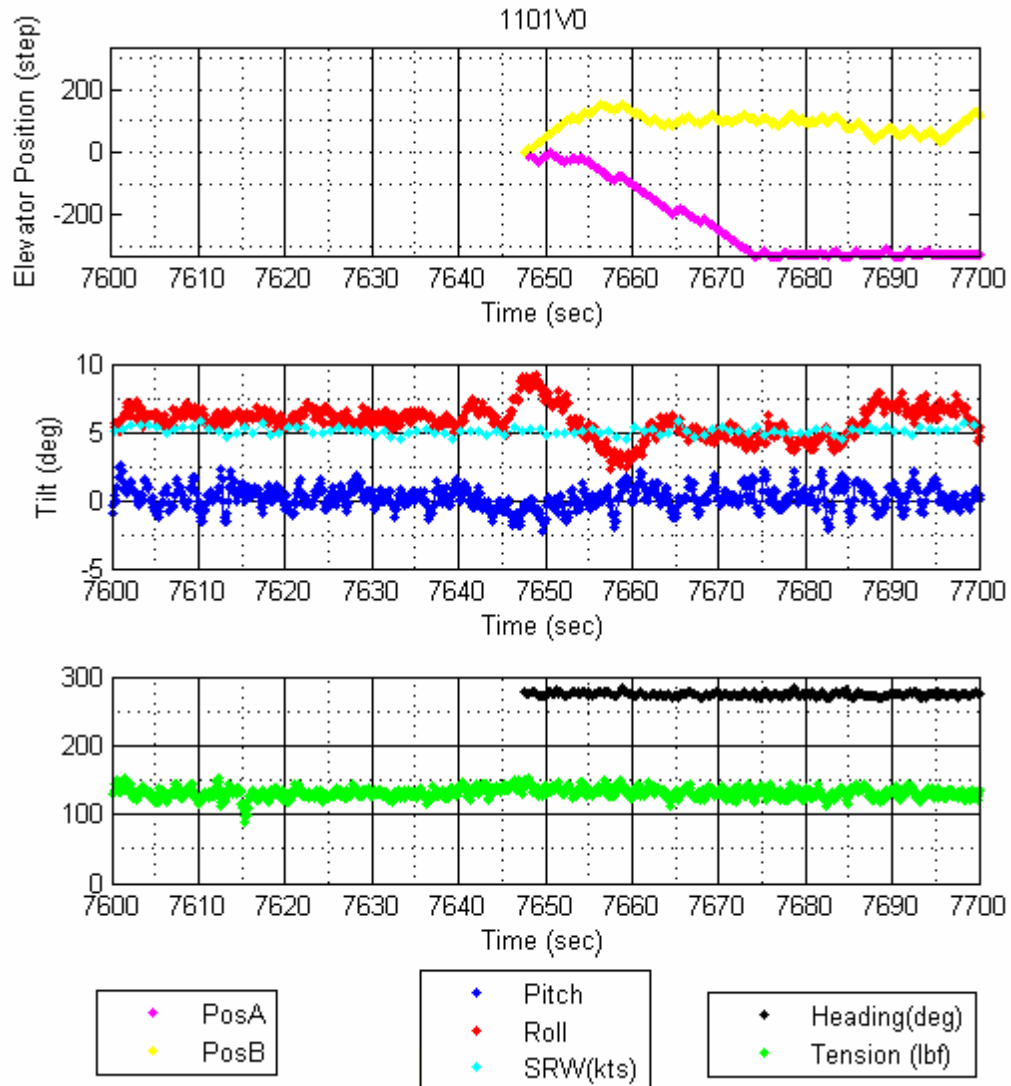


Figure 9.3.4: Startup condition and reaction of the towfish from the 1101V0 control sequence.

At startup of the controller, there were a small negative offset in pitch, however there was a +6.5 degree roll offset. A decoupled roll and pitch command was immediately executed to correct the positive roll and negative pitch. The decoupling command sequences are evident in Figure 9.3.4 by asymmetrical separation of the elevators. The controller reduces the roll from + 6.5 degrees to + 5 degrees until the roll range of elevator motion was exceeded

at $t = 7675$ seconds. In an attempt to correct the +5 degree roll, the difference in elevator position was approximately 430 steps. According to the plant steady state gain in Table 5.3.1, a 430 step difference corresponds to a 40.7 degree correction for 4 kts. tow speed and above. Again it is evident that the elevator position was inaccurate and/or the actual plant gain for roll was less than expected. A longer sequence of the data set is shown in Figure 9.3.5.

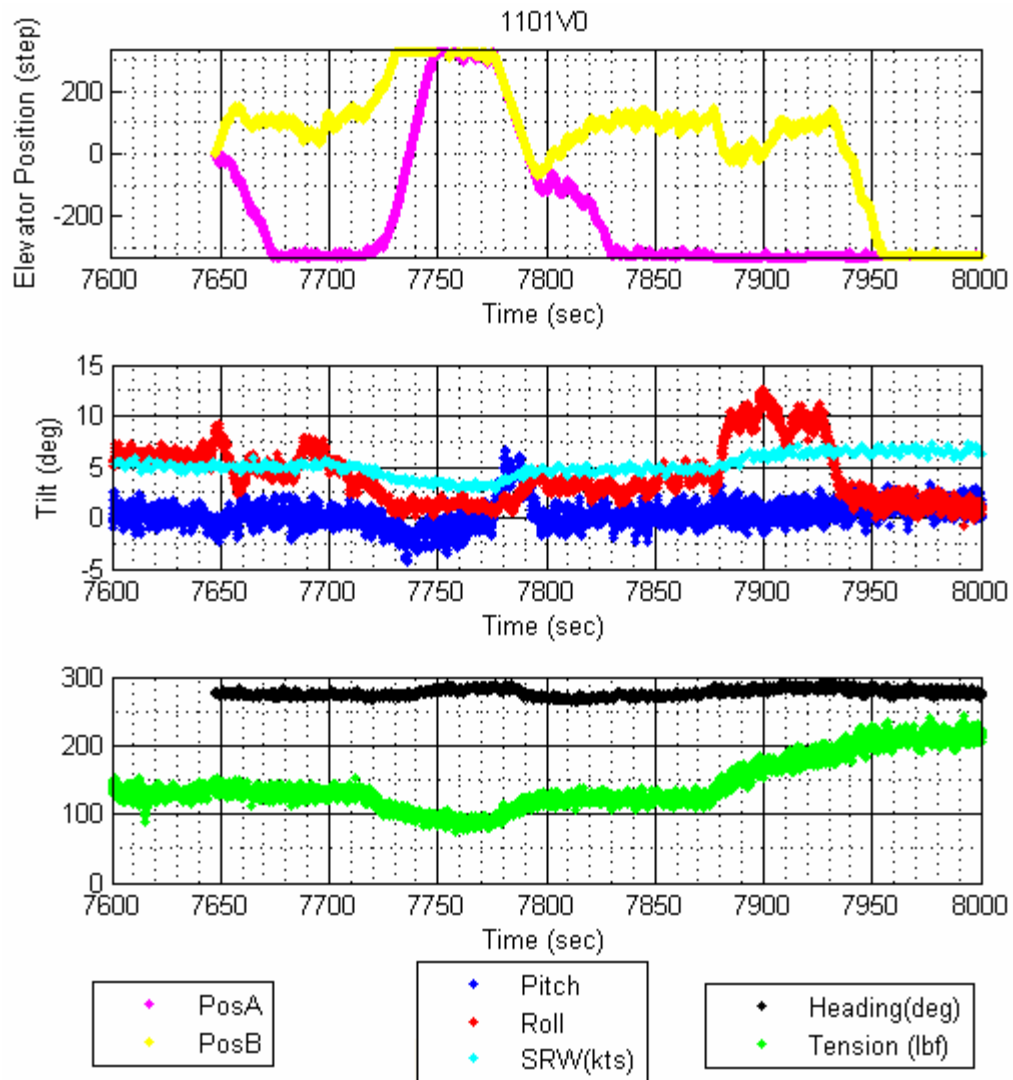


Figure 9.3.5: Section from 11:01 am of data from October 24th, 2006 survey with control Version 0 active.

In this dataset, there were three major changes in speed through water. The first major change was when the mean speed of 5 knots dropped down to 3 knots after the 7700 second mark. Control effort was evident by the major increase of elevator Position A and Position B to the +330 step upper limit of the elevator motion. Over the period of approximately 50 seconds ($t = 7725-7775$), the controller was able to maintain pitch and roll values within ± 2.5 degrees of horizontal.

The second major speed change occurred at $t = 7775$ seconds; when the speed rapidly increased from a mean of 3 knots to 4.5 knots. As the pitch increased from zero to +7 degrees, the pitch correction was given precedence over the roll correction. Elevator positions begin to decrease immediately after the zero crossing of pitch (from negative to positive) until the pitch was returned within ± 2.5 degrees of horizontal. Roll correction was withheld, despite the zero to 5 degree increase, until the pitch was within the ± 2.5 degree range. After roll correction commenced at $t = 7800$ seconds, the roll control range of elevator motion was exceeded.

The third major speed change occurred at $t = 7880$ by increasing from 4.5 knots to 7 knots in approximately 75 seconds. The mean pitch value was maintained during this time period, as shown by the decrease in elevator Position B. However, because the Smart Tail was already operating at its positive roll correction limit, a 10 degree positive roll resulted that could not be corrected.

9.4 High Frequency Performance

Two ten-minute segments of data were selected for high frequency performance examination. One segment was from the 11057V1 dataset and the other was from the 1101V0

dataset, both of which are during periods when both elevators were within their controllable limits.

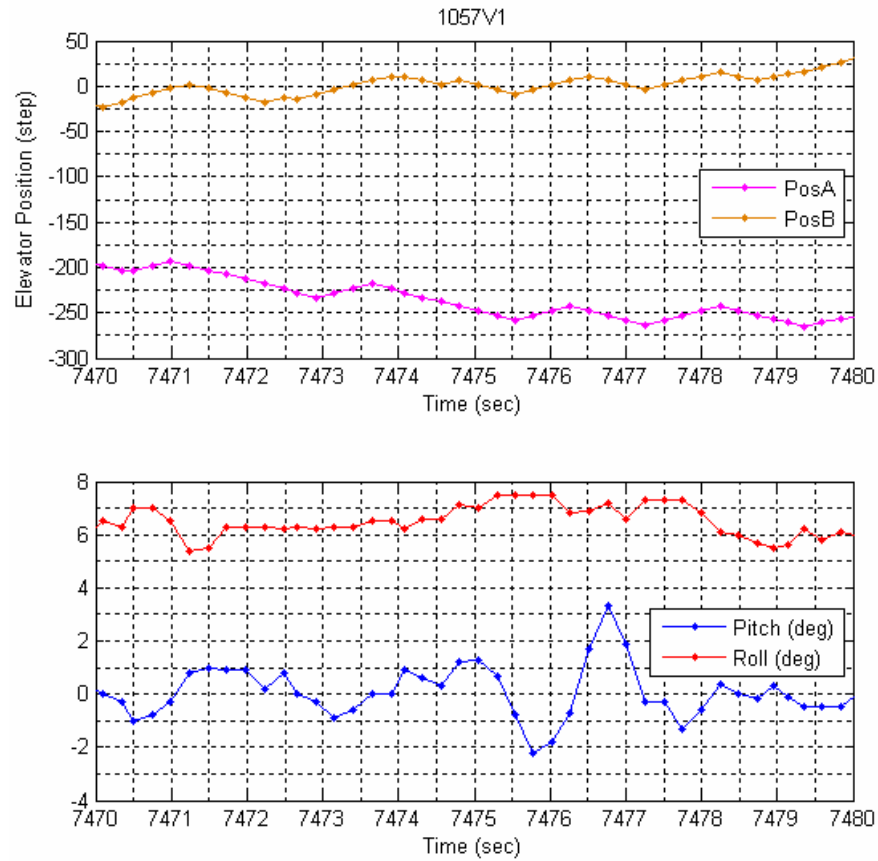


Figure 9.4.1: A 10 second segment of the 1057V1 dataset.

Figure 9.4.1 indicates that the pitch derivative feedback by virtue of the change in direction of elevator Position A and Position B occurring one to two samples after a change in the sign of the slope of the pitch.

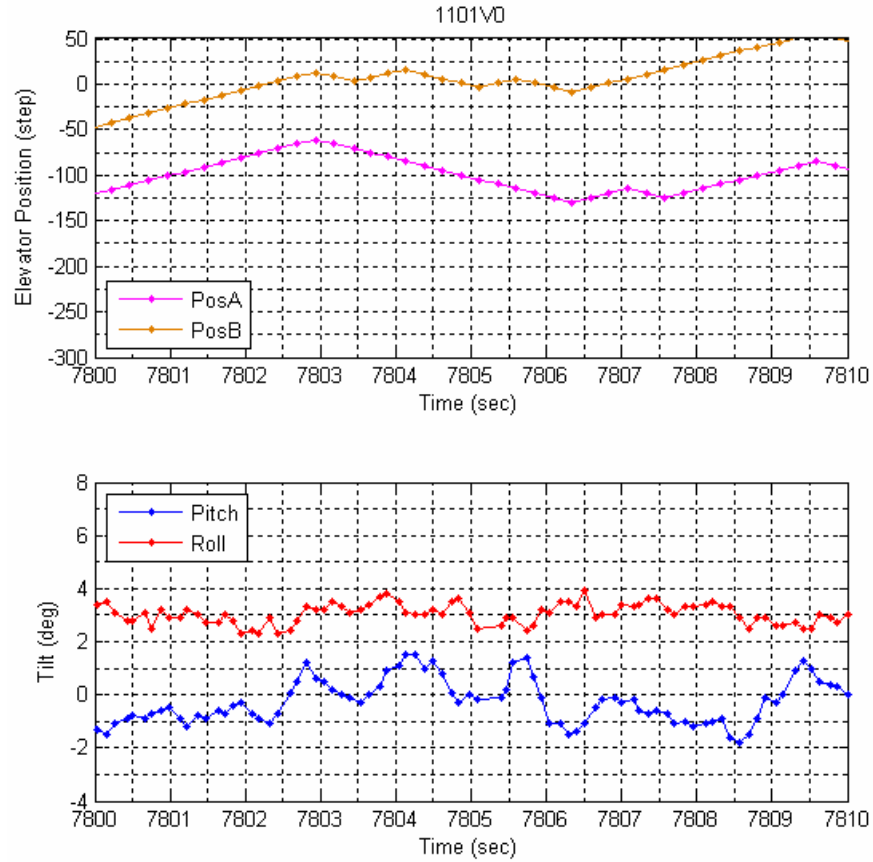


Figure 9.4.2: A 10 second segment of the 1101V0 dataset.

Figure 9.4.2 shows after a change in direction of elevator Position A and Position B occurring at a one sample delay after a zero crossings of the pitch signal. With the derivative feedback so low in Version 0, the change of the pitch between 2 sample intervals was not enough to influence the pitch command.

CHAPTER 10

CONCLUSIONS

This study has successfully addressed the development of a closed loop controller for the Smart Tail elevators that are intended to maintain near-zero tilt of a towfish under survey conditions. In the progression of this study, it was necessary to perform engineering characterization of individual components that made up the system. The towfish motion was characterized under realistic survey conditions, both with and without the benefit of the Smart Tail attempting to actively stabilize the attitude to zero tilt. The former was conducted in the early stages of the study in order to estimate bounds on the frequencies and range of motions that the Smart Tail control plant may encounter. The latter was a necessary element of proving the study objectives had been met. Several items like a reduced-length test tow body, the PEL Swivel device, and a tow tank carriage apparatus (TCA) that were purpose-built for this study will be useful tools for future developments that require side scan sonar towfish testing.

Extensive engineering tests were conducted in the UNH tow tank to establish behavior of the towfish/ Smart Tail assemblage at different tow speeds. Separate engineering tests were conducted to evaluate the following: (a) different static balance conditions of the test tow body with the Smart Tail attached; (b) tow body attitude as a function of the elevator

positions and the tow speed; (c) lift/drag forces on the tow body as a function of the towfish attitude, elevator positions and the tow speed; and (d) the relationship between tow speed and recovery-time-to-level from an imposed initial non-level state. Analysis and interpretation of the test data provided information about the steady state righting forces that the Smart Tail could impart to the towfish and the dynamics associated with employing the controllable elevators to modify those forces. It is important to note that the forces exerted by the non-movable elements of the Smart Tail were approximately ten times greater than the variable forces that could be exerted by the control elevators of the Smart Tail.

The information acquired from the tow tank experiments and the initial early field experiments were integrated into a mathematical model that was based on first principles. Results from laboratory testing of Smart Tail's electronic and mechanical components also contributed in the development of this model. A multiple-input, multiple-output (MIMO) system model was developed in the Matlab™ Simulink workspace. That model was decoupled into two single-input, single-output systems (SISO), one for pitch, and the other for roll. PD control was successfully implemented in each of the two feedback loops and the controller gains were tuned using classical control techniques. The controller gains were then incorporated into the original MIMO system. Ultimately, two versions of the SmartTail.exe control software were prepared. The form of the different versions (Version 0 and Version 1) were identical, however there was a difference in the derivative feedback gains. Visitors that came into the electronics lab while the Smart Tail was being put through its paces by the SmartTail.exe control software were fascinated to see the elevators autonomously running up and down.

A field test was designed whereby the final performance of the system could be evaluated. Field testing of the Smart Tail was then conducted on the R/V Gulf Challenger. The performance of the Smart Tail controller during the field testing clearly indicated that the elevator actions for correcting non-zero pitch and roll conditions of the towfish were of the proper form. As a result of the controller decoupler, the pitch commands were given precedence over roll commands. The pitch performance of the Smart Tail showed adequate capability of correcting disturbances that might be described as low frequency towfish motion and a non-zero mean trim in pitch. The pitch control maintained towfish attitude within ± 3 degrees from horizontal for tow conditions where speed changed up to 3 knots in an interval of 50 seconds. However, the change in towfish pitch, observed in the field test for a given change in the position of the elevators, was about half of what had been expected based on the tow tank tests. This resulted in a greater portion of the total range of elevator control motion being required to achieve level condition of the towfish than had been anticipated. Based on this observation it would be advisable to increase the area of the control elevators relative to the area of the non-movable structural elements of the Smart Tail. The roll low frequency performance suffered due to the pitch corrections being given precedence over roll corrections. This resulted in the bounds of the available roll control, in terms of elevator range of motion, limiting the roll performance during the field tests. Furthermore, the ratio of the towfish roll response to any roll command was markedly less than predicted based on the tank tests. The possible root causes for this reduced roll response should be included in future studies that may be conducted on the Smart Tail.

Derivative feedback on pitch and roll, which was intended to improve the responsiveness of the control plant to high frequency deviations from zero tilt, did not

significantly improve overall stabilization performance. This was due to limitations stemming from the simple 2-point approximation of the derivative that was imposed by the low (8 Hz) update rate of the towfish TCM™ 2.5 tilt sensor in the closed-loop controller and due to the noise in the tilt feedback sensor. However, evidence that the derivative feedback gain was impacting the performance did show up when comparing the high frequency performance of the Version 0 and Version 1 of SmartTail.exe. In Version 0, which had a lower derivative feedback gain than was used in the Version 1, it was clear that the motor control commands were changing signs based on the value of the tilt feedback signal and not based on the sign of the derivative of the feedback signal. In Version 1 it appeared that the sign changes of the motor control were more in line with the derivative of the tilt feedback signal than with the value of the tilt feedback signal. Implementing the intended derivative feedback scheme was part of the decision to run the elevator motor controller in a single step mode where the motor control could be modified after each step, if necessary. Designing and programming a Kalman Filter for the SmartTail.exe controller is an excellent recommendation for future development.

The alternate mode for the elevator motor controller was a ramp mode where a single command that was issued to make a large move was internally broken into a variety of different move commands based on considerations of torque/speed. However, the down side of the ramp mode was that the elevator motor controller was constrained to carry any command to completion even though the tilt feedback sensor may begin indicating that conditions had changed and the end point of the previous command was no longer valid.

This work has demonstrated that implementation of a side scan sonar stabilization device based on tail elevator adjustment is feasible. A stability performance of ± 2 degrees in

pitch and roll over an interval of 10 seconds was achieved using the Smart Tail. However, the peak-to-peak variations of towfish attitude at frequencies higher than 0.1 Hz were still larger than one would have preferred them to be. Based on the susceptibility of the TCM™ 2.5 output to include effects of horizontal accelerations, it is not clear if the higher frequency “tilts” were real or systematic errors due to surge. That gives ample justification to improve the quality of the tilt feedback sensor as part of any future work with the Smart Tail.

Future development should include the integration of continuous hardware elevator shaft positioning feedback and an increase in the power available for running the elevator control motors. The increased power for the motors will provide improved torque/speed characteristics and the continual hardware feedback of elevator position will give assurance that the intended effect of a motor command was achieved.

REFERENCES

- Brogan, William L. *Modern Control Theory*, 3d ed. Upper Saddle River, NJ: Prentice Hall, 1991.
- Franklin, Gene F., Powell, J. David, Enami-Naeini, Abbas *Feedback of Dynamic Systems*, 4th ed. Upper Saddle River, NJ: Prentice Hall, 2002.
- Fussell, Barry *ME 951: Advanced Control Systems I*, Lecture Notes University of New Hampshire, Dec. 1st 2005.
- Latchman, Sonia *Effect of Cable and Towbody Parameters on Tension and Cable Length when Towing at 200 m depths and 10 knots*, Oceans '93 proceedings, Issue Oct 18-21 1993, Volume 3.
- McClellan, James H., Schafer, Ronald W., Yoder, Mark A., *DSP First: A Multimedia Approach*, Upper Saddle River, NJ: Prentice-Hall Inc., 1998.
- McGillicuddy, Glenn *Characterization of Weak Rope Through the Design and Construction of a Portable Tensile Testing Machine*, Master of Science Thesis, University of New Hampshire, Dec. 2005.
- Ogata, Katsuhiko *System Dynamics*, 4th ed. Upper Saddle River, NJ: Prentice Hall, 2004.
- Shigley and Mischke, *Mechanical Engineering Design*, 5th ed., New York: McGraw-Hill, Inc., 1989.
- Smith, Chris. *Theory and the Art of Communications Design*. State of the University Press, 1997.
- Unlu, Ahmet Nuri. *A Study of the Effects of Tonfish Motion on Side Scan Sonar Imagery through Simulation*, Master of Science Thesis, University of New Hampshire, 1999.

APPENDICES

APPENDIX A:
CALCULATIONS

Raising the Load

Calculation for torque on Thumb Screw head T required to overcome thread friction and raise the load F. (ACME threads).

$$F := \frac{180}{4} \cdot \text{lbf} \quad d := \frac{5}{8} \cdot \text{in} \quad d = 0.625 \text{ in}$$

$$\text{thrdsp Erin} := 11$$

$$F = 45 \text{ lbf}$$

Pitch

Coefficient of Friction

$$\mu := 1.8$$

$$p := \frac{1 \cdot \text{in}}{\text{thrdsp Erin}}$$

Threads per turn

$$p = 0.091 \text{ in}$$

$$n := 1$$

Mean Diameter

lead

$$d_m := d - \frac{p}{2}$$

$$l := p \cdot n$$

$$l = 0.091 \text{ in}$$

$$d_m = 0.58 \text{ in}$$

$$T := \frac{F \cdot d_m}{2} \cdot \left[\frac{1 + \pi \cdot \mu \cdot d_m}{(\pi \cdot d_m - \mu \cdot l)} \right]$$

Eqn 8-5 Mechanical Engineering Design - Shigley and Mischke

$$T = 2.209 \text{ lbf} \cdot \text{ft}$$

APPENDIX B:
PARTS INFORMATION

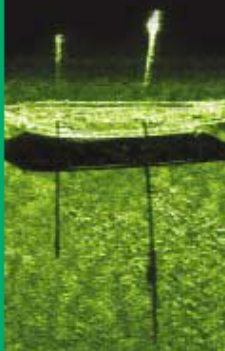
Tow Carriage Assembly Parts and Materials						
Manufacturer/distributor	Part Name	Part Number	Dim 1	Dim 2	Material	Qty Description
McMaster-Carr	Thumb Screw	90165A533	5/8" - 11 Thread	3-1/8" Length	Steel	4 Thumb Screw with removable swivel pad Fluted Knob
	Hex Cap Screw	92186A632	3/8 - 16" Thread	2" w/ 1" should	Stainless 316	1 Packs of 10 Partially Threaded - side bolts for clamps
		93190A638	3/8 - 16" Thread	3" 1/2"	Stainless 316	2 Packs of 5 Fully Threaded - Top bolts for clamps
		93190A644	3/8 - 16" Thread	4 1/2"	Stainless 316	1 Packs of 5 Fully Threaded - Bottom bolts for clamps
	Rectangular Bar	8975K313	1" Thick	3" X 1'	Aluminum 6061	1
	Rectangular Bar	8975K417	0.75" Thick	3" X 1'	Aluminum 6061	1
	Rectangular Bar	8975K414	0.5" Thick	3" X 3'	Aluminum 6061	1
	Large Washer	92141A044	1-13/16" ID	.140" Thick	316 Stainless	1 Loose washer to go on shaft
	Machine Srew	91500A624	3/16 Thread	1" Length	317 Stainless	1 for fairings to ride on - packs of 5 Screws for cheek plates in shaft_sub.asm
						www.mcmaster.com
Online Metals	Plate	Custom Cut to	0.5" thick	26" X 26"	Alum 6061 T6	1
	Round Bar	Custom Cut to	1.625" Diameter	4'	Stainless 304	1
		Custom Cut to	4" Diameter	0.5"	Stainless T-304	1
						http://www.onlinemetals.com/
Odium Spectrum	Tufnose Fairings	TN1600	1.60" Diam Cable	2 ft section		http://www.odium-spectrum.com/fairings.html
Smart Tail Components						
RS Components	Hybrid Stepper Motor	440-442				3 http://www.rsnewzealand.com/
John Crane	Elastomer Bellows Seal	502				3 www.johncrane.com
PNI Corporation	TCM2 - 50 2.82K 10467	10651				1 www.pnicorp.com/
	TCM2.5 Module 1001218	12403				1
KAGA Electronics (USA)	SPN Series Universal Input	SPN15-12S				1 Power Supply Unit
Newark InOne	Honeywell Humidity Sensor	19C6680				www.kacom.com
	HIH - 3610-003					1 www.newark.com
Weeder Technologies	Stepper Motor Driver	WTSMD-M				3 www.weedtech.com



communications
Klein Associates, Inc.

Side Scan Sonar Division
Navigation Division
Waterside Security and
Surveillance Division

11 Klein Drive,
Salem, N.H. 03079-1249, U.S.A.
Phone: (603) 893-8131
Fax: (603) 893-8907
klein.mall@L-3.com
www.L-3klein.com



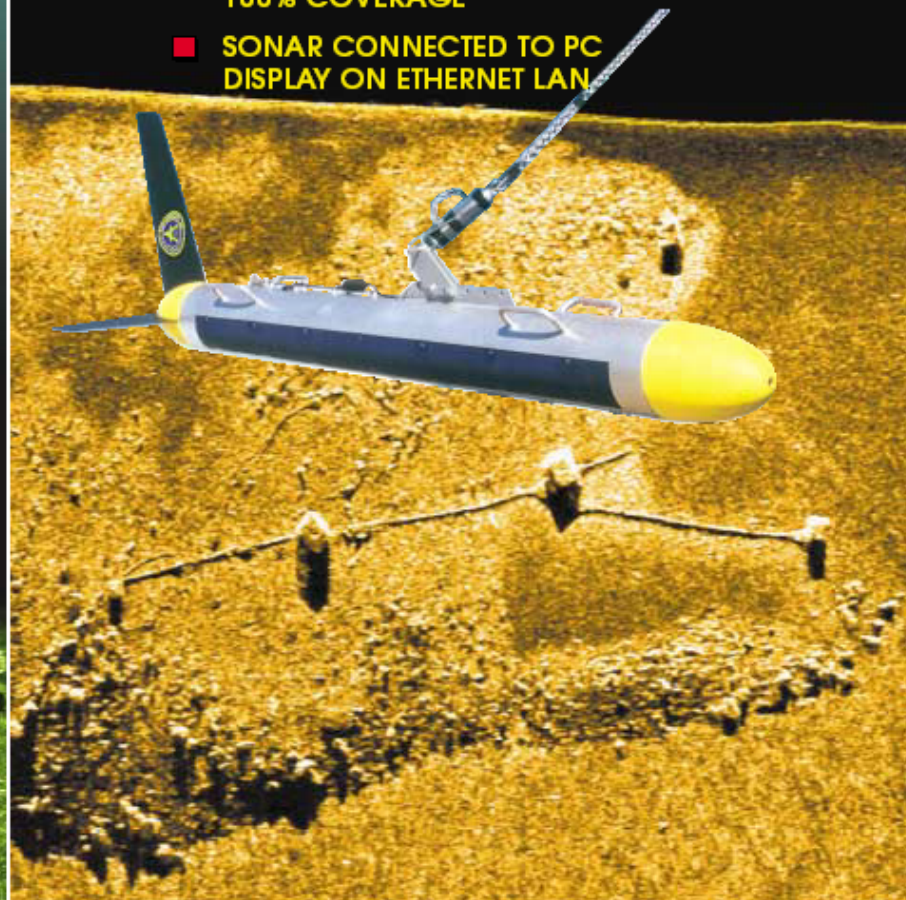
Klein System 5000

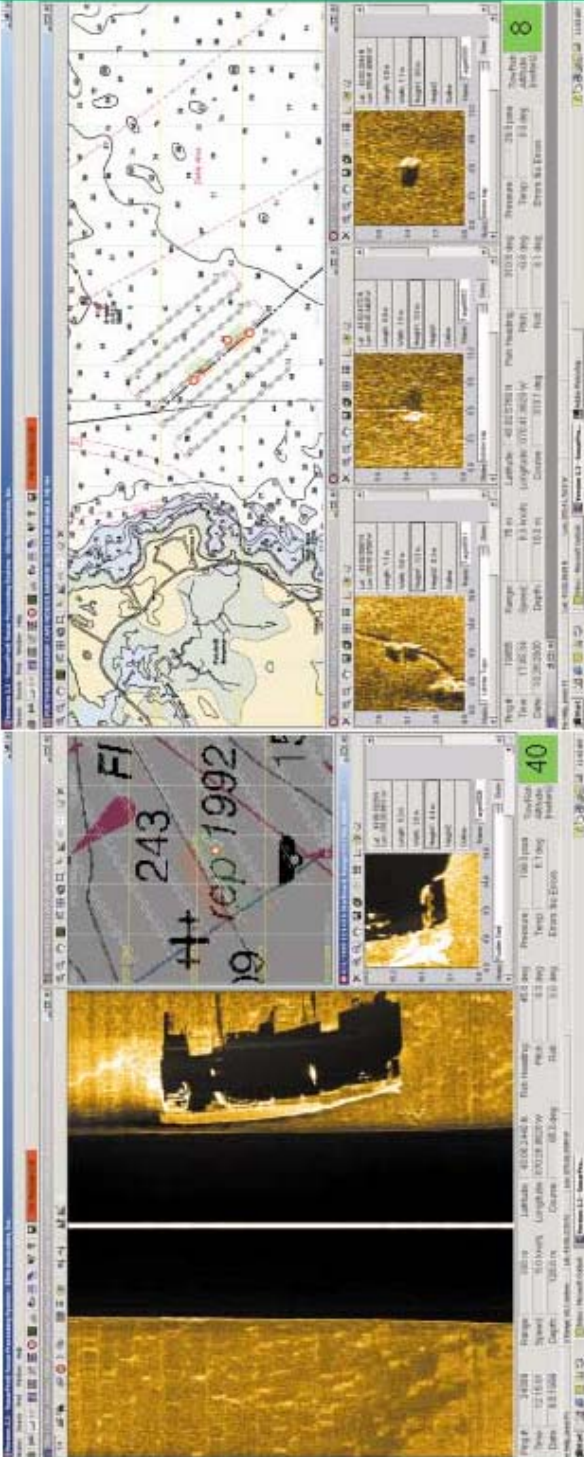
HIGH RESOLUTION, DYNAMICALLY FOCUSED, MULTI-BEAM SIDE SCAN SONARS

"The difference is in the Image!"

The System 5000 is a 5 beam side scan sonar designed for hydrographic military and commercial applications requiring high resolution images of the seafloor and bottom obstructions, while operating at tow speeds up to 10 knots and with an overall swath width of 300 meters.

- **MULTIPLE SIMULTANEOUS BEAMS PER SIDE EACH PING**
- **HIGH TOW SPEED CAPABILITY**
- **DYNAMIC DIGITAL AUTO-FOCUSING**
- **VERY HIGH RESOLUTION AND 100% COVERAGE**
- **SONAR CONNECTED TO PC DISPLAY ON ETHERNET LAN**





INTRODUCTION

Conventional side-scan sonar systems use a single sonar beam per side to generate an image of the seafloor. The physics of this type of sonar results in degradation of image resolution with range, poor along track resolution, and requires speeds of 5 knots or less to insure 100 percent bottom coverage.

From a design perspective, these shortcomings can be eliminated by designing a sonar that, through beam steering and focusing techniques, simultaneously generates several adjacent, parallel beams per side. With multi-beam design approach, parallel higher towing speeds with 100 percent bottom coverage, while providing high resolution imaging is, there is a vast range of the sonar.

This design approach is primarily employed by military side scan sonar systems designed for high speed mine hunting applications. When accurate is the first commercial company to offer a Multi-Beam Side Scan Sonar using similar design techniques to military sonar, but at a fraction of the cost.

The two main benefits of the High Speed, High Resolution Series 3000 systems are: higher towing speeds with no loss of bottom coverage, and range independent high resolution image capability.

Since operation costs are dependent on the amount of data that is required to complete a survey, the new Multi-Beam Side Scan Sonar systems with survey speeds are more than twice that of conventional side scan sonar, minimize the time of sonar use, thus greatly reducing survey costs.

SPECIFICATIONS

Towfish*

- Number of Beams
- Frequency
- Range Scales
- File Length
- Resolution Along Track

Resolution Across Track

- Operating Speed Envelope
- Sonar Configuration
- Minimum Operating Range
- Along Length
- Along Length
- Along Length
- Weight (in air)

Sensors: Heading/Pitch & Roll/ Temperature/ Pressure/ Altimeter Depth Rating

Options

- Yow Rate & High Resolution Roll Sensors
- Responder/Transponder
- South Bodymount
- Splash Proof IP67 Housing

Transceiver Processor Unit

- Width
- Height
- Depth
- Weight
- Voltage
- Power
- Humidity Tolerant
- Data Output
- PC Display Control Unit

Tow Cable


- Type
- Material

5 Pin / 5 Standard
455 kHz ± 1%
50, 75, 100, 150 m
50 m 200 pps.
20 m to 75 m, five cables increasing to maximum of 36 m @ 150 m maximum range
7.5 to 30 m
2-10 knots @ 150m Sonar Range
16 bit / channel
150 m (500 m South)
120 m (47-21m)
184 m (74-11m)
15.2 m (16 ft.)
70 kg (155 lbs.)

Standard
100 m Standard

Optional
Optional
Optional
Optional

19 in. rack mount
13.2 in (5.2 in.)
56.6 in (21.5 in.)
122.7 kg (271 lbs.)
115/200 VAC 50/60 Hz
120 watts include two fish
WHEA 0113
100 Amp, Ethernet LAN
Main Ruggedized or Customer Supplied PC
Cable or Fibre optic double armored
Contact Klen for specifications.



L3 COMMUNICATIONS

11 Main Drive, Suite 100, R.H. 03091-2009, U.S.A.
Phone: (603) 893-6131 Fax: (603) 893-8807
Email: info@l3.com Web site: www.l3.com

TCMTM 2.5

Tilt Compensated 3-Axis Compass Module



The TCM2.5 is a **drop-in replacement** for PNI's original TCM2 family of products. It offers improved accuracy and performance for compass heading, tilt and magnetometer measurements. It is the **same size**, has the **same 10-pin RS-232** interface connector and is **completely backwards compatible** with the original TCM2 ASCII protocol. These features make the TCM2.5 the choice for existing applications that require compatibility the TCM2 family of products.

The TCM2.5 integrates 3-axis magnetic field sensing, 2-axis tilt sensing and compass heading into a single module. Advantages include compatibility with existing systems, low power consumption, large signal noise immunity under all conditions, and a large magnetic field measurement range. The TCM2.5 combines PNI Corporation's patented Magneto-Inductive (MI) magnetic sensors and a MEMS accelerometer for unparalleled cost effectiveness and performance. MI sensors change inductance by 100% over the wide field measurement range. This variable inductance property is used in a cost and space efficient ASIC, incorporating a temperature and noise stabilized oscillator/counter circuit which is inherently free from offset drift.

Applications

- ROV/AUV's
- Remote terrestrial antenna direction indicators
- Side-scan sonar
- Survey equipment
- Robotics systems
- Vehicle detection
- Buoys

Features

- High accuracy compass heading: 0.8°
- High resolution compass heading: 0.1°
- High repeatability: 0.1°
- Wide tilt range: +/- 50°
- Multiple measurement modes:
compass heading, magnetic field and 2-axis tilt
- Calibrated magnetic field measurement range:
+/- 80 μ T (+/- 0.8 Gauss)
- High resolution magnetic field measurement:
0.05 μ T (0.0005 Gauss)
- Reliable calibration:
hard-iron calibration with quality of calibration score
- Low Power: < 20 mA typical current draw
- **Backwards compatible digital interface:**
RS-232
- **Backwards compatible footprint:**
TCM2 hole spacing

* The TCM2.5 was designed as a transitional product to replace the original TCM2 family. For any new applications, the TCM2.6 is highly recommended.

Ordering Information

NAME	PART NUMBER
TCM2.5 Module	12413
TCM2.5 Interface Kit	90011
TCM2.5 Evaluation Kit	90018

Interface kit includes: module, manual, evaluation software and 18" pigtail cable

Evaluation kit includes: module, manual, evaluation software, 18" pigtail cable and oft finished DB-9 cable with power supply

Developed by America's premier sensor technology company.
PNI Corporation, 133 Aviation Blvd. Suite 101, Santa Rosa CA 95403 • Tel: 707.566.2260 • Fax: 707.566.2261 • www.pnicorp.com



TCM2.5 Specifications

Parameter	Typical	Units	
Heading Specifications			
Accuracy	0.8°	Deg RMS	
Resolution	0.1°	Deg	
Repeatability (1)	0.1°	Deg RMS	
Max Dip Angle	85°	Deg	
Magnetometer Specifications			
Calibrated Field Measurement Range	± 80	µT	
Magnetic Resolution	± .05		
Magnetic Repeatability	± .1		
Tilt Specifications			
Pitch Accuracy	0.2°	Deg RMS	
Roll Accuracy	0.2°		
Tilt Range	± 50°	Deg	
Tilt Resolution	0.1°		
Tilt Repeatability (1)	0.1°		
Calibration			
Hard Iron Calibration	Yes		
Soft Iron Calibration	No		
Limited Tilt User Calibration	No		
Mechanical Specifications			
Dimensions (L x W x H)	6.4 x 5.1 x 1.4	cm	
Weight	20	grams	
Mounting Options	Screw Mounts/Standoffs horizontal		
Connector for RS-232 Interface	10-pin		
I/O Specifications			
Latency from Power-On	< 50	mSec	
Latency from Sleep Mode	< 1		
Maximum Sample Rate	20	samples/sec	
RS-232 Communication Rate	300 to 115200	baud	
Output Formats	TCM2 Protocol NMEA0183		
Power Specifications			
Supply Voltage	5 V (Regulated) 6 to 18 V (Unregulated)	VDC	
Typical Current Draw (Continuous Output)	Maximum	22	
	Typical	< 20	
Idle Mode	18	mA	
Sleep Mode	0.6		
Environmental Specifications			
Operating Temperature	-20° to 70°	C	
Storage Temperature	-40° to 85°		
Shock	50–2500 G's, Half Sine Wave Shock with 2 drops at each level		
Vibration	Z-Axis, Skewed Block, at 1, 2 & 4 Grms @ 10–1000 KHz for 30 min. per level		
Humidity	70°C with 95% R.H. for 168 hrs.		

(1) Repeatability is based on statistical data at ± 3 sigma limit about the mean.

These specifications are preliminary and are subject to change without notice.
For the most current specifications, please visit our website at www.pnicorp.com.

Stepper Motor Driver Module

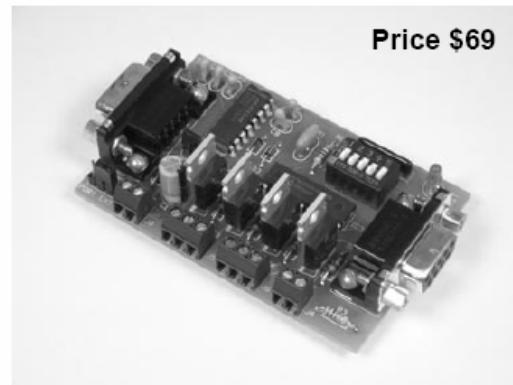
FEATURES

- Drives a unipolar stepper motor rated up to 30VDC @ 2A.
- DIP switch addressable; stack up to 32 modules on the same port for multiple axes.
- S-curve acceleration and deceleration slope profiles provide smooth start/stop motion.
- Software programmable ramp rate, velocity, and idle current.
- 24-bit absolute motor position counter.
- Normally-open limit switch input.
- Supports single phase, dual phase, and half-step drive modes.
- All user configuration data and motor position counter stored in non-volatile memory.
- Industry standard RS-232 interface. Meets all EIA/TIA-232E and V.28 specifications.
- Screw-terminal connectors used on all inputs and outputs.

DESCRIPTION

Connects to the RS-232 serial port of a PC, laptop, or other host. Directly drives a unipolar stepper motor using precise positioning and tracking algorithms. Simple coordinates sent from the host will advance stepper motor to an exact position in the range of 0 to 16,777,215. Host can also instruct motor to move in either direction until a limit switch has been triggered, or use a basic single-step mode which is host incremental.

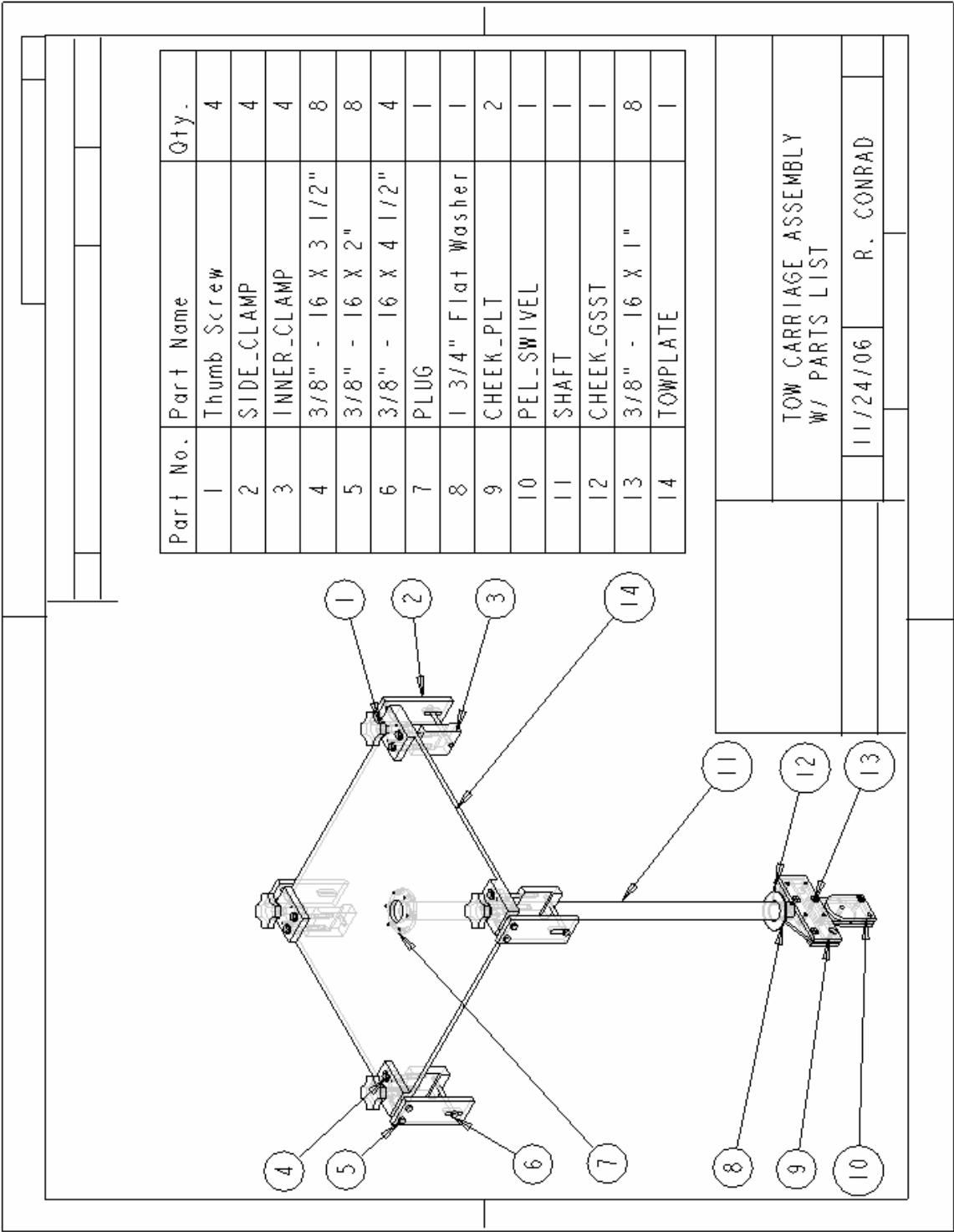
S-curve acceleration/deceleration slope profiles are automatically generated and incorporated into any multiple step sequence, independent of host. Thus reducing stall conditions during acceleration, and overrun conditions during deceleration. Ideal for use in cost sensitive, open-loop, precision motion control applications requiring a minimal user learning cycle.

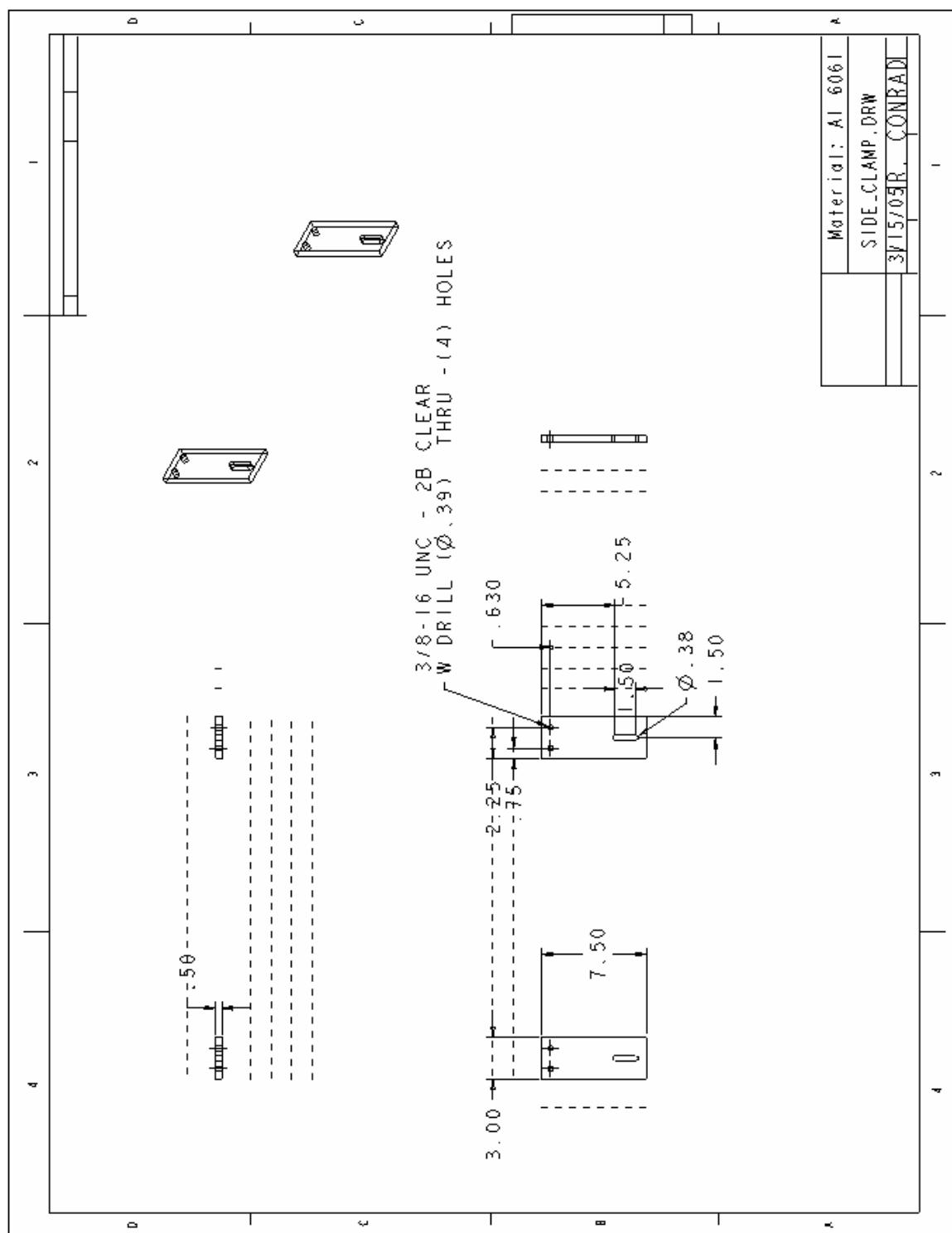


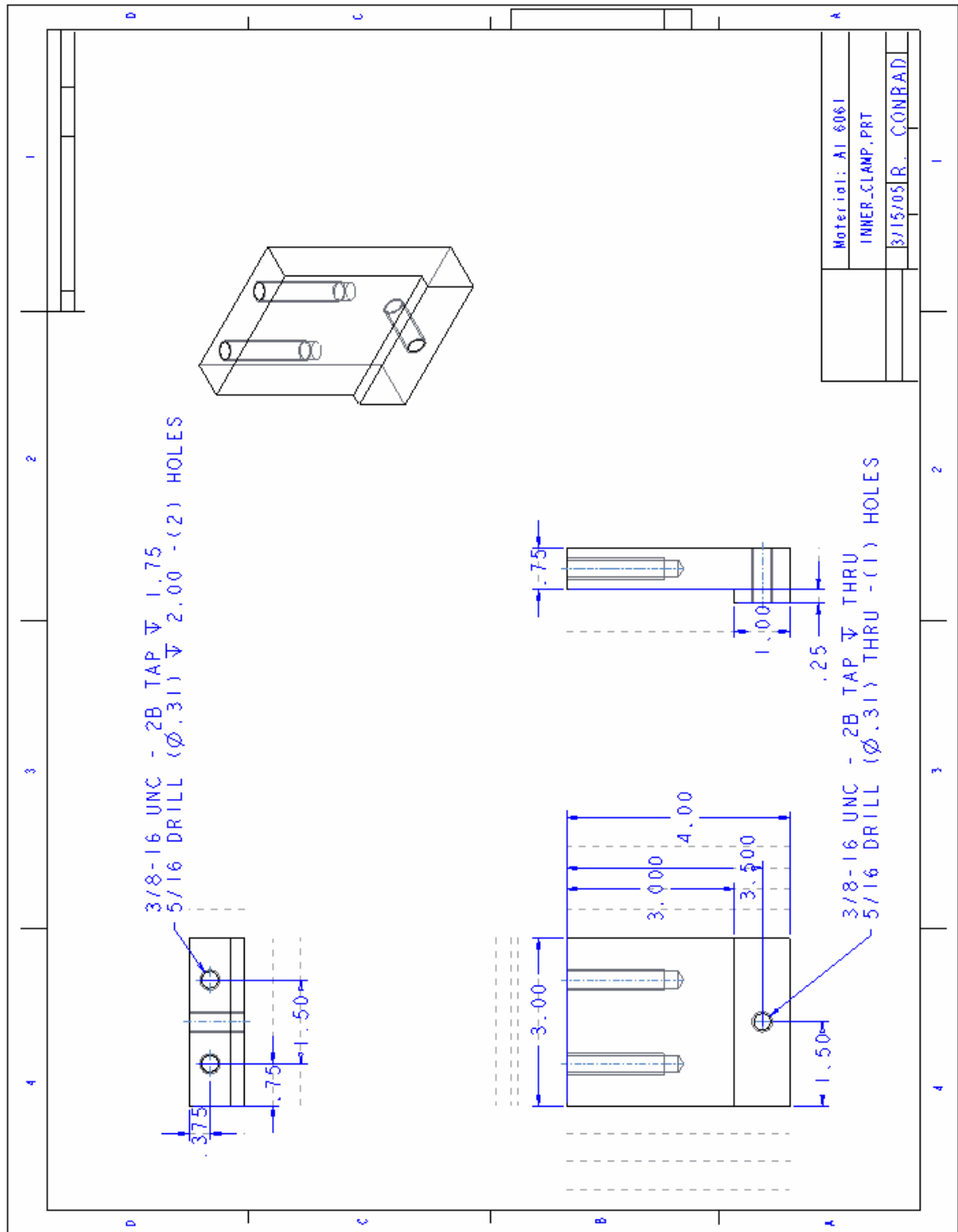
SPECIFICATIONS

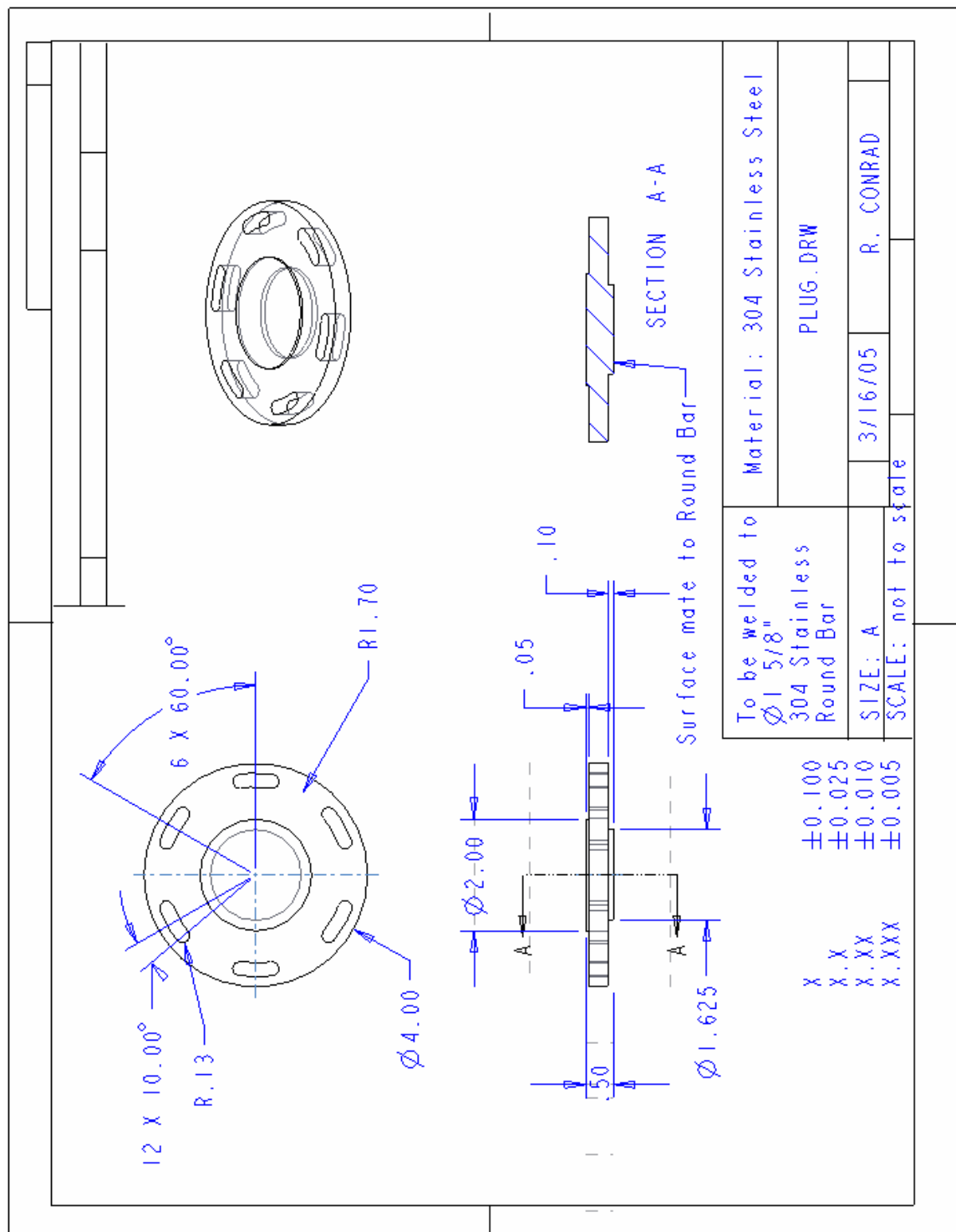
Drive Type	Quad, open-drain MOSFET
Drive Current	2A continuous max
Limit Switch	Normally-open, direction sensitive
Idle Current	PWM, selectable in 10% increments
Processor	PIC16CE625
Clock	4 MHz
Communications	9600 Baud, N, 8, 1
Power Requirements	+8 to +30 VDC
Current Draw	9 mA, plus current drawn by motor
Operating Temperature	-20°C to +80°C
Board Dimensions	3.1" x 2.0" x 1.0"
Weight	1.9 oz

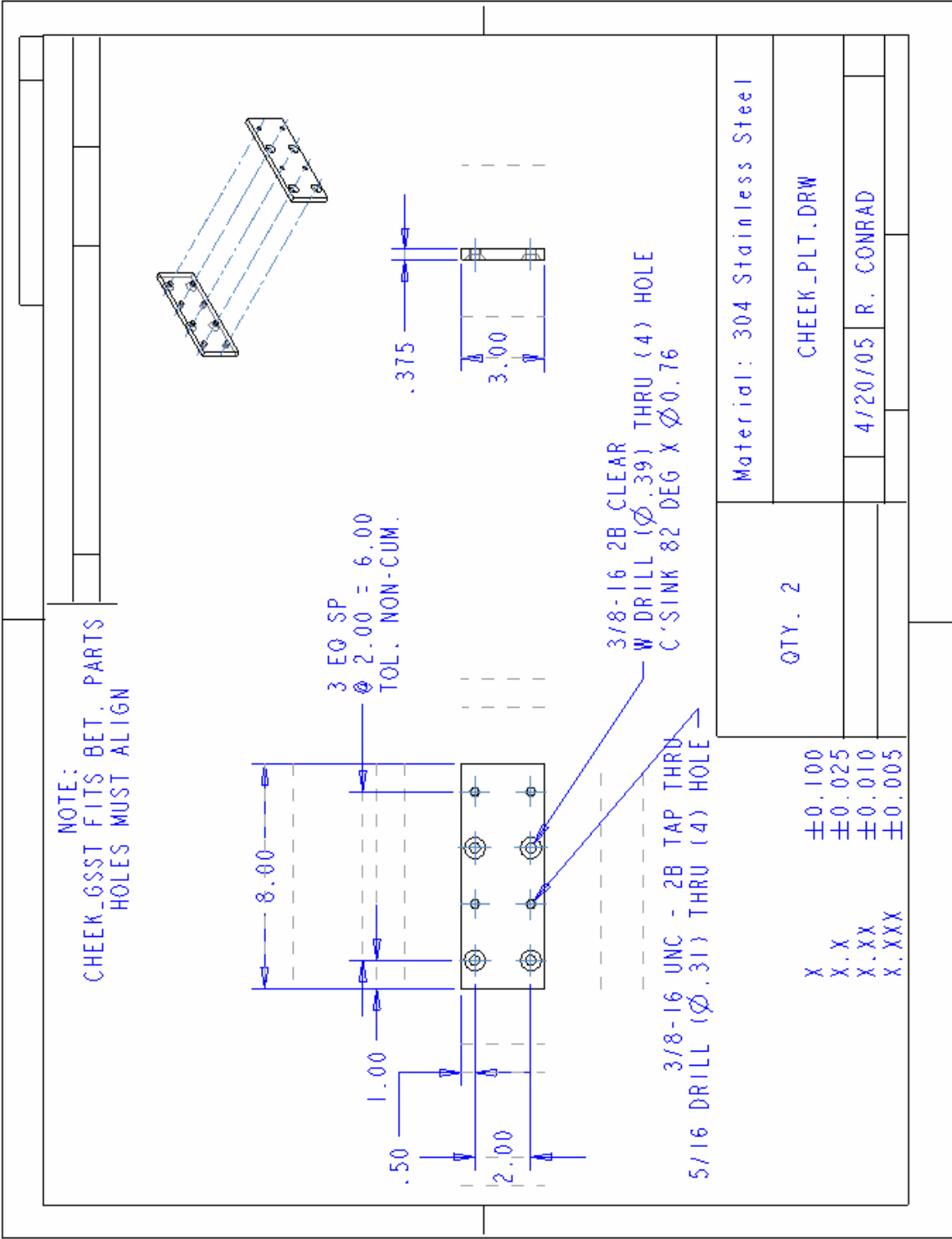
APPENDIX C:
PRINTS

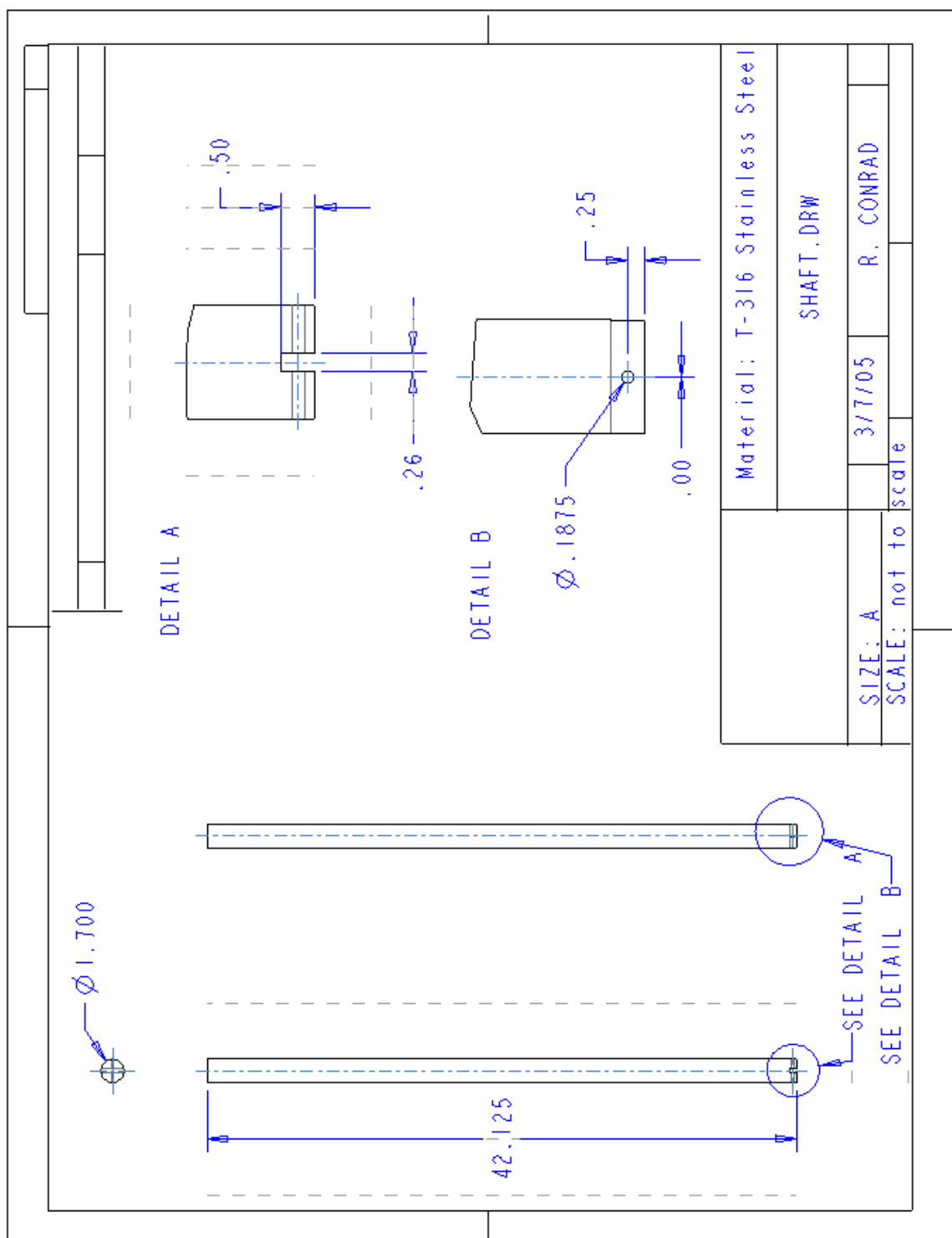


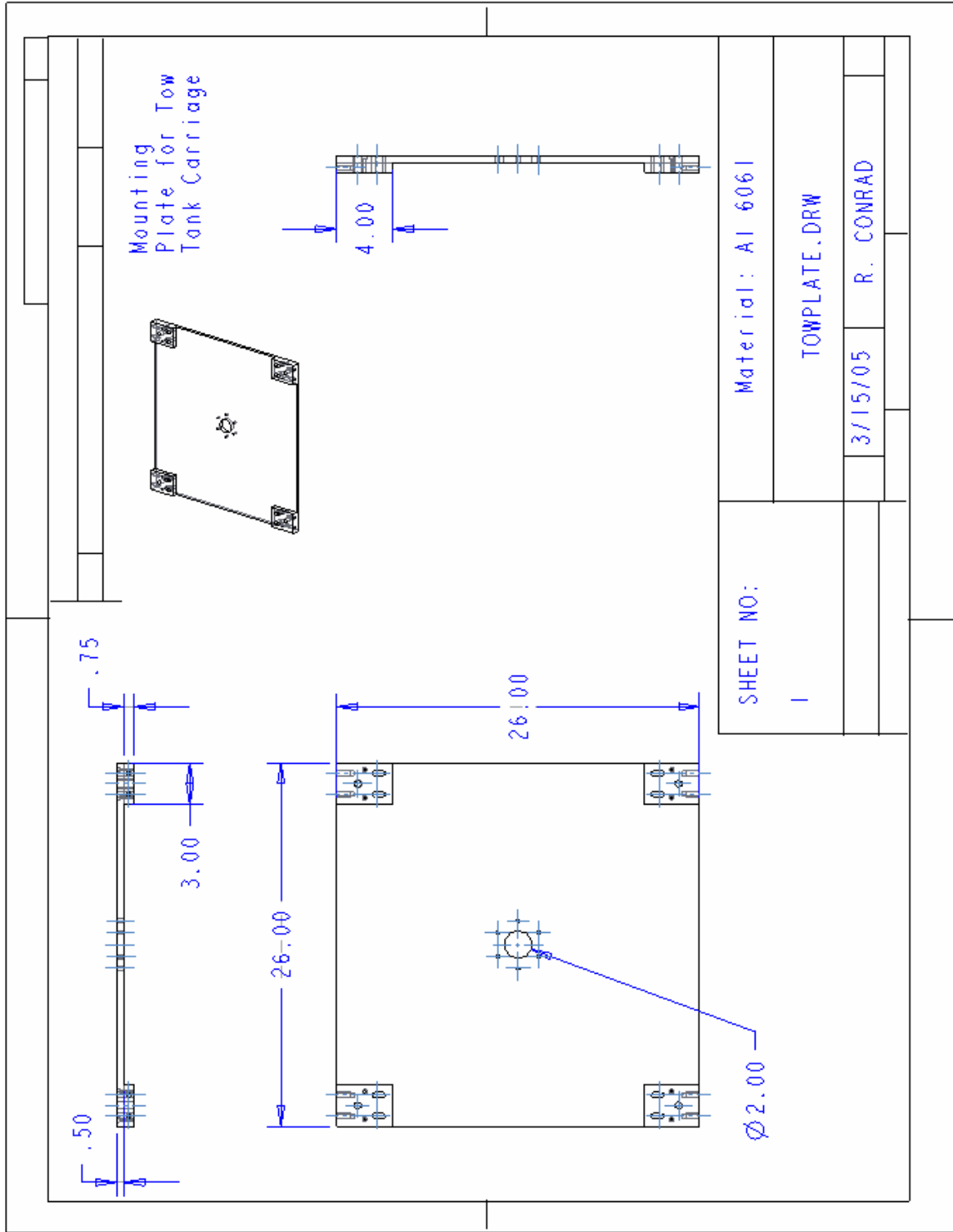


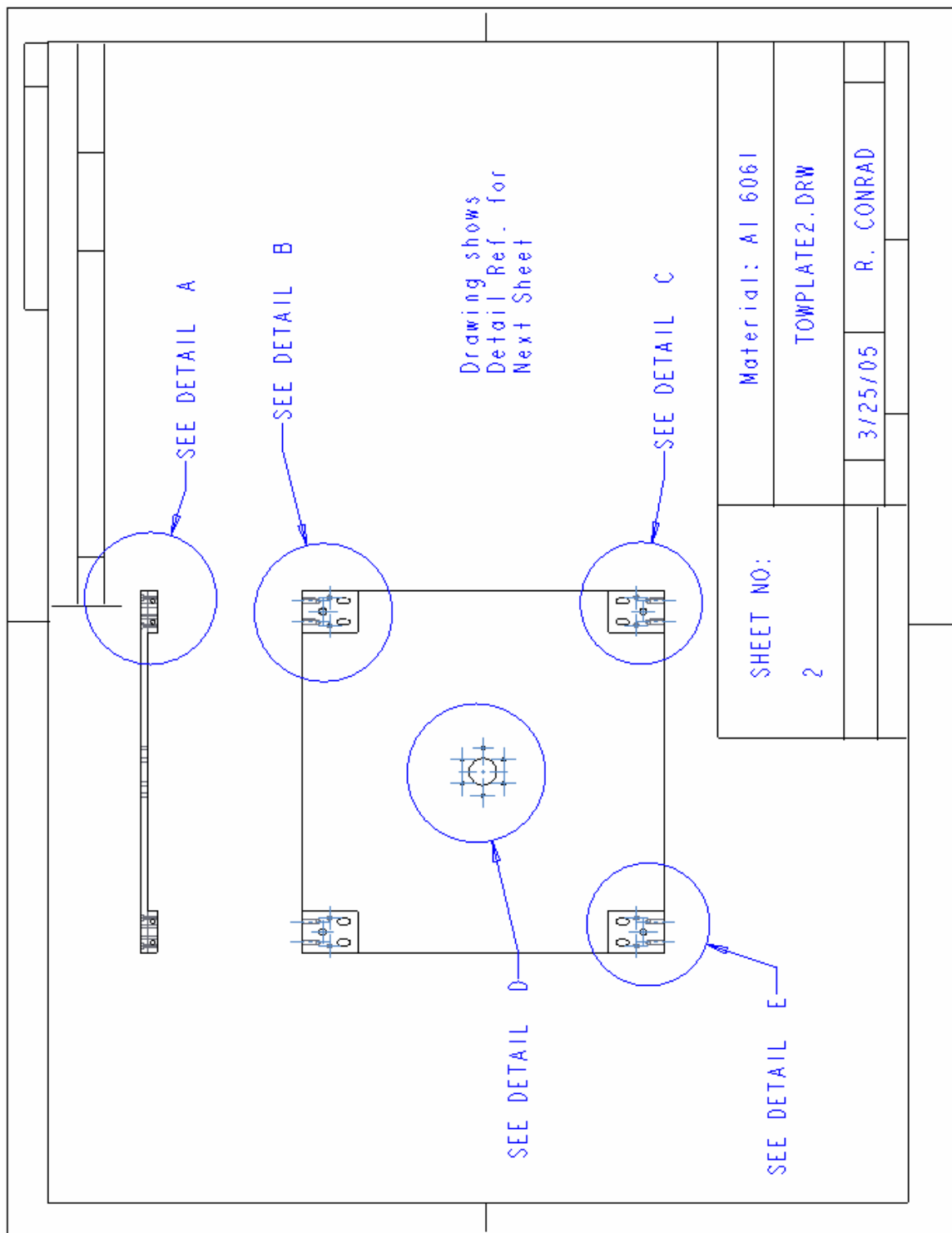


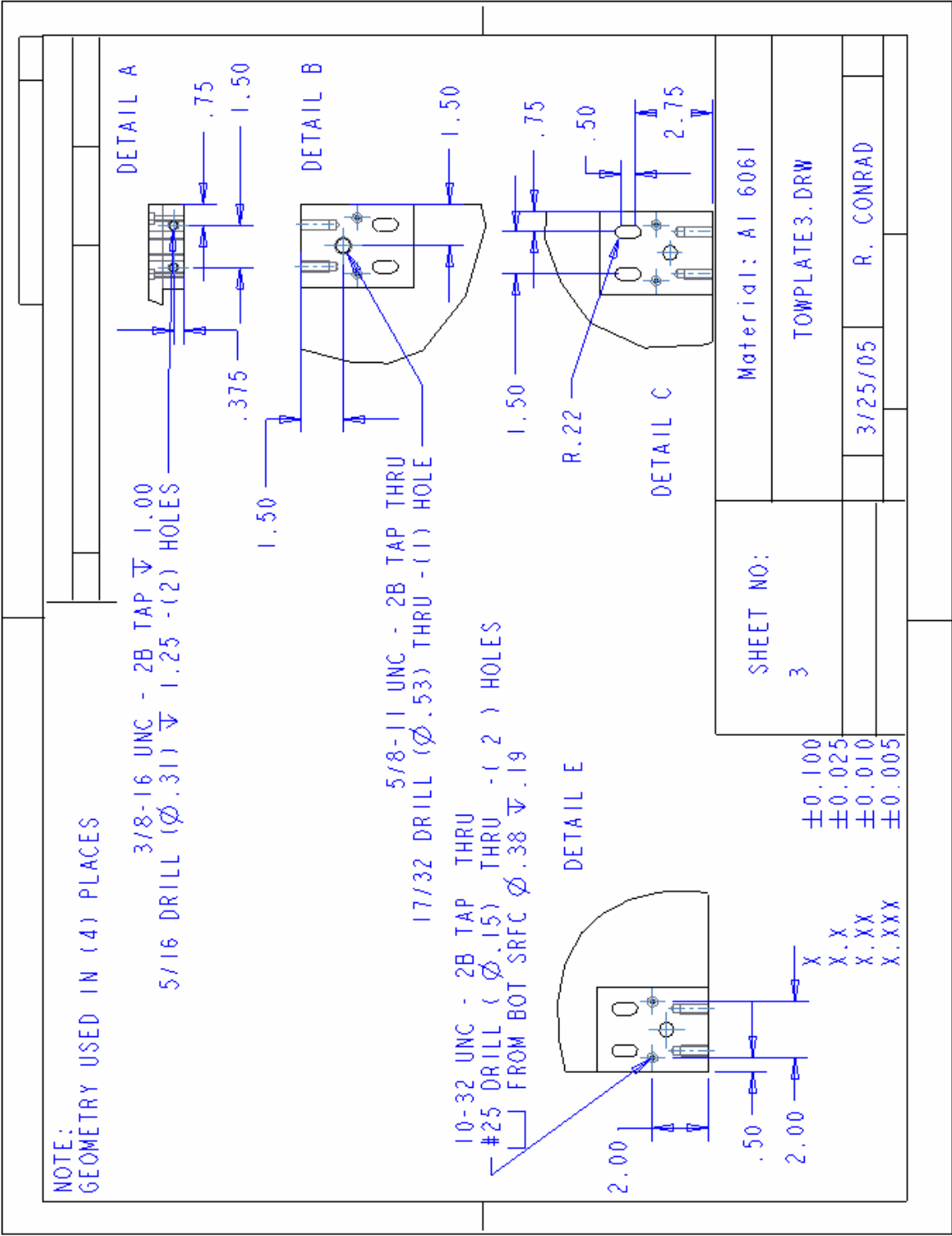


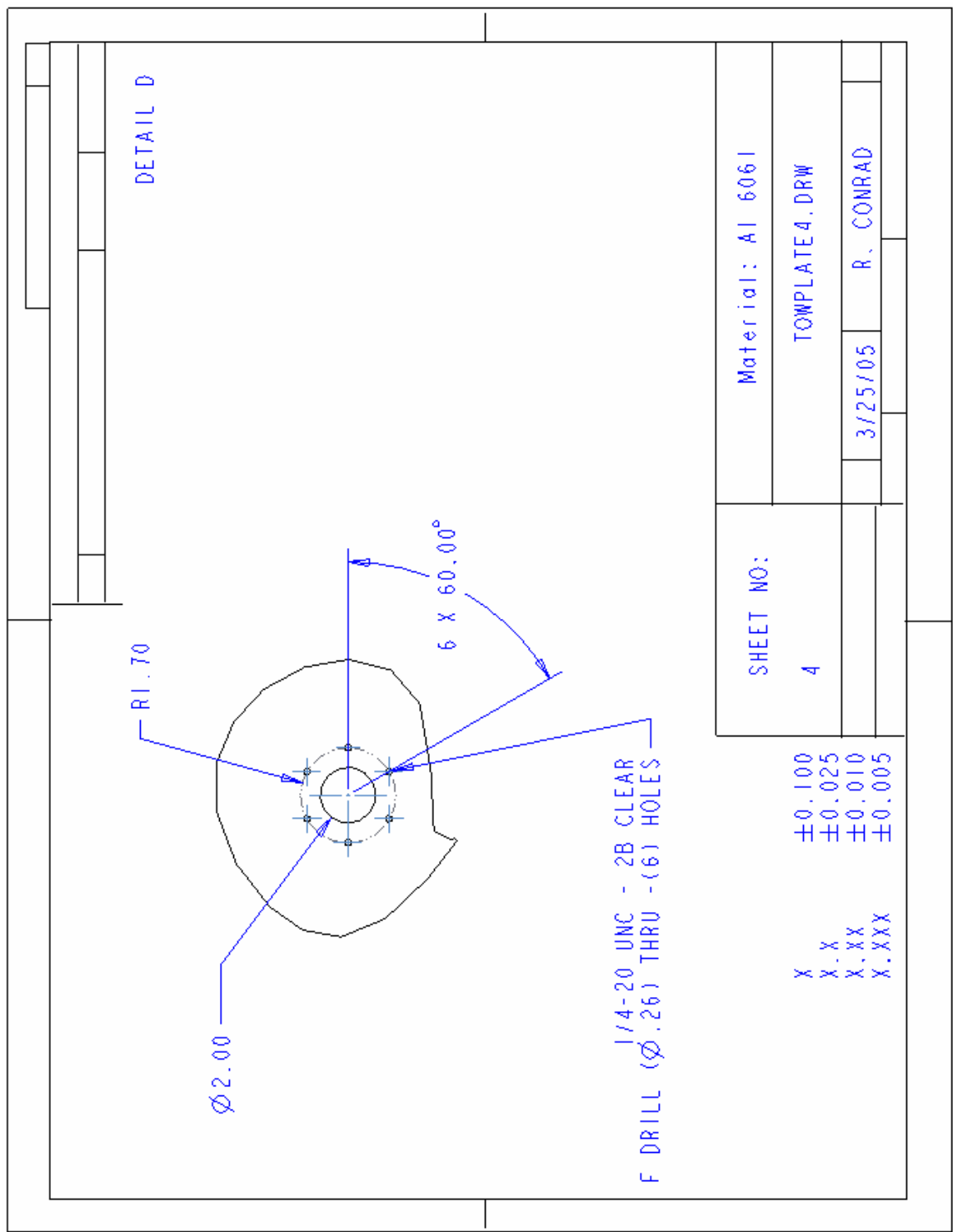




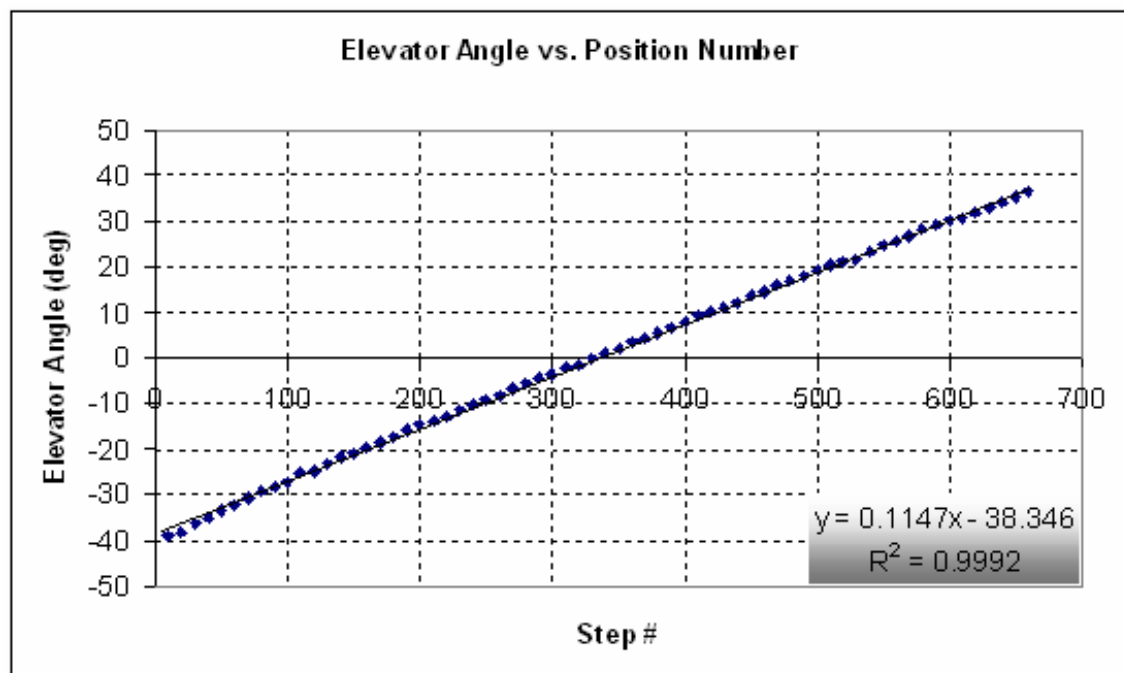
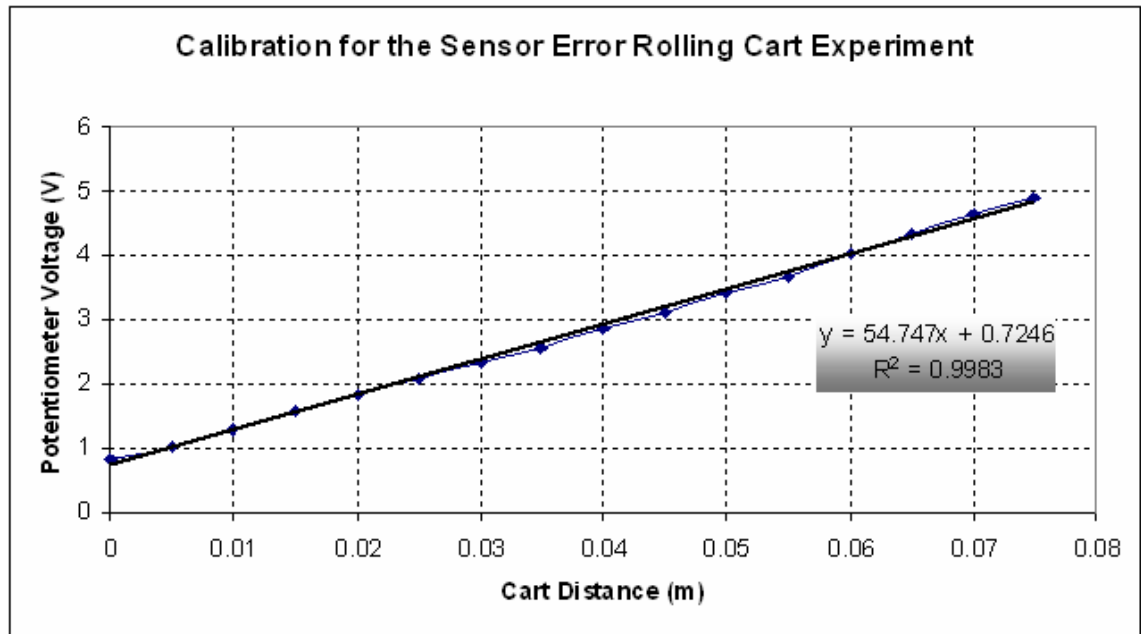




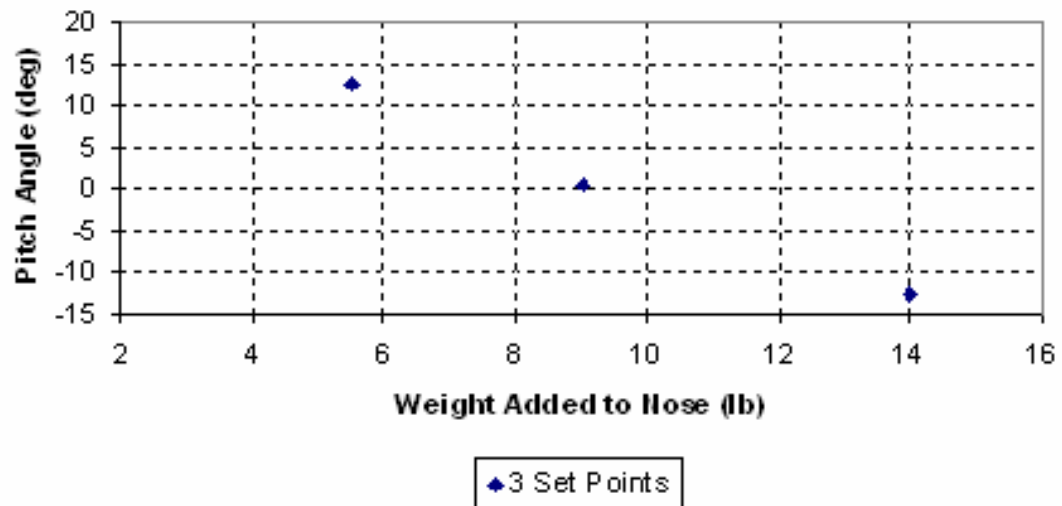




APPENDIX D:
CALIBRATIONS



Balance vs Ballast for Smart Tail Test 19 Oct 05
(In water for nose heavy, neutral, and nose light ballast conditions)



APPENDIX E:
SMART TAIL SOFTWARE

SmartTail Reference Manual

Generated by Doxygen 1.4.6

Wed Nov 8 20:18:02 2006

Contents

1	SmartTail Hierarchical Index	1
1.1	SmartTail Class Hierarchy	1
2	SmartTail Class Index	3
2.1	SmartTail Class List	3
3	SmartTail Class Documentation	5
3.1	Command Class Reference	5
3.2	CommandProcessor Class Reference	7
3.3	DoubleCommand Class Reference	8
3.4	DoubleStepCommand Class Reference	9
3.5	PassiveCommand Class Reference	11
3.6	SingleCommand Class Reference	12

Chapter 1

SmartTail Hierarchical Index

1.1 SmartTail Class Hierarchy

This inheritance list is sorted roughly, but not completely, alphabetically:

Command	5
DoubleCommand	8
DoubleStepCommand	9
PassiveCommand	11
SingleCommand	12
CommandProcessor	7

Chapter 2

SmartTail Class Index

2.1 SmartTail Class List

Here are the classes, structs, unions and interfaces with brief descriptions:

Command	5
CommandProcessor	7
DoubleCommand	8
DoubleStepCommand	9
PassiveCommand	11
SingleCommand	12

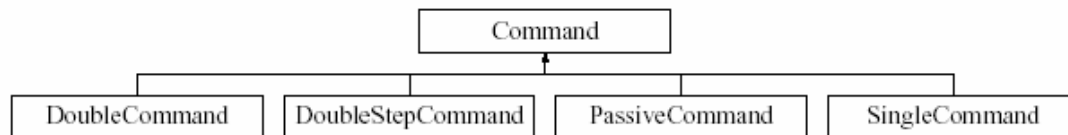
Chapter 3

SmartTail Class Documentation

3.1 Command Class Reference

```
#include <Command.h>
```

Inheritance diagram for `Command`:



Public Member Functions

- virtual bool **execute** (`ComPort &`, `ostream &`)=0

Friends

- `ostream & operator<<` (`ostream &co`, const `Command &c`)

3.1.1 Detailed Description

This is the base class for all `Command`(p. 5) classes that will be utilized by the SmartTail program. It is an Abstract class that will never be instantiated but will define a common interface to all Commands in the system.

Author:

Ian Berry <iberry@unh.edu>

3.1.2 Member Function Documentation

3.1.2.1 virtual bool `Command::execute` (`ComPort &`, `ostream &`) [pure virtual]

All concrete subclasses of `command` MUST implement an `execute` method having the signature:

bool execute(ComPort &, ostream &)(p. 5)

The ComPort object MUST already be connected and initialized.

The boolean return should indicate that the command was sent and an appropriate confirmation message was received.

Implemented in **DoubleCommand** (p. 8), **DoubleStepCommand** (p. 10), **PassiveCommand** (p. 11), and **SingleCommand** (p. 12).

The documentation for this class was generated from the following file:

- src/Command.h

3.2 CommandProcessor Class Reference

```
#include <CommandProcessor.h>
```

Public Member Functions

- **CommandProcessor** (ComPort *cmd)
- **CommandProcessor** (ComPort *cmd, ostream * _logger)
- const CString & **getPromptString** ()
- void **setPromptString** (CString &cstring)
- bool **executeCommandSequence** (vector< Command * > &, ostream &)
- bool **processInput** (istream &, ostream &)
- void **setDebug** (bool state=true)

3.2.1 Detailed Description

The **CommandProcessor**(p.7) class is responsible for ensuring proper orderly access to the WTSMD cards.

Author:

Ian Berry <iberry@unh.edu>

3.2.2 Constructor & Destructor Documentation

3.2.2.1 **CommandProcessor::CommandProcessor** (ComPort * *cmd*) [inline]

Constructor that takes the ComPort that shall be sent the commands.

3.2.3 Member Function Documentation

3.2.3.1 **bool CommandProcessor::executeCommandSequence** (vector< Command * > &, ostream &)

Execute a sequence of commands.

3.2.3.2 **const CString& CommandProcessor::getPromptString** ()

get/set prompt string.

3.2.3.3 **bool CommandProcessor::processInput** (istream &, ostream &)

Build command sequences from the given (user) input stream.

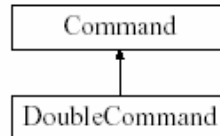
The documentation for this class was generated from the following files:

- src/CommandProcessor.h
- src/CommandProcessor.cpp

3.3 DoubleCommand Class Reference

```
#include <DoubleCommand.h>
```

Inheritance diagram for DoubleCommand::



Public Member Functions

- **DoubleCommand** (CString &cmd1, CString &cmd2)
- bool execute (ComPort &, ostream &)

Friends

- ostream & **operator**<< (ostream &, const **DoubleCommand** &)

3.3.1 Detailed Description

Double **Command**(p.5) Class provides the ability to send a command to each of the Weeder controller cards, `~~nearly~~ simultaneously(++)`.

(++) Through some testing we have found that if the `ComPort::Transmit(cmd,timeout)` method is utilized with any timeout of less than 17 milliseconds, there is a high probability of "collisions" in the multi-drop RS232 network which will significantly increase the delay between commands. This is less of an issue when utilizing only one WTSMD card, but for addressing multiple cards this can lead to excessive retransmissions and possibly multiple collisions before the line is clear for sending again.

3.3.2 Member Function Documentation

3.3.2.1 bool DoubleCommand::execute (ComPort & *in*, ostream & *out*) [virtual]

Implementation for **DoubleCommand**(p. 8) class.

Implements **Command** (p. 5).

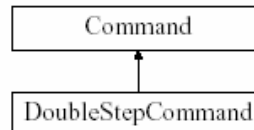
The documentation for this class was generated from the following files:

- src/DoubleCommand.h
- src/DoubleCommand.cpp

3.4 DoubleStepCommand Class Reference

```
#include <DoubleStepCommand.h>
```

Inheritance diagram for DoubleStepCommand::



Public Member Functions

- **DoubleStepCommand** (CString &)
- **DoubleStepCommand** (int stepsA=0, int stepsB=0, char addrA='A', char addrB='B')
- bool **execute** (ComPort &, ostream &)
- void **setStepA** (int sA)
- void **setStepB** (int sB)

Friends

- ostream & **operator<<** (ostream &, const **DoubleStepCommand** &)

3.4.1 Detailed Description

DoubleStepCommand(p.5) Class provides the ability to send a command to each of the Weeder controller cards, nearly simultaneously.

See constructor documentation for syntax of the command.

3.4.2 Constructor & Destructor Documentation

3.4.2.1 DoubleStepCommand::DoubleStepCommand (CString &)

DoubleStepCommand Constructor This command takes a CString of the form "A-123" or "A123:B-321". These strings indicate the number of Steps in the given direction that each motor should be instructed to move.

3.4.2.2 DoubleStepCommand::DoubleStepCommand (int *stepsA* = 0, int *stepsB* = 0, char *addrA* = 'A', char *addrB* = 'B') [inline]

Default and explicit constructor. Defaults to A+0, B+0 but may be explicitly constructed to go anywhere. At runtime, the bounds of the fin will be checked so that the fins stay in the range 0-660.

3.4.3 Member Function Documentation

3.4.3.1 `bool DoubleStepCommand::execute (ComPort &, ostream &) [virtual]`

All concrete subclasses of command MUST implement an execute method having the signature:

`bool execute(ComPort &, ostream &)`(p. 10)

The ComPort object MUST already be connected and initialized.

The boolean return should indicate that the command was sent and an appropriate confirmation message was received.

Implements `Command` (p. 5).

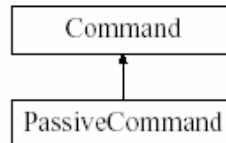
The documentation for this class was generated from the following files:

- `src/DoubleStepCommand.h`
- `src/DoubleStepCommand.cpp`

3.5 PassiveCommand Class Reference

```
#include <PassiveCommand.h>
```

Inheritance diagram for `PassiveCommand`:



Public Member Functions

- `PassiveCommand (CString &cmd)`
- virtual `bool execute (ComPort &, ostream &)`

Friends

- `ostream & operator<< (ostream &co, const PassiveCommand &c)`

3.5.1 Detailed Description

A single weeder command which has no action corresponding, just information (i.e. AE or BP)

3.5.2 Member Function Documentation

3.5.2.1 `bool PassiveCommand::execute (ComPort &, ostream &) [virtual]`

All concrete subclasses of command MUST implement an execute method having the signature:
`bool execute(ComPort &, ostream &)(p.11)`

The ComPort object MUST already be connected and initialized.

The boolean return should indicate that the command was sent and an appropriate confirmation message was received.

Implements `Command` (p.5).

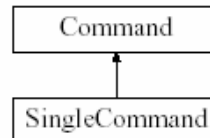
The documentation for this class was generated from the following files:

- `src/PassiveCommand.h`
- `src/PassiveCommand.cpp`

3.6 SingleCommand Class Reference

```
#include <SingleCommand.h>
```

Inheritance diagram for SingleCommand::



Public Member Functions

- **SingleCommand** (CString &cmd=CString(""))
- virtual bool **execute** (ComPort &, ostream &)

Friends

- ostream & **operator**<< (ostream &, const **SingleCommand** &)

3.6.1 Detailed Description

Single Command(p. 5) Class provides the ability to send a command to only one of the Weeder controller cards.

author: Ian Berry <iberry@unh.edu>

3.6.2 Member Function Documentation

3.6.2.1 bool **SingleCommand::execute** (ComPort &, ostream &) [virtual]

All concrete subclasses of command **MUST** implement an execute method having the signature:

bool **execute**(ComPort &, ostream &)(p. 12)

The ComPort object **MUST** already be connected and initialized.

The boolean return should indicate that the command was sent and an appropriate confirmation message was received.

Implements **Command** (p. 5).

The documentation for this class was generated from the following files:

- src/SingleCommand.h
- src/SingleCommand.cpp

Index

- Command, 5
 - execute, 5
- CommandProcessor, 7
 - CommandProcessor, 7
- CommandProcessor
 - CommandProcessor, 7
 - executeCommandSequence,
 - getPromptString, 7
 - processInput, 7
- DoubleCommand, 8
- DoubleCommand
 - execute, 8
- DoubleStepCommand, 9
 - DoubleStepCommand, 9
- DoubleStepCommand
 - DoubleStepCommand, 9
 - execute, 10
- execute
 - Command, 5
 - DoubleCommand, 8
 - DoubleStepCommand, 10
 - PassiveCommand, 11
 - SingleCommand, 12
- executeCommandSequence
 - CommandProcessor, 7
- getPromptString
 - CommandProcessor, 7
- PassiveCommand, 11
- PassiveCommand
 - execute, 11
- processInput
 - CommandProcessor, 7
- SingleCommand, 12
- SingleCommand
 - execute, 12